ARO 21637.12-MS

(2)

Fatigue, Fracture and Wear Properties of Rubber

Final Report

James A. Donovan

January 19, 1989

U.S. Army Research Office
21637-MS

University of Massachusetts
Amherst, Massachusetts 01003

ADA204743

UNCLASSIFIED
SECURITY CLASSIFICATION OF THIS PAGE

MASTER COPY - FOR REPRODUCTION PURPOSES

REPORT DOCUMENTATION PAGE

1a. REPORT SECURITY CLASSIFICATION Unclassified	1b. RESTRICTIVE MARKINGS
2a. SECURITY CLASSIFICATION AUTHORITY	3 DISTRIBUTION / AVAILABILITY OF REPORT Approved for public release; distribution unlimited.
2b. DECLASSIFICATION / DOWNGRADING SCHEDULE	
4. PERFORMING ORGANIZATION REPORT NUMBER(S)	5. MONITORING ORGANIZATION REPORT NUMBER(S) ARO 21637.12-MS
6a. NAME OF PERFORMING ORGANIZATION University of Massachusetts 6b. OFFICE SYMBOL (If applicable)	7a. NAME OF MONITORING ORGANIZATION U. S. Army Research Office
6c. ADDRESS (City, State, and ZIP Code) Mechanical Engineering Amherst, MA 01003	7b. ADDRESS (City, State, and ZIP Code) P. O. Box 12211 Research Triangle Park, NC 27709-2211
8a. NAME OF FUNDING / SPONSORING ORGANIZATION U. S. Army Research Office 8b. OFFICE SYMBOL (If applicable)	9. PROCUREMENT INSTRUMENT IDENTIFICATION NUMBER DAAG29-85-K-0030
8c. ADDRESS (City, State, and ZIP Code) P. O. Box 12211 Research Triangle Park, NC 27709-2211	10. SOURCE OF FUNDING NUMBERS PROGRAM ELEMENT NO. / PROJECT NO. / TASK NO. / WORK UNIT ACCESSION NO

11. TITLE (Include Security Classification)
Fatigue, Fracture and Wear Properties of Rubber

12. PERSONAL AUTHOR(S)
James A. Donovan

13a. TYPE OF REPORT	13b. TIME COVERED	14. DATE OF REPORT (Year, Month, Day)	15. PAGE COUNT
FINAL	FROM 85-01-01 TO 88-12-31	89/1/19	130

16. SUPPLEMENTARY NOTATION
The view, opinions and/or findings contained in this report are those of the author(s) and should not be construed as an official Department of the Army position, policy, or decision, unless so designated by other documentation.

17. COSATI CODES		
FIELD	GROUP	SUB-GROUP

18. SUBJECT TERMS (Continue on reverse if necessary and identify by block number)
Carbon black reinforcement, fatigue, fractal analysis, fracture, J-Integral, strain induced crystallization, wear, ( )

19. ABSTRACT (Continue on reverse if necessary and identify by block number)
cont. pg 1

This is the final report on the research program to study the fracture resistance of rubber and its relation to microstructural change in the crack tip region. Fracture was characterized by the J-integral and carbon black increased fracture resistance by increasing strain induced crystallization. The research results as published papers are included.

20 DISTRIBUTION / AVAILABILITY OF ABSTRACT ☐ UNCLASSIFIED/UNLIMITED ☐ SAME AS RPT. ☐ DTIC USERS	21. ABSTRACT SECURITY CLASSIFICATION Unclassified
22a. NAME OF RESPONSIBLE INDIVIDUAL	22b. TELEPHONE (Include Area Code) / 22c. OFFICE SYMBOL

DD FORM 1473, 84 MAR 83 APR edition may be used until exhausted. All other editions are obsolete.

SECURITY CLASSIFICATION OF THIS PAGE
UNCLASSIFIED

TABLE OF CONTENTS

I Statement of Problem Studied.....1

II Summary of Most Important Results.....2

III Publications.....3

IV Presentations.....129

V Participating Scientific Personnel.....130

Statement of Problem Studied

Characterizing the fracture properties of technologically important elastomers (non-linear, non-elastic materials) has been uncertain because of the extensive energy dissipation during deformation. The objective of the research was to evaluate the J-integral concept of fracture as a fracture characterizing parameter and to relate the fracture resistance to crack tip microstructure in carbon black filled natural rubber. Wear rate of rubber, thought to be primarily related to fracture resistance, was studied and correlated by fractal analysis to the wear surface.

Summary of Most Important Results

1. Carbon black increased the extent of strain induced crystallinity and thereby contributed to fracture resistance. This has been an overlooked carbon black reinforcement mechanism.

2. J-integral concept is valid for characterizing fracture initiation and correlation of fatigue crack growth rate in carbon black filled natural rubber.

3. J can be used for single edge cracked, pure shear, and mixed mode I and II crack growth studies.

4. Crack initiation was shown to be controlled by the local crack tip strain.

5. Crack initiation conditions in single edge and pure shear specimens (both mode I loading) differ because of the greater biaxial stress state in the pure shear specimen.

6. Differential scanning calorimetry of uniaxially and biaxially stressed specimens showed that biaxial stresses hindered strain induced crystallization.

7. Rubber wear surfaces are fractal, and the fractal analysis linked the wear rate to the topography of the wear surface.

Publications **Page**

A. "J-Integral and Crack Opening Displacement as Crack Initiation Criteria in Rubber," Rubb. Chem. and Tech., 59 (1986), 787-799 (with R.F. Lee). 4

B. "Fractographic Survey of Polymeric Materials," in Microscopy, Fractography and Failure Analysis, Ed., M.R. Louthan and T.A. Place, (1986), VPI, Blacksburg, VA. 17

C. "Applications of the J-Integral to Fracture of Non-Elastic Rubber," Elastomers and Rubber Technology, Eds. R.E. Singler and C.A. Byrne, U.S. Gov. Printing Off. (1987), 175-190. 39

D. "J-Integral and Crack Opening Displacement as Crack Initiation Criteria in National Rubber in Pure Shear and Tensile Specimens," Rubb. Chem. and Tech. 60, (1987) 674-688. 55

E. "Effect of Carbon Black on the J-Integral and Strain Energy in the Crack Tip Region in a Vulcanized Natural Rubber," Rubb. Chem. and Tech., 60, (1987), 893-909. 63

F. "Microstructural Changes in the Crack Tip Region of Carbon Black Filled Natural Rubber," Rubb. Chem. and Tech., 60, (1987), 910-923. 72

G. "Mixed Mode I and II Fracture of Carbon Black Filled Natural Rubber," Int. J. of Fract., 34, (1987) 41-55. 79

H. "Fractal Analysis of Rubber Wear Surfaces and Debris," J. of Mat. Sci., 23, (1988), 2230-2242. 93

I. "The Effect of Carbon Black and Stress State on Strain Induced Crystallization in Natural Rubber" draft to be submitted to Rubber Chem. and Tech. 106

J. Several additional papers will be prepared based on unreported results.

J-INTEGRAL AND CRACK OPENING DISPLACEMENT AS CRACK INITIATION CRITERIA IN RUBBER*

R. F. LEE AND J. A. DONOVAN

DEPARTMENT OF MECHANICAL ENGINEERING, UNIVERSITY OF MASSACHUSETTS, AMHERST, MA 01003

INTRODUCTION

Rivlin and Thomas[1] showed thirty years ago that the fracture properties of nonlinear elastic rubbers could be characterized by the tearing energy T defined as

$$T = -\frac{1}{B}\cdot\frac{\partial U}{\partial a}, \tag{1}$$

where B is the thickness of the specimen, U is the stored energy, and a is the crack length. T is, therefore, the critical strain energy release rate required to advance the crack unit area. T accurately characterizes the fracture properties of nonlinear elastic rubbers[2]. However, if the rubber is nonelastic and dissipates significant energy it is not suitable, and the approach requires subtraction of the dissipated energy.

The J-integral concept[3] has been applied to rubber since it successfully characterizes ductile, highly dissipative fracture in metals and has been shown to satisfactorily characterize fracture in nonlinear, nonelastic rubbers also[4]. However, this method requires several specimens to determine the critical J-integral for fracture.

Thomas[5] was the first to focus attention on the crack tip region as a means for determining the critical fracture parameters in rubber. Instead of studying the behavior of sharp cracks, he measured the conditions for crack initiation of blunted cracks and derived the following equation for the tearing energy:

$$T = R\int W\cdot d\sin\theta,$$

where W is the stored strain energy, R is the crack tip radius, and θ is the angle from notch center line to the point of interest (Figure 1). Thus, by knowing the local stored energy as a function of position, the critical tearing energy could be determined. From the local extension ratio along the crack surface and using the Mooney–Rivlin equations for energy density as a function of extension ratio, he was able to calculate the critical tearing energy.

It is interesting to note that precisely the same equation can be derived from Rice's definition of the J-integral[3]. The J-integral is defined as

$$J = \int_\Gamma \left(W(x,y)dy - T_J\frac{du}{dx}ds\right), \tag{2}$$

* Received November 1, 1985; revised May 19, 1986. B.

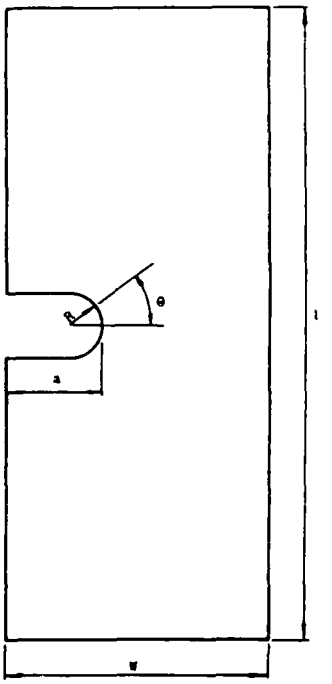

FIG. 1.—Characteristic dimensions of prenotched specimens.

where W is the strain energy density of any element on any integration path Γ surrounding the crack tip, T_J is the traction vector of the element, u is the displacement vector, and s is the arc length.

If the integration path is taken along the blunted notch, then the traction vector T_J is everywhere zero and

$$J_\theta = \int W dy = R \int W \cdot d \sin\theta, \tag{3}$$

which is exactly the same as Thomas derived some thirty years ago.

Application of the J-integral to the Barrenblatt–Dugdale model[3] for a long plastic zone in front of a crack shows that

$$J_\delta = \int \sigma d\delta, \tag{4}$$

where σ is a restraining stress in an elastic, perfectly plastic material and δ is the crack tip opening. Thus, within the assumptions of this model, the criterion of a critical J for crack initiation is completely equivalent to specification of a critical crack opening displacement[3]. Based on this result and recognizing that the highly strained region in front of a crack in rubber may not satisfy the Dugdale model, the possibility that a critical crack tip displacement would also be satisfactory was investigated. Specifically, the $\int \sigma d\delta$ where σ is the net section stress and δ is the crack tip opening was evaluated as a possible fracture characterizing parameter.

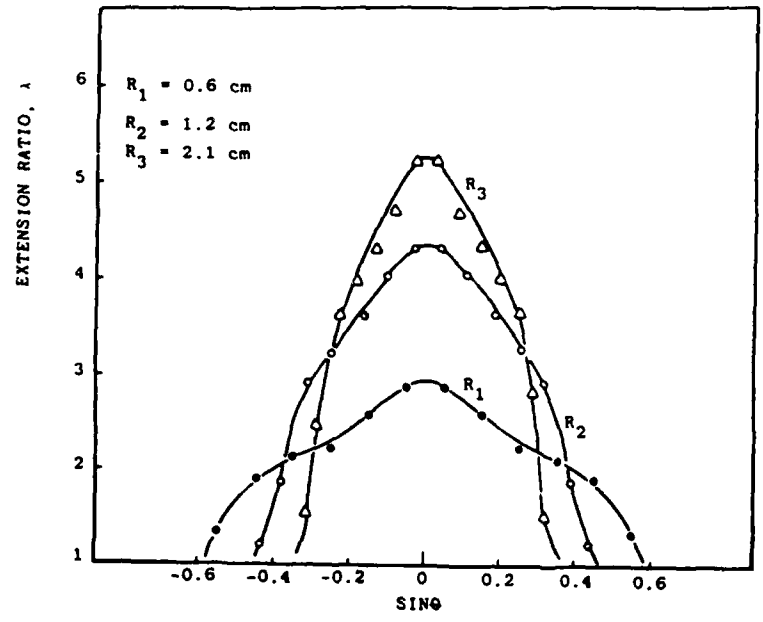

FIG. 2.—Extension ratio as a function of sin θ for a specimen with an initial radius of 2 mm.

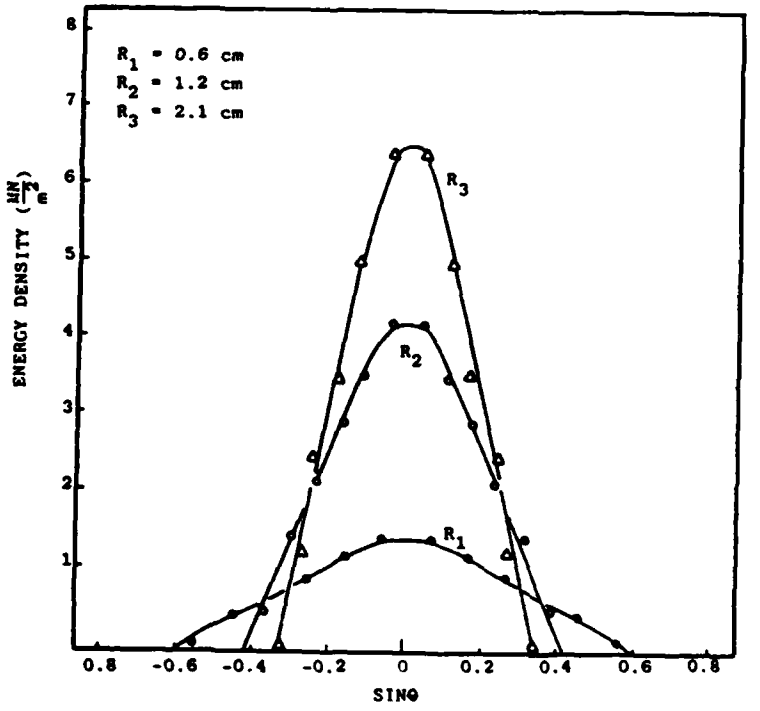

FIG. 3.—Energy density as a function of sin θ for a specimen with an initial radius of 2 mm.

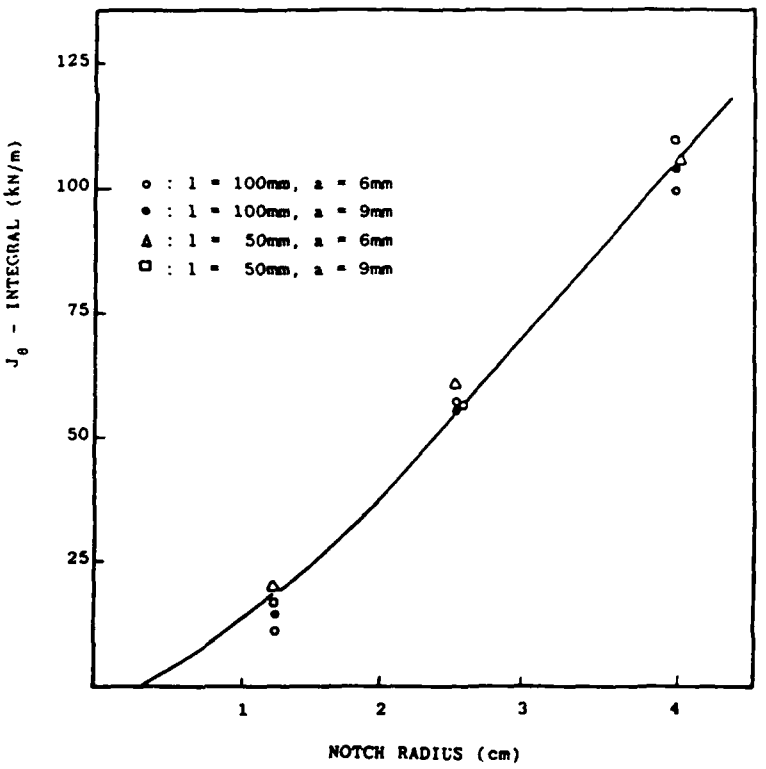

FIG. 4.—J_θ as a function of deformed notch tip radius for a specimen with an initial notch radius of 2 mm in unfilled NR.

Since carbon-black-filled NR is a highly dissipative system, it was chosen as a severe test of the validity of the J-integral approach to characterizing fracture in rubber. The J-integral based on the Thomas–Rice relation in prenotched specimens is compared to the value of the J-integral based on the Dugdale model, and results on the effect of carbon black content on the fracture properties are presented.

EXPERIMENTAL PROCEDURE

An NR recipe, compounded by BFGoodrich, with carbon black contents of 0, 10, 25, and 40 pph was used for all tests.

Single-edge notched specimens with sharp or blunt notches of different lengths, widths, and precrack lengths were tested at 21°C and a displacement rate of 1 cm/min. The sharp cracks were made by cutting the rubber with a razor blade. The blunt notches were made by drilling a hole with a sharp, hollow, circular

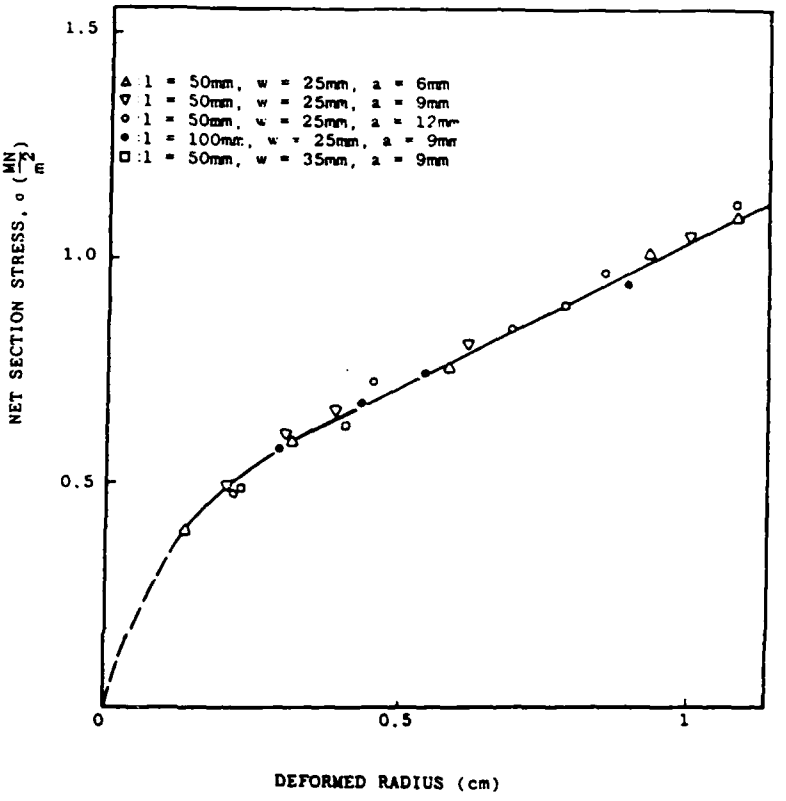

FIG. 5.—Net section stress as a function of deformed crack tip radius in different geometry precracked specimens in unfilled NR.

cutter lubricated with water. Blunt notches with radii 1, 2, and 3 mm were made, then the sides of the notches were cut away with a sharp razor blade (Figure 1).

The region around the notch tip was coated with white powder so that a series of fine, equally spaced radial lines could be made in the crack tip region. The spacing between the lines was measured with the aid of a 10 × filar eyepiece. Based on these measurements, the extension ratio as a function of position was determined and was the basis for calculating the critical J integral at initiation.

The above procedure is not applicable for sharp cracks, therefore J_i was determined by measuring the crack opening radius with a radius gage as a function of load.

Crack initiation was identified by coating the crack surface with the white powder; as loading increased, the region in the crack tip developed a new surface delineated by the white powder which then slowly peeled. The first observation of peeling was taken as crack initiation. However, the true initiation event is thought to slightly precede the initiation of peeling; but, initiation was consistently

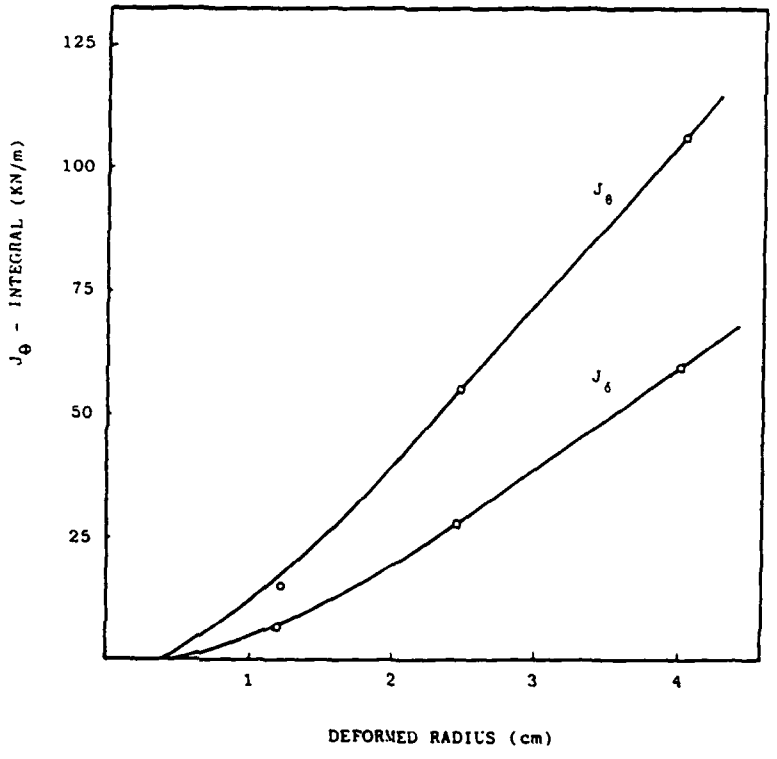

FIG. 6.—J_θ and J_δ as a function of deformed notch radii.

identified as described. Additional work is being done to refine identification of the initiation event.

Conventional tensile tests (smooth specimens) to determine stress–extension ratio curves and the stored energy as a function of extension ratio were measured at 21°C and a displacement rate of 1 cm/min.

RESULTS

The extension ratio as a function of position along the notch tip for different values of the radius of the notch were measured and are shown in Figure 2 as a function of sin θ.

These data were obtained in specimens of different length (l) width (w), precrack radius (R_ρ) and precrack length (a). The data were independent of these variables, except for R_ρ, within experimental error. The stored energy (W) as a function of the extension ratio was obtained from tensile tests by integrating the area under the stress–extention ratio curve and used to determine the energy stored as a function of position along the blunted notch and is shown in Figure

3 for different imposed notch radii. The J-integral was then determined according to Equation (3) by integrating the area under the W-sin θ curve and is shown in Figure 4 as a function of the deformed notch tip radius and shows that it is independent of w, l, and a. Similar data were obtained as a function precrack notch tip radius, specimen geometry, and carbon black content.

This curve (Figure 4) serves as the basis for determining the critical J value required for initiation of crack growth from a blunted precrack. However, it is obvious that this procedure is tedious and cannot be applied to sharp cracks. Therefore, the net section stress was measured as a function of deformed crack

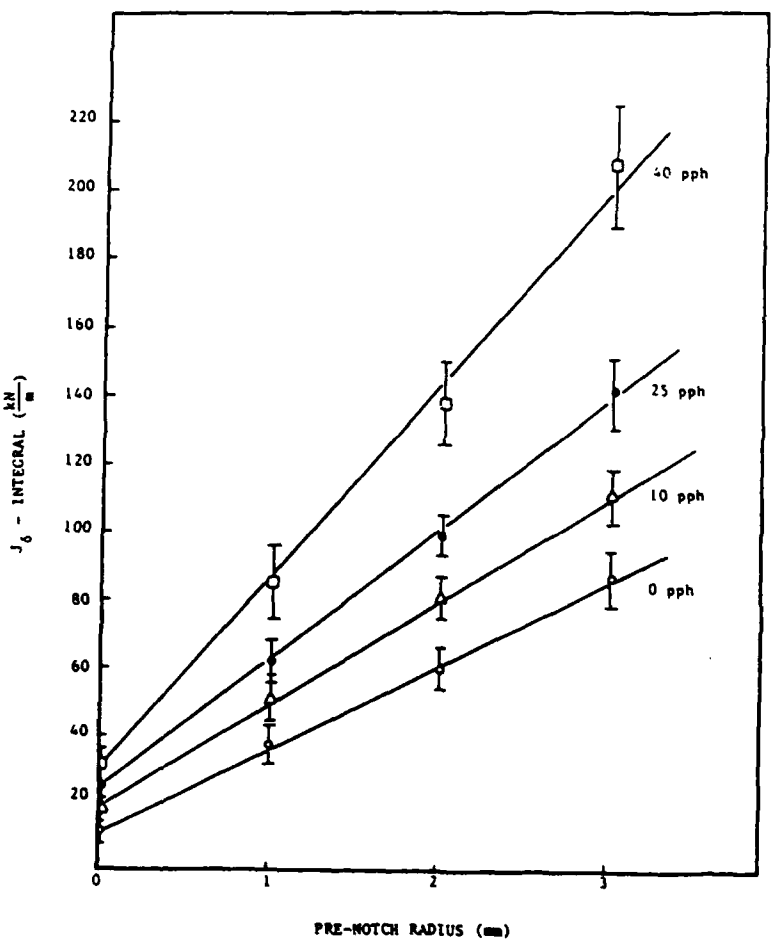

FIG. 7.—J_δ at crack initiation as a function of prenotch radii for 4 contents of carbon black.

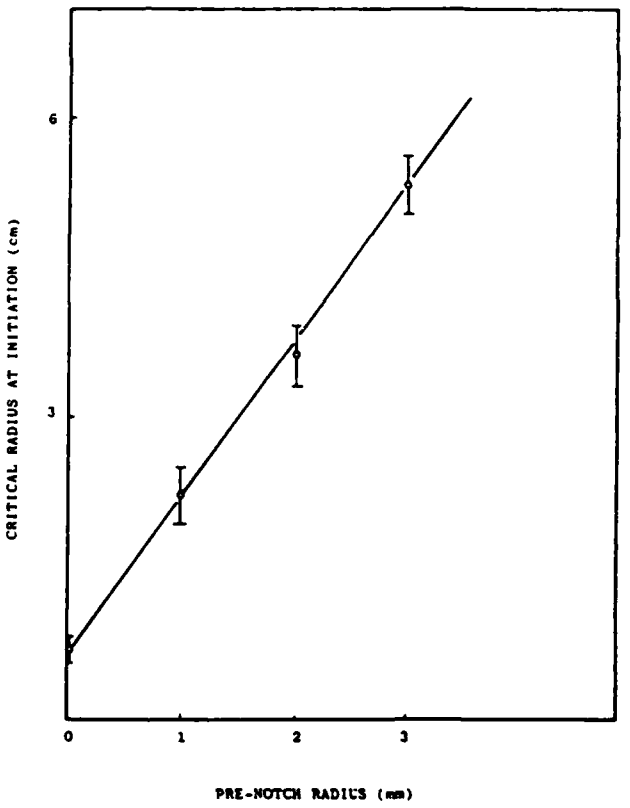

FIG. 8.—Critical radius at crack initiation as a function of prenotch radius.

tip radius and found to be independent of l, w and a (Figure 5). These data were used in Equation (4) to calculate J_s and are shown in Figure 6. The two curves are related by a factor of two; additional verification of this will be given below in the discussion of the critical J value for initiation.

The critical values of J_o and J_s were determined by following the above procedures and noting the critical radius at crack initiation. J_s is shown in Figure 7 as a function of the prenotch radius; the value for a sharp crack ($R_\rho = 0$) is also shown.

The critical conditions for initiation as a function of loading and specimen geometry were determined for precracked and prenotched specimens. Figure 8 shows that the relationship of the critical radius at initiation was linearly related to the prenotch crack tip radius. The critical radius was independent of the other specimen dimensions such as length, width, and precrack length. Therefore, for prenotched specimens the critical J-integral could be calculated based on Equation (3) (J_o), as well as with Equation (4) (J_s). Table I shows the values of the critical

parameters determined by both methods and that J_i is one-half J_θ, and therefore Equation (4) is a basic method to calculate the J-integral for initiation for sharp cracks or blunt notches as given by Equation (3).

Four levels of carbon black were studied to determine its effect on the critical conditions for crack initiation. Figure 9 shows the net section stress as a function of crack tip opening for precracked specimens. As discussed above, the area under these curves up to the point of initiation is one-half the critical J_i-value. The J_i-value was determined as a function of carbon black for prenotched and precracked specimens, and the combined data as a function of carbon black concentration are shown in Figure 10. The critical radius for crack initiation depended on the prenotch radius, but not on the carbon black content.

The J integral is an averaged measure of the stress–strain field in the crack tip region, while the critical radius is a local measure of the strain; therefore, their ratio is an averaged measure of the stress in the crack tip region required to initiate crack growth. Figure 11 shows that this average stress in the crack tip region increases linearly with carbon black content.

DISCUSSION

The calculation of the critical J value for initiation from the local strain field at the tip of a blunt notch is theoretically correct as proposed originally by

TABLE I

REPRESENTATIVE VALUES OF J_θ AND J_i FOR CRACK INITIATION IN NR FOR DIFFERENT SPECIMEN GEOMETRIES AND CARBON-BLACK CONTENTS[a]

CB, pph	R_ρ, mm	l, mm	a, mm	w, mm	J_θ, kN/m	J_i, kN/m	J_θ/J_i
40	2	100	17	35	287	126	2.28
40	2	100	12	25	301	137	2.20
40	2	100	9	25	316	143	2.21
40	2	50	9	25	283	124	2.28
40	1	100	9	25	176	85	2.07
25	2	100	12	25	204	103	1.98
25	2	100	9	25	189	100	1.89
25	2	50	9	25	208	104	2.00
25	3	100	9	25	284	131	2.17
10	2	100	12	25	165	75	2.2
10	2	100	9	25	159	83	1.92
10	2	50	9	25	163	78	2.09
10	3	100	9	25	200	110	1.82
0	2	100	9	25	106	57	1.86
0	2	100	6	25	121	61	1.98
0	2	50	6	25	115	59	1.95
0	1	100	6	25	101	50	2.02

[a] CB, carbon black content; R_ρ, precrack radius; l, specimen length; a, crack size; w, specimen width.

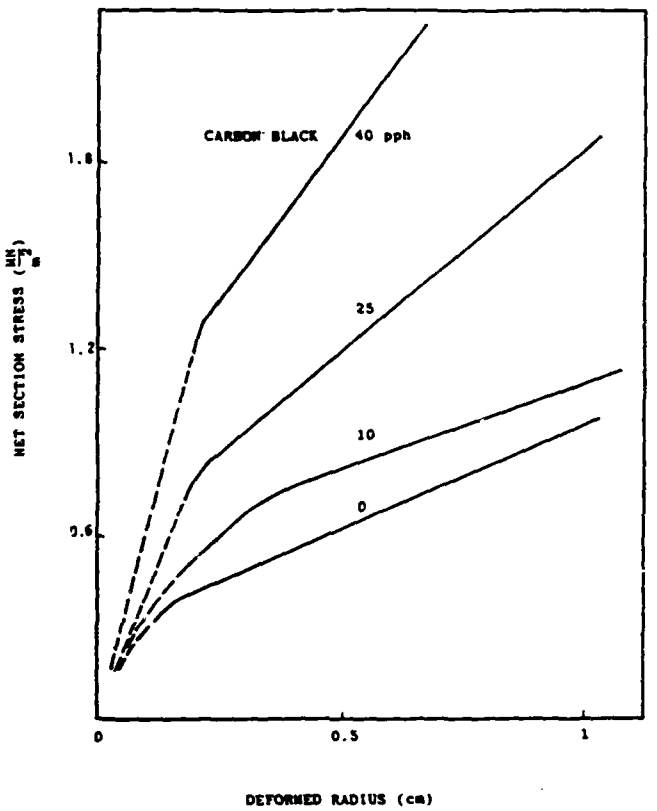

FIG. 9.—Net section stress as a function of deformed notch radius for 4 contents of carbon black.

Thomas[5] and shown to follow directly from Rice's definition of the *J*-integral. A small error may exist in the calculated values because the strain energy density was determined from uniaxial extension data, but a biaxial state of stress exists in the notch tip region. However, this is considered to be small since the extension ratios are large and predominately uniaxial.

The geometry independence, except for the prenotch tip dependence, justifies the *J*-integral as a valid fracture-characterizing parameter. This method of calculating *J* is experimentally involved, as is the multiple specimen method[4]. Therefore, the approach of measuring the J_δ, which requires only one specimen and the measurement of the crack tip opening as a function of stress is a simple, efficient method to characterize the conditions for crack initiation. In addition, this procedure is valid for sharp precracks. The correlation with the true J_δ-value from J–δ curves (Figure 6) and from the critical conditions (Table I) is found to be about a factor of 2. This simple procedure, therefore, is valid; it can characterize

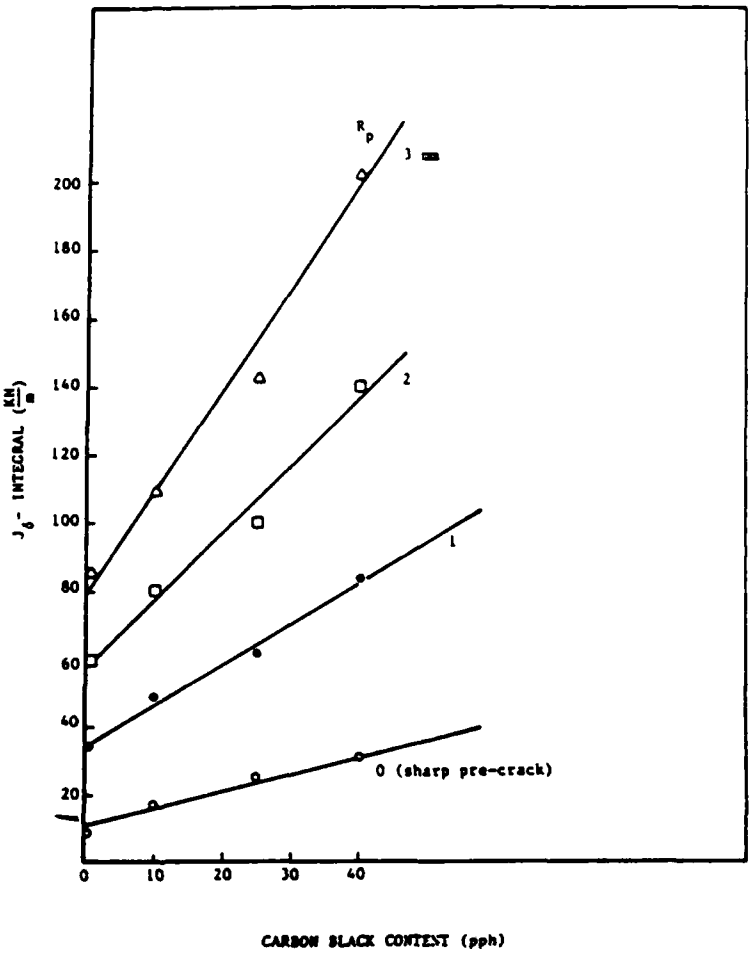

FIG. 10.—J_i at crack initiation as a function of carbon black content for specimens with different prenotch radii.

the critical fracture properties of a highly dissipative rubber with a sharp crack, and it requires only one specimen.

The observation that the critical radius at initiation was independent of carbon black content suggests that the critical strain is not dependent on the carbon black content but that the required stress increases linearly with carbon content. This can be seen in Figure 12, where the ratio of J_i to critical radius is independent of the prenotch diameter and increases linearly with carbon content. This ratio represents a general state of stress in the crack tip region. It is well known that carbon black increases the stress–extension curve, but these data, to

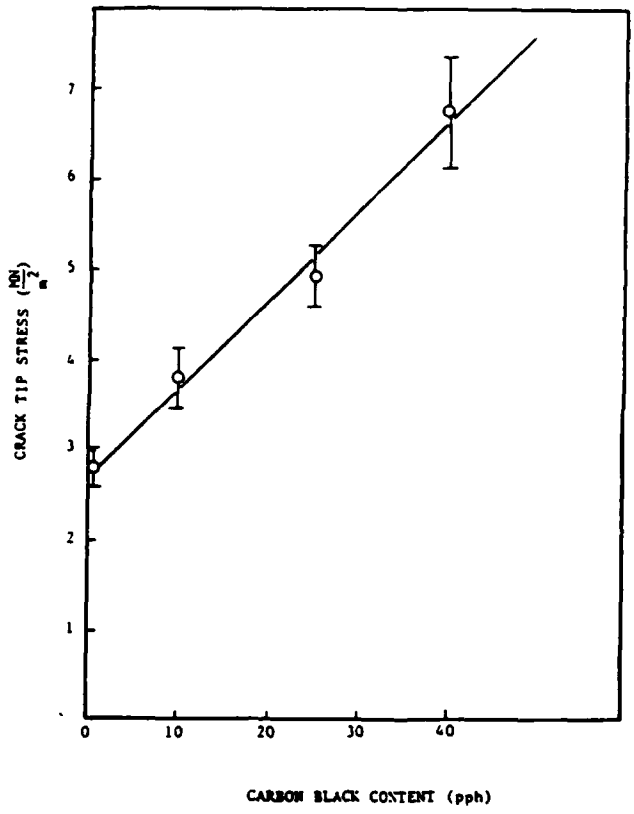

FIG. 11.—Average stress in crack tip region at initiation for 4 different contents of carbon black.

the best of our knowledge, are the first to show the effect of carbon black on the state of stress and strain in the crack tip region at the critical condition for crack initiation.

CONCLUSIONS

1. Evaluation of $\int \sigma d\delta$ where σ is the net section stress and δ is the deformed crack tip diameter requires only one specimen to characterize the initiation of crack growth in unfilled and carbon-black-filled NR.
2. $\int \sigma d\delta$ is equal to one half of the J-integral for crack growth initiation, which is identical to the Thomas tearing energy for a blunt notch.
3. The critical J-integral for crack initiation increases linearly with carbon black content.
4. The critical crack tip radius for crack initiation is independent of carbon black content, and the required crack tip region stress increases linearly with carbon black content.

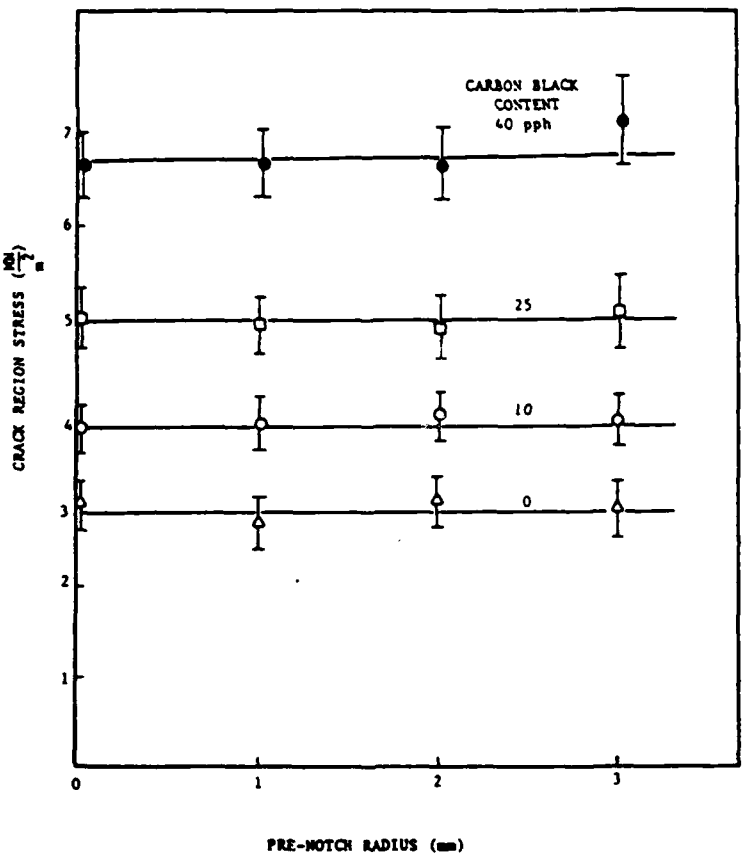

FIG. 12.—Crack tip region stress at initiation as a function of prenotch radius for 4 different contents of carbon black.

ACKNOWLEDGMENTS

The financial support of this work by the U.S. Army Research Office - Durham and the Cabot Foundation is gratefully acknowledged and appreciated. We would also like to thank Dr. S. Parhizgar and The BFGoodrich Co. for supplying the materials.

REFERENCES

[1] R. S. Rivlin and A. G. Thomas, *J. Polym. Sci.* 10, 291 (1953).
[2] H. W. Greensmith and A. G. Thomas, *J. Polym. Sci.* 18, 198 (1955).
[3] J. R. Rice, *J. Appl. Mech.* 35, 379 (1968).
[4] D. J. Lee and J. A. Donovan, *Theor. Appl. Fract. Mechanics* 4, 137 (1985).
[5] A. G. Thomas, *J. Polym. Sci.* 18, 177 (1955).

FRACTOGRAPHIC SURVEY OF POLYMERIC MATERIALS

J. A. Donovan
N. P. Francisco
N. R. Goldberg
R. F. Lee
H. Liu
P. R. Stupak

Mechanical Engineering
University of Massachusetts
Amherst, MA 01003

INTRODUCTION

POLYMERS, materials made up of long covalently bonded molecules, are replacing at an increasing rate conventional materials such as metals, wood and inorganic glass in engineering applications. Therefore, concern and understanding of polymer fracture, its mechanisms and modes are increasing. Consequently many tests have been developed to measure the fracture resistance of polymeric materials which recently are more and more based on fracture mechanics concepts. Fractography of polymeric materials has already aided the design of more fracture resistant materials. Yet, it is not as well developed as fractography of metals and its use in failure analysis of polymeric materials is not firmly grounded.

But, before discussing the fractography of polymeric materials the classification and microstructure of polymeric materials will be outlined. As already mentioned the basic characteristic of polymers is that they are made of long molecules that are covalently bonded, therefore the bonds within the molecule are strong and directional, but the bonds between the molecules can be of two types: 1) weak van der Waals bonds including hydrogen bonds or 2) strong chemical bonds if the polymer is cross-linked. It is the type of inter-molecular bonding which distinguishes the two principal classes of polymers: thermoplastics and thermosets.

Thermoplastic polymers, as their name implies, when heated becomes formable (plastic) because the thermal energy decreases the secondary bonding and the molecules easily slide past each other. But, when cooled they become rigid. This process can be repeated many times with limited degradation (due primarily to oxidation). Common thermoplastic polymers are: polyethylene (PE), polypropylene (PP), polystyrene (PS), polyvinyl chloride (PVC), polymethyl methacrylate (PMMA), polycarbonate (PC), and nylon. Nylon is the most common polymer with significant hydrogen bonding between the molecules.

Thermosets are long chain polymers chemically bonded into a network by strong primary chemical bonds called crosslinks. These crosslinks are formed by chemical reaction as when the two components of the epoxy react during curing or the sulfur joins the rubber molecules during vulcanization. The mechanical properties are strongly dependent on the extent of crosslinking. Heat will soften the thermoset polymer, but it will not

become "plastic" as the thermoplastics. Sufficient heat severely degrades thermosets by disrupting the primary bonds.

Each of these classes of polymers can be sub-divided. The thermosets can be divided into two classes based on the extent of crosslinking. The most common example of a lightly crosslinked polymer is an elastomer, with its characteristic long elongation and rapid recovery when the stress is removed. Examples of heavily crosslinked materials are the rigid epoxies, phenolics and Bakelite (the product of the reaction of urea with formaldehyde). It is common to refer to these two groups as rubbers or elastomers and thermosets respectively even though their basic structure is similar.

The thermoplastic polymers are made up of two sub-classes of materials based on their structure (or lack of structure): amorphous or glassy polymers (PS, PC, PMMA) and semicrystalline polymers (PE, PP, nylon).

Glassy polymers form because the molecular architecture is too irregular to allow the formation of crystals or because the kinetics of crystallization are sufficiently slow so that crystallization is suppressed; however if given sufficient time they may crystallize. Therefore, even polymers which under normal processing are semi-crystalline can frequently be produced in the amorphous condition, for example polyethylene terephthalate (PET) and nylon; and normally glassy polymers can crystallize, for example PC.

After a few brief words about specimen preparation and radiation damage during examination in the scanning electron microscope (SEM). The fracture surface as revealed by SEM will be surveyed for the four classes of polymers: glassy, semi-crystalline, thermosets and elastomers.

The objective is to survey fractography of polymers in the sense of selecting the main characteristics of the materials rather than a critical review of the field. Therefore, it is superficial, but we hope informative and an introduction to a rapidly changing area of investigation.

SPECIMEN PREPARATION

Specimen preparation of polymeric samples for scanning electron microscopy (SEM) is basically the same for metallic samples. But, to prevent local charging because their electrical conductivity is low the samples must be coated with a conductor usually gold, gold/pallidium alloy or carbon by evaporation or sputtering.

Another reason for coating is to prevent oxidation or other aging reactions from occurring since the fracture surface may be very active due to the scission of the molecules. This is especially true with rubbers for which it is recommended that the specimens be coated within twenty four hours of fracture.

Another concern when examining polymeric samples in the SEM is the possibility of radiation damage which may lead to artifacts. Polymeric materials react to the electron radiation in specific ways and must be taken into account during any study.

For a thorough discussion of the physics as well as the practical aspects of SEM of polymeric materials see the recent excellent review of White and Thomas (1).

SEM OF GLASSY POLYMERS

In unoriented glassy polymers the molecules are arranged in random loose coils that are entangled; therefore, if the glassy polymer is formed in the absence of stress fields the mechanical properties are isotropic. Fractography of only isotropic glass polymers will be discussed.

The deformation behavior of glassy polymers is determined by their

molecular architecture, molecular weight, temperature and strain rate among other things. Two types of inhomogeneous deformation of glassy polymers can occur where the local strain is much greater than the average strain: sheer banding and crazing. Shear bands form at 45° to the principal stress (Figure 1), are easily visible and within the shear band the molecules become highly oriented. There is no volume change due to the formation of the shear band. Shear bands are important for understanding the fracture properties of glassy polymers because they dissipate energy and can toughen the material.

However, since we are focussing on fractography the crazing process dominates the appearance of the fracture surface. In Figure 1 the formation of a craze is clearly visible bisecting the shear bands at 90° to the applied stress. Figure 2, a transmission micrograph of a craze, shows that the craze has crack like features except that the craze surfaces are connected by load carrying fibrils with 40-60% void space. Crazes have been successfully modelled as Dugdale zones (4). Fracture in glassy polymers seems to always be preceeded by the formation of a craze or craze bundle which then fails and becomes a crack.

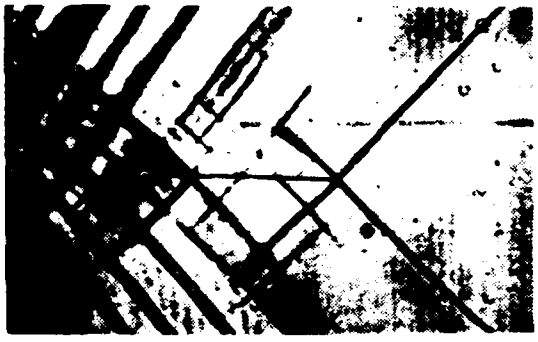

Figure 1. Craze (horizontal line in center) and shear bands formed by bending a notched PC specimen. Ishihama and Narisawa (2).

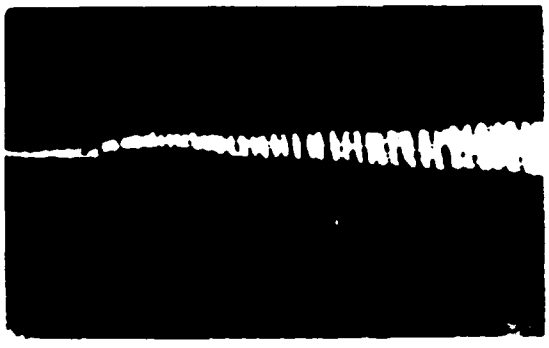

Figure 2. Transmission election micrograph of fibril structure in a craze. Behan, Berris and Hull (3).

Figure 3 is the fracture surface of a rod of PMMA showing a central region where fracture initiated, probably from a defect such as a pre-existing void or inclusion (dust particle), then a region of "mackerel" bands and finally the outer region which is frequently rougher.

IX-5

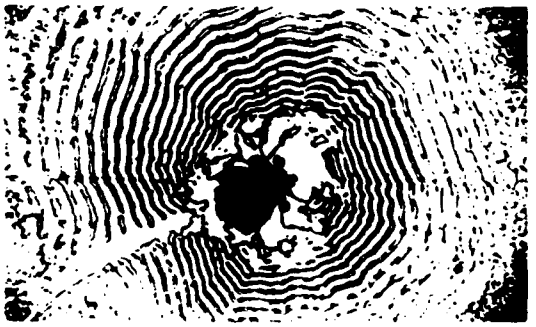

Figure 3. The "mackerel" pattern due to fracture of a craze in PMMA. Doyle (5).

The mirrored zone is relatively smooth and thought to form by the slow failure of the fibrils along the mid plane of the craze. As the crack grows the fracture pattern becomes distinctly different and has been studied by Doyle (5,6,8) and Hull and co-workers (3,7) most extensively. Figure 4 is a higher magnification SEM photo of the transition from the mirror zone into the "mackerel" zone which illustrates the striped and banded nature of this zone. Murray and Hull (9) in matching photos (Figure 5) from the two halves of the fracture showed that the striped area on one surface corresponded to the banded region on the other surface. At still higher magnification, Figure 6, the detail of the stripe described as "mist" and the band as "hackle" from the failure of the craze fibrils is apparent.

The development of the mist and hackle is shown schematically in Figure 7 showing that the crack jumps from one craze surface to the other and that fracture occurs near the fibril bulk interface.

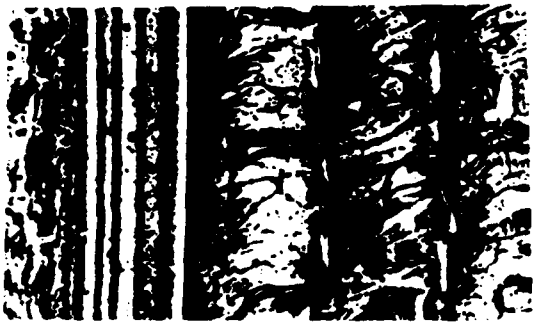

Figure 4. Higher magnification view of the transition region from the mirror zone (left) to mackerel bands. Doyle, Maranci, Orowan and Stork (6).

Figure 5. Opposite fracture surfaces showing that "misc" on one surface corresponds to the "hackle" on the other. Murray and Hull (7).

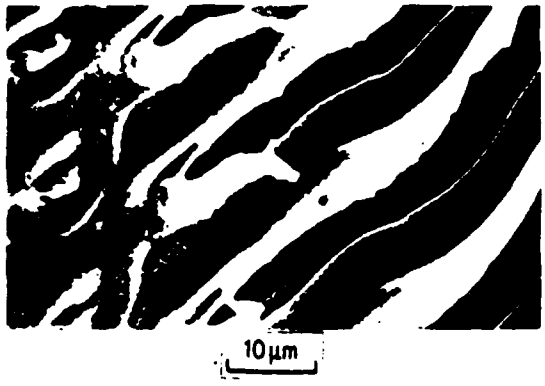

Figure 6. Mackerel pattern showing fibril roots (mist) on left and strips of fractured fibrils (right). Doyle (5).

The fracture near the bulk/fibril interface appears to have two possibilities, that is the fibril can fail and results in the fracture surfaces described as mist or hackel which is representative of the "roots" of the failed fibrils. But, there is some evidence that the fracture can occur below the craze boundary with no evidence of fibrils or fibril roots as shown in Figure 8, dark area. Also, apparent in this figure is the hackle region thought to be fibril roots Region A and a bundle of fibrils that create the "mist".

Another unique characteristic of fracture of polymers most apparent in glassy polymers is the development of diamond cavities, most extensively studied by Howard and co-workers (9). Figure 9 shows the development of a single diamond cavity develops from the failure of a particular craze with the blunt edges perpendicular to the applied stress. Diamond cavities of similar structure have been observed in many glassy polymers and their growth is controlled by the shear deformation in the adjacent bulk polymer. The reorientation of the crazes in the vicinity of the diamond cavity due to the plastic deformation near the cavity is apparent in Figure 9.

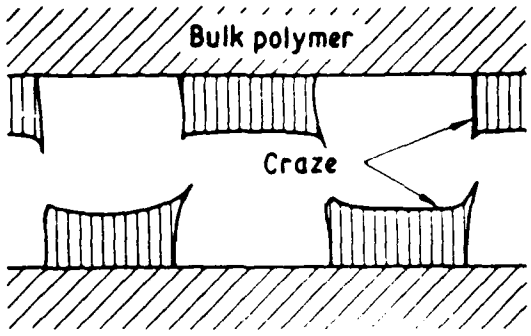

Figure 7. Schematic of the formation of the mackerel pattern by the crack alternating between craze surfaces. Doyle (5).

Figure 8. Bundle of fractured fibrils, with roots of fibrils to the left and a cleavage like fracture surface to the right. Doyle (8).

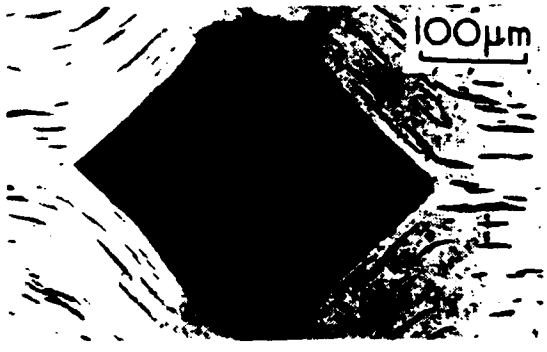

Figure 9. Diamond cavity in field of deformed crazes. Carnes and Howard (9).

Crazes also influence the fatigue crack growth rate in glassy polymers because the tip of a fatigue crack is also a craze, and therefore the fatigue and failure characteristics of the craze affect the mode of fatigue growth. The effect of crazing on the fatigue fracture surface appearance is critical for proper interpretation.

The fracture surface of a fatigued sample shows discontinuous growth bands (DGB) which look like the classic fatigue striations (Figure 10). However, the extensive work by Hertzberg and Manson and co-works (10) have shown conclusively that it requires up to thousands of fatigue cycles to form one DGB at low ΔK values. The number of cycles for one DGB decreases exponentially with increasing ΔK. They have shown that during DGB formation a craze forms at the crack tip which when it (the craze) grows up to a limiting size the crack propagates to the tip of the craze by a void coalescence mechanism. Figure 11 shows the fine structure on one DGB indicating that as the crack propagated through the craze the fracture path alternated between craze surfaces. Hertzberg, et al. point out that for failure analyses a misinterpretation of DGB's as fatigue striations could lead to an underestimation of the propagation stage of fatigue crack growth by three orders of magnitude.

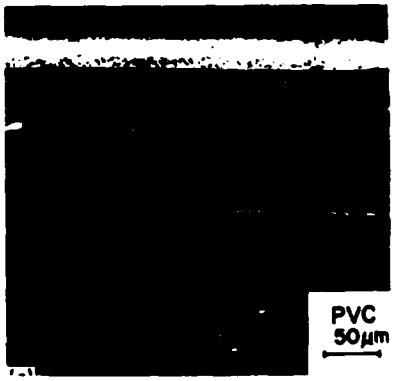

Figure 10. Fractograph of discontinuous growth bands. Skibo, Hertzberg, Manson and Kim (10).

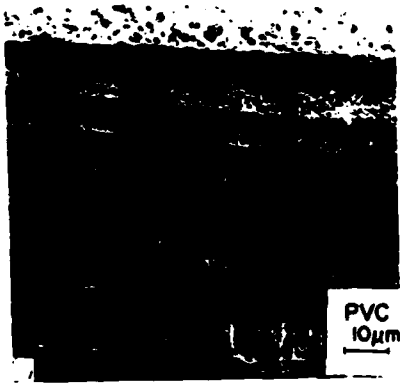

Figure 11. Fine structure on a DGB indicating that fracture path alternated between the craze surfaces. Skibo, Hertzberg, Manson and Kim (10).

A further complication to understanding fatigue crack propagation are the observations of Takemori of an intersecting "ξ" plastic zone that develops in PC in smooth bar fatigue tests (11). The ξ plastic zone consists of central arm that is a craze similar to the previous discussion, but at 45° to the craze emanating from the crack tip shear bands develop giving the appearance of the Greek letter ξ. ξ plastic zones have not been observed to grow from notched samples, but only in fatigue cracks that develop from surface crazes. The development of the shear bands tends to stabilize the craze thus craze breakdown requires more cycles before forming a discontinuous growth band. The development of the shear bands is thought to be due to the effect of state of stress on whether shear bands (plane stress) or crazes (plane strain) develop. Thus life predictions based on fatigue data generated from notched samples may not be relevant for fatigue cracks initiating from smooth surfaces.

SEMICRYSTALLINE POLYMERS

Crystals in semicrystalline polymers are folded chain crystals, in which the long molecules fold back upon themselves to form thin (100A) platelets called lamellae. An individual molecule may be in several crystals as well as in the amorphous material that separates the lamellae. The properties of the crystals are very anisotropic; in the chain direction they are very strong (chemical bonds), but in the transverse direction (van der Waals bonds) they are very weak. Therefore, the crystal orientation, easily affected by processing, is a major factor in the strength properties of semicrystalline polymers. For example, the modulus of PE may easily vary from 10 to 200 GPa depending on how the material was processed.

The crystalline lamellae are separated by the amorphous intercrystalline phase which contains chain ends, loops, other less crystallizable material (lower molecular weight chains), and tie molecules. Tie molecules are incorporated into more than one crystal and are extremely important for the mechanical properties. Figure 12 shows intercrystalline links between crystals of PE which are more than one molecule, but illustrate the concept of tie molecules graphically. True tie molecules would wander through the amorphous phase rather than be direct links between the crystals.

Figure 12. Intercrystalline links, analogous to tie molecules, between PE crystals. Keith, Padden and Vadimsky (12).

The organization of the crystal lamellae depends on the processing conditions. If the crystals from under quiescent conditions the lamellae grow radially from a nuclei, similar to the growth of a metal grain, to form a spherulite. However, unlike a metal grain the spherulite consists of many crystals and amorphous material. Figure 13 is an example of the crystalline portion of a spherulite. These spherulites will grow until they fill space and form a solid which can be characterized by its

Figure 13. Crystalline lamellar in a spherulite of PP. Keith and Padden (13).

spherulite size, an example is shown in Figure 14; the diameter of the spherulites can range from 0.1 to 1000 μm. The complex spherulitic structure is "clearly" shown in a replica of a fracture surface in Figure 15.

Figure 14. Impinging spherulites; in concentric rings are due to the twist that occurs in the lamellar as they grow (14).

Figure 15. Replica of a fracture surface showing the complex structure of a spherulite. Norton and Keller (15).

If the crystallization conditions are not quiescent then the microstructure and properties will be significantly different. Also, the kind and distribution of defects will be affected by the processing history. Thus just as in metals the processing history determines properties, but even more so. An excellent review of the relation of properties to structure of semicrystalline polymers has recently been published by Schultz (16).

Two of the most important structural parameters that determine the mechanical behavior and specifically fracture properties are the molecular weight and the percent crystallinity of the polymer. The higher the molecular weight the easier the crystallization, the greater the number of tie molecules, and the greater the number of entanglements or knots in the amorphous phase. All of these decrease the ability of the polymer to deform viscously and tend to increase the brittleness of the polymer. Freidrich and Fakirov (17) have recently presented a fracture map representing the effect of molecular weight and degree of crystallinity on failure mode; three types of behavior are found: ductile, semi-ductile (crazing) and brittle. For example, the plane strain fracture toughness of commercial PE decreases from 6 to 1 $mN/m^{3/2}$ when the crystallinity increases from 60 to 77 percent (16). Therefore, as you might expect the molecular weight affects the fracture appearance. Figure 16 shows that the fracture surface of nylon 66 during fatigue changes from a patchy appearance to highly drawn when the molecular weight doubles, which also increases the modulus and decreases the fatigue crack growth rate.

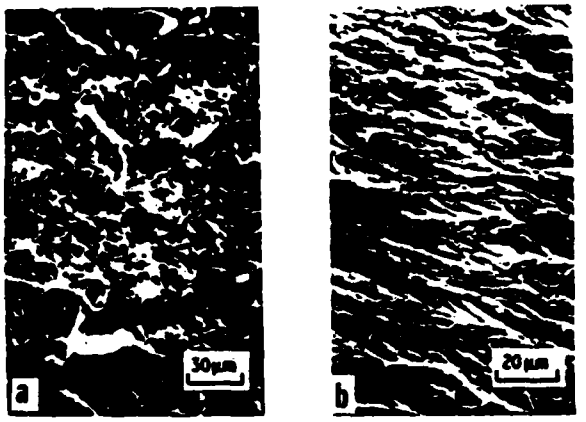

Figure 16. Fatigue fracture surface showing the effect of doubling the molecular weight in nylon 66: a) MW: 17,000 and b) MW: 34,000. Bretz, Hertzberg and Manson (18).

Since polymers at their service temperatures are usually viscoelastic, strong strain rate effects are expected and found in most polymer systems. Figure 17 shows how the strain rate affects the fracture path through spherulitic PP; at low deformation rates the fracture path follows the spherulitic boundaries, but at higher strain rates the path becomes increasingly trans-spherulitic.

The effect also manifests itself if the material is susceptible to tearing instability where ductile fracture initiates the fracture, but as the crack grows the elastic contraction exceeds the plastic opening and drives the crack faster. The effect of tearing instability on the fracture surface is quite dramatic as shown in Figure 18, with evidence of diamond cavities in the ductile region.

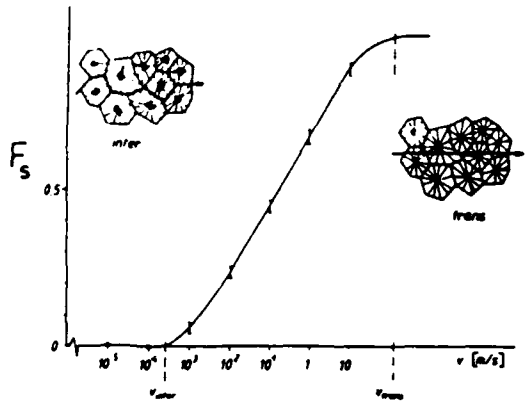

Figure 17. The effect of deformation rate on the fraction of trans-spherulitic fracture. Schultz (16).

Figure 18. Fractograph of a PP specimen that failed by tearing instability; ductile failure on left and brittle on right. Prabhat and Donovan (19).

Finally, the effect of environment can be very pronounced on many polymers. Ubiquitous water has dramatic effects on fracture properties as shown in Figure 19. The rather brittle fracture in air shows much greater evidence of plasticity when tested in water, the water has plasticized the material. Many of the common polymers owe their good fracture properties to their hydroscopic nature, for example nylon.

THERMOSETTING POLYMERS

Fracture of thermosetting polymers strongly depends on the test temperature and loading rate: at low temperatures/high rates crack growth is brittle, at intermediate temperatures and rates fracture is discontinuous (stick/slip) and at the highest temperature and lowest loading rates fracture is ductile. Also, the environment, amount of hardner (crosslink density), curing temperature and time, and aging all affect the fracture toughness. Examples of the effect of these variables on the fracture surface will be discussed for unfilled epoxies because of their widespread use. Significant work has been done on filled epoxy systems because many

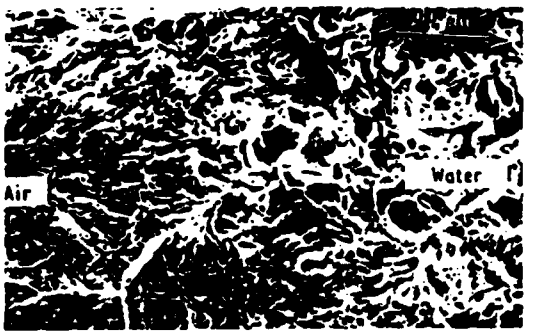

Figure 19. The effect of water on the fracture surface of PBT. Takemori and Morelli (20).

of these systems are of great engineering interest as adhesives and composites, but they will not be discussed here.

Crack growth in epoxies is discontinuous in specimens (tapered double cantilever beam or double torsion) for which the stress intensity is independent of crack size. The phenomenon is not well understood, but the effect of the various variables have been studied most extensively by Young and co-workers (21,23). Figure 20 is a typical load-time curve during crack growth in a double torsion specimen. Initial crack growth requires a larger load than to propagate the crack; the crack grows for a while with falling load until it arrests. Figure 21 shows the fracture surface in which the crack arrest lines are clearly visible and the surface between the arrest lines is nearly featureless. The detail of the arrest lines varies with experimental conditions, but Figure 22 is representative. The arrest lines are out of the continuous crack plane, suggestive of high local plastic deformation and crack tip blunting. The fine lines parallel to the growth direction are also usually found, but unexplained.

The experimental conditions that lead to continuous crack growth produce nearly featureless fracture surfaces like the regions between the crack arrest lines.

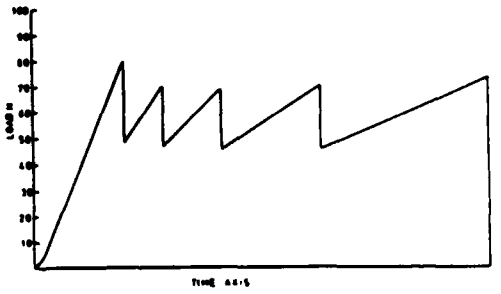

Figure 20. A typical load-time curve for an epoxy during stick-slip crack propagation.

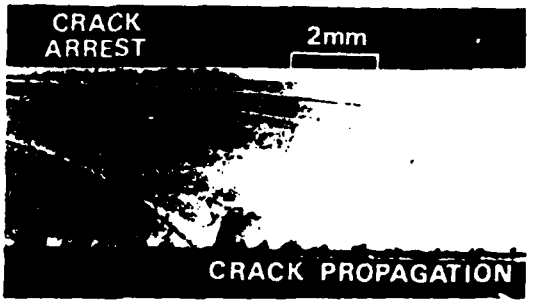

Figure 21. Fracture surface of double torsion epoxy specimen showing the arrest bands. Young and Beaumont (23).

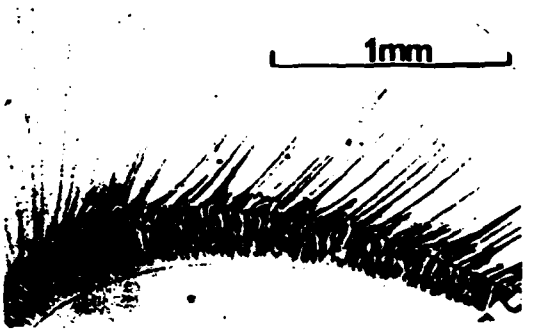

Figure 22. Fine structure of a crack arrest band in epoxy. Phillips, Scott and Jones (23).

Increasing the loading rate decreases the difference between the load for initiation and at arrest, which are proportional to the critical strain energy release rate for both conditions; the strain energy release at arrest is independent of the deformation rate of the test.

A recent study (24) of the temperature dependence of fracture in an epoxy resin found that not only was discontinuous crack growth found at high temperatures, but reappeared at very low temperatures. The fracture surface had the same general appearance as stick/slip fracture at high temperatures, but the arrest regions were somewhat different.

Other variables, such as percent cure, curing temperature, amount of hardner affect the details of stick/slip fracture. For example, aging after curing decreases the height of the arrest lines. All of the data suggests that the stick/slip phenomenon is related to the ability of the crack tip to blunt which is related to the ability of the epoxy to deform viscously; the low temperature stick/slip phenomenon may be an exception to this generalization.

ELASTOMERS

Rubber as an engineering material has long played a distinctive role which continues to increase, with the design demands also increasing. New thermoplastic elastomers based on better understanding of the relationship of properties to structure are being developed continuously. However, this survey of the fractography of elastomers will be restricted to the classical rubbers, which is beginning to be studied to increase our understanding of the fracture properties. Fracture in rubber, not unlike other materials, is a complex process with stress induced microstructural changes occurring in the crack tip region and various fillers, primarily carbon black (CB) being added for reinforcement, and various other ingredients which may or may not alter the fracture properties and surfaces.

There is a general consensus, as in other materials, the rougher the fracture surface the greater the toughness. Failure initiated in the central region of Figure 23, with the roughest region due to slow crack growth from a defect possibly an inclusion or simply an inhomogenity as shown in Figure 24. Inhomogenities can exist due to poor mixing during compounding. The region removed from the rough zone are characteristic of rapid growth with tear lines. Figure 25 shows a more developed and complex pattern of interconnected tear lines. Understanding the origin of the fracture characteristics is just developing and Gent and Pulford (27) have recently suggested that many of the fracture features are related to the linking of secondary cracks in the crack tip region.

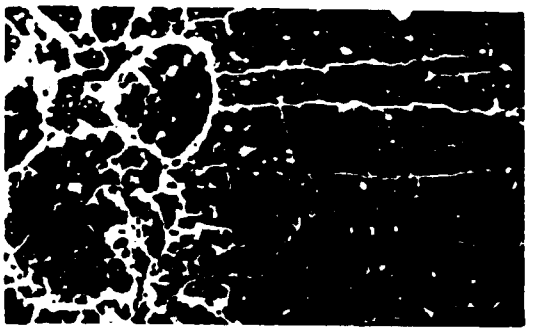

Figure 23. Fracture surface of an unfilled natural rubber tensile specimen with initiation site on left. Mathew and De (25). X50

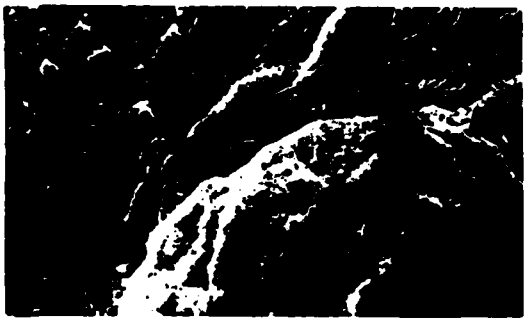

Figure 24. Gel particle that could serve as a crack initiator in rubber. Eldred (26).

Figure 25. Fracture surface of a pre-cracked unfilled rubber specimen showing many tear ridges. Mathew and De (25). X50

As in any other material fatigue is a major source of failure in rubber. However, fatigue striations are not usually observed, but surface roughness decreases as the fatigue crack growth increases.

Reinforcement of rubber has been a major goal of rubber science and technology for many years; two ways to affect the failure properties is to change the crosslink density via the vulcanization process and to add carbon black. Recently De and co-workers (25,28,29) have been studying the effects of processing variables on ultimate properties and the effect of these variables on the fracture surface. Figure 26 accentuates the change in fracture topography that occurs by comparing a relatively highly crosslinked but unfilled rubber, with a lower crosslink density, but reinforced with carbon black.

The toughness of the rubber seems to be correlated with the nature of the tear ridges; Figure 27 at higher magnification shows that some of the tear lines are relatively linear while in a material with higher toughness the tear lines are more complex with many branches, this latter type of fracture has been described as knotty tearing.

One of the common ingredients of most commercial rubbers is an anti-oxidant, to delay environmental degradation of the rubber. The effect of anti-oxidant on the fracture surface after aging the same amount of time is shown in Figure 28; the rubber containing the antioxidant shows more complex tear lines or more knotty tearing and retains its resistance to fracture longer. It is thought that the anti-oxidant reacts with the fracture produced free radials and decreases subsequent degradation.

Finally, although carbon black is a remarkable reinforcing agent there has been a search for other reinforcing fillers; to optimize the properties or to provide the possibility of tough rubber products other than black ones. Silica treated with a bonding agent works, but untreated silica separates from the rubber creating voids that degrade the fracture resistance. However, the economics of bonding agents is prohibitive for all but exceptional cases.

ABRASION OF RUBBER

Abrasion of rubber, a form of polymer fracture, perhaps the least understood, affects the service life of many engineered products. The primary, and obvious example is the abrasion of tires. Many advances in tire wear resistance have occurred through design (radial tires) and through reinforcement. Carbon black reinforcement generally leads to an order of magnitude improvement by adding a cheaper ingredient (CB) to the more expensive rubber matrix.

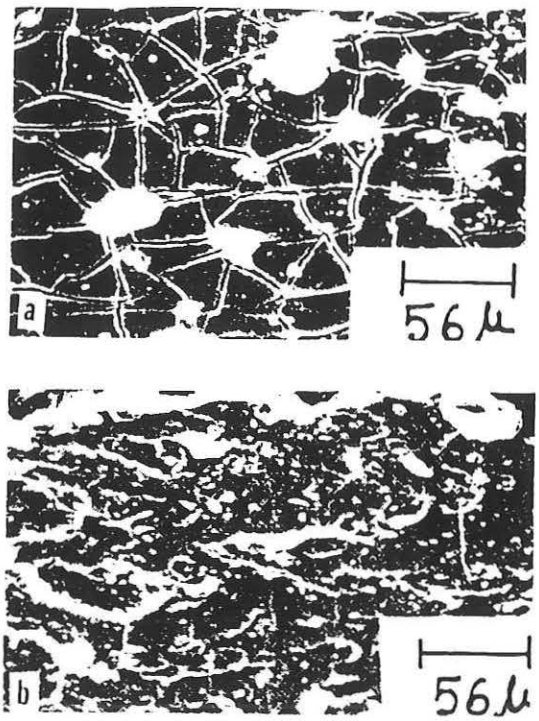

Figure 26. a) Fracture surface of an unfilled but highly cross-linked rubber sample; b) Same rubber but CB filled and low cross-link density. Pal and De (28).

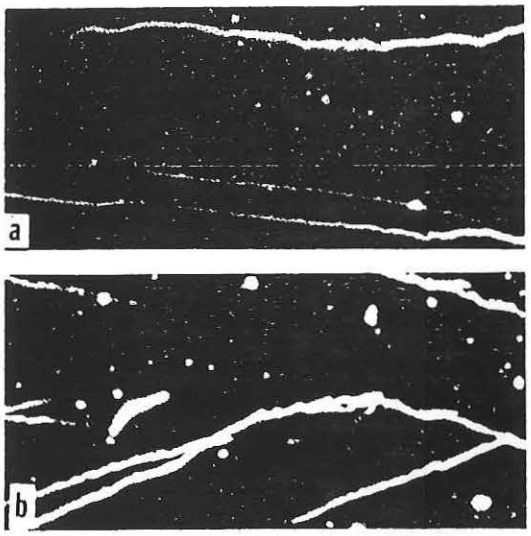

Figure 27. a) Linear tear ridges associated with low tear resistance and b) knotty tearing with branched ridges and higher tear resistance. Chakraboty, Bhowmick and De (29). X45

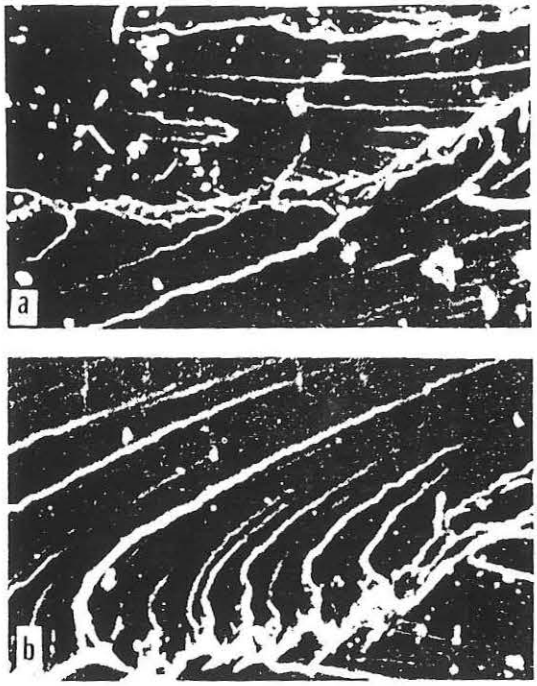

Figure 28. The effect of anti-oxidant a) natural rubber recipe without anti-oxidant and b) with anti-oxidant both after the same aging treatment. Mathew and De (25). X50

Tire abrasion has been studied with SEM, but it is not a mature field. Because of its great technological interest there have been efforts to develop a laboratory abrader that would duplicate abrasion during service, it probably will be no surprise that these efforts have not been successful. The goal of a laboratory abrasion test would be to rank different tire compounds, but the different tests do not always rank the test compounds the same nor in the same order as field tests. Nevertheless, useful insight has been gained from abrasion tests and from the study of the abraded surface, which will now be briefly surveyed.

First Figure 29 shows a typical abrasion pattern that frequently develops on an abraded rubber sample. The origin of the abrasion pattern was first studied by Schallamach (31) to understand its relation to wear rate, but the complex processes involved are not well understood.

Figure 30 shows the development of "macroridges" from a laboratory wear test, similar ridges are observed on tires. The origin of these ridges may best be understood with the schematic shown in Figure 31 for abrasion with a laboratory devide called a knife abrader - the knife is usually a razor blade. As the blade passes the ridge the abrasion is concentrated on the base folding the ridge over the trailing material which is protected. As would be predicted the wear pattern on the leading edge, top of ridge and trailing edge are significantly different as shown in Figure 32. The base takes the brunt of the wear. Southern and Thomas (32) have analyzed this process in terms of the fracture mechanics and fatigue crack growth from the base of the ridge. However, this is probably not the only process since the ridge tip is finally weakened and fractured forming a wear particle. Thus, it is probable that the complex wear process consists of both crack growth and tensile fracture. The fracture mechanics model correlates fatigue crack growth data and wear data for unfilled, non-crystallizing rubbers, but not for other rubbers.

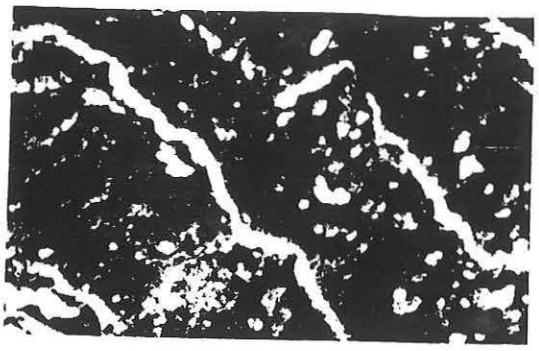

Figure 29. Typical abrasion pattern that develops on rubber. Zhang (30).

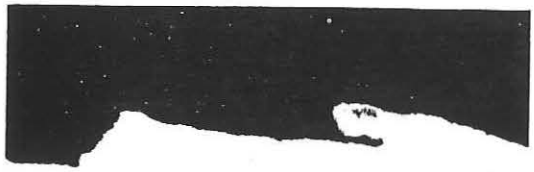

Figure 30. A cross-section showing the development of the abrasion pattern that develops in tire and laboratory tests. Southern and Thomas (32).

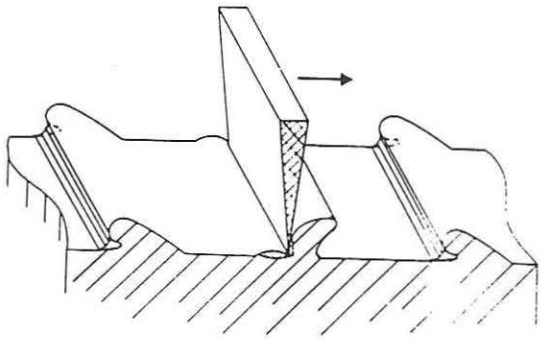

Figure 31. Schematic of abrasion pattern development during a knife abrasion test. Zhang (30).

The effect of CB filler on the abrasion pattern is particularly interesting, since the filler leads to significant wear resistance. Figure 33 compares the abrasion surface of filled and unfilled natural rubber which appear very different; the filled rubber develops the abrasion pattern which is clearly visible; but, the surface of the unfilled rubber is covered with debris. The debris forms from the detachment of small rubber particles that aggregate and adhere to the rubber surface.

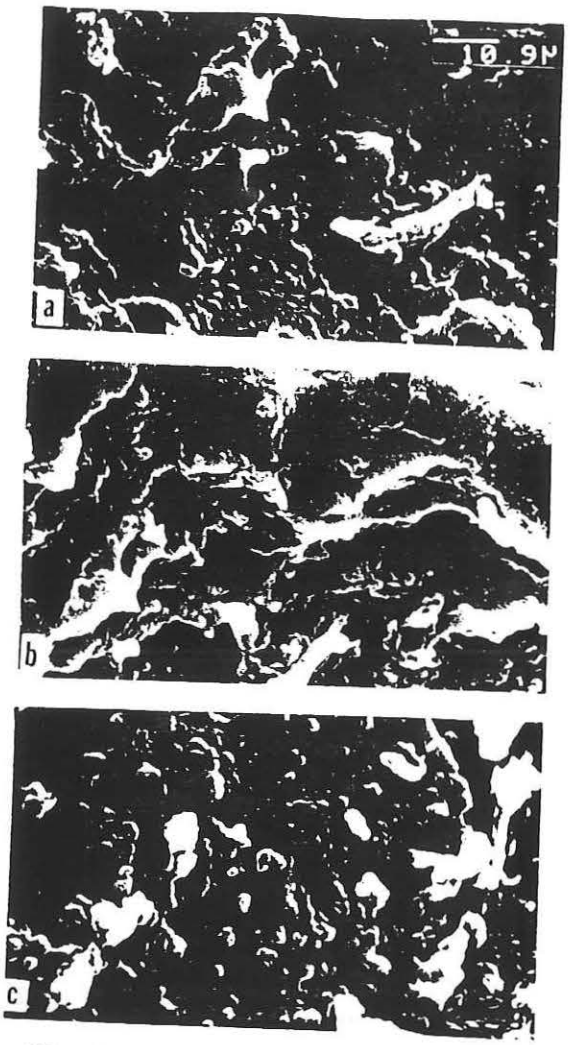

Figure 32. Fracture surfaces of abrasion ridge a) base, b) top and c) protected surface. Stupak and Stupak (33).

Since the discovery of synthetic rubber much has been done to blend the different rubbers for optimum properties. Butyl rubber (BR) has very good abrasion resistance and is frequently blended with natural rubber for tire tread. A study of the effect of composition on mechanical properties as well as abrasion resistance showed that a 50/50 blend of NR/BR had better fatigue crack growth resistance than a 75/25 blend, but about the same tensile strength. Figure 34 shows the resulting wear surface of the 50/50 blend to be much finer than the 75/25 blend; the abrasion resistance of the 50/50 blend was superior. Supporting the fatigue crack growth theory of Southern and Thomas.

However, another major variables that affects abrasion resistance is the temperature of the rubber. Many of the most important properties of tires are related to the mechanical hysteresis characteristics of the rubber. The energy dissipated each time the tire is deformed increases the tire's temperature. SBR heats up more quickly and to a higher temperature

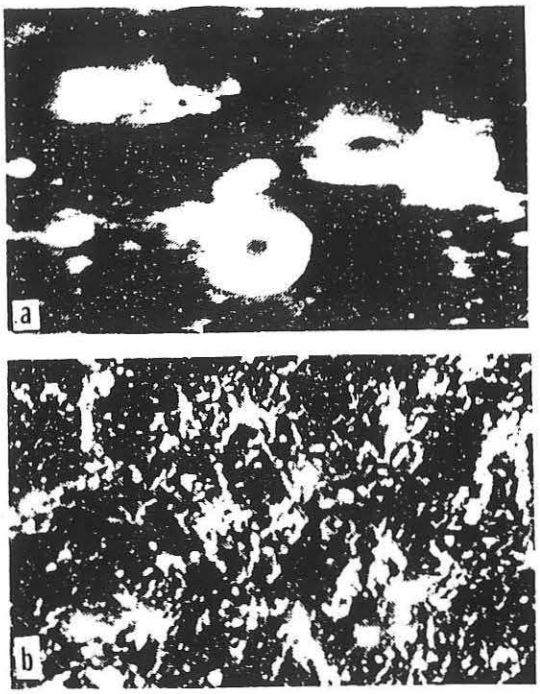

Figure 33. Abrasion surface of a) unfilled natural rubber and b) filled natural rubber. Bhowmick (34). X350

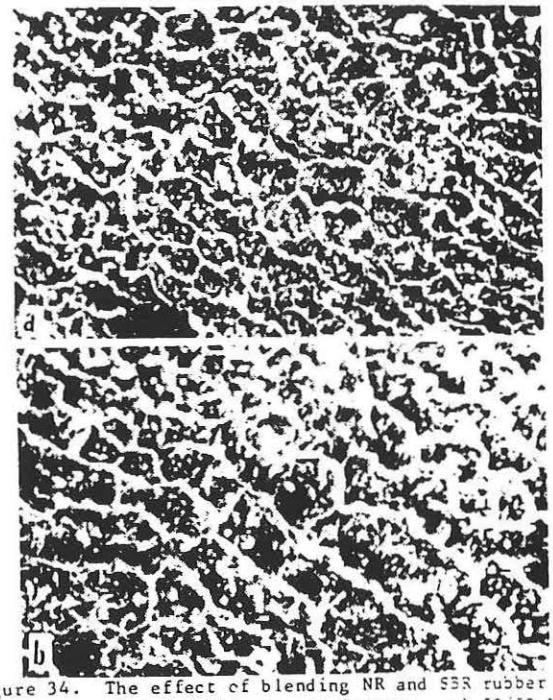

Figure 34. The effect of blending NR and SBR rubber to optimize abrasion resistance. a) 50/50 NR/BR and b) 75/25 NR/BR. Both rubbers were filled with CB. Mathew and De (35). X20

than BR. Since the fracture properties are related to the viscoelastic properties the SBR rubber shows a deeper wear pattern and greater wear rate than the BR rubber tested under similar conditions.

However, the increase in fatigue crack growth rate is much greater than the increase in wear rate. Which suggests that the fatigue crack growth model for wear is not the complete story.

The effect of load on wear, which would increase the frictional forces and the fatigue crack growth rate leads to greater abrasion and the establishment of different abrasion patterns on the samples as shown in Figure 35.

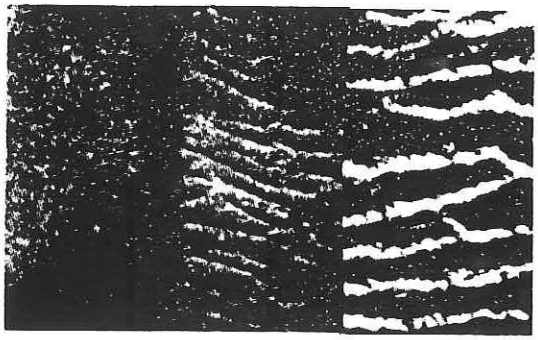

Figure 35. The effect of load on the abrasion pattern developed on filled SBR. Southern and Thomas (32).

SUMMARY

Fractography of glassy, semi-crystalline thermoset and rubbery polymers were surveyed. The unique features of each class, such as crazing in glassy polymers, stick/slip fracture and abrasion of rubber as a form of fracture were discussed. Evidence for the effects of molecular weight, percent crystallinity and environment on fracture of specific polymers was presented. Such fractographic evidence has been very helpful in understanding the fracture characteristics of polymers; and as the use of fractography of polymers increases, and techniques develop even greater understanding will be achieved.

REFERENCES

1. White, J. R. and E. L. Thomas, Rubb. Chem. and Tech. 57, 457 (1984).

2. Ishihawa, M. and I. Narisawa, J. Mat. Sci. 18, 1947 (1983).

3. Beahan, P., M. Berris and D. Hull, Phil. Mag. 24, 1267 (1971).

4. Kramer, E. J. in Development in Polymer Fracture, ed. E. H. Andrews, App. Sci. Pub. London 55 (1979).

5. Doyle, M. J., J. Mat. Sci. 17, 204 (1982).

6. Doyle, M. J., A. Maranci, E. Orowan and S. T. Stork, Proc. R. Soc. Lond. A. 329, 137 (1972).

7. Murry, J. and D. Hull, J. Poly. Sci. 8, 583 (1970).

8. Doyle, M. J., J. Mat. Sci. 17, 760 (1982).

9. Cornes, P. L. and R. N. Howard, Polymer 15, 149 (1974).

10. Skibo, M. D., R. W. Hertzberg, J. A. Manson and S. L. Kline, J. Mat. Sci. 12, 531 (1977).

11. Takemori, M. T., Poly. Eng and Sci. 22, 937 (1982).

12. Keith, H. D., F. J. Padden and R. G. Vadimsky, J. App. Phy. 42, 4585 (1971).

13. Keith, H. D. and F. J. Padden, J. App. Phys., 35, 1286 (1964).

14. Keller, A. J., Poly Sci. 39, 151 (1959).

15. Norton, D. R. and A. Keller, J. Mat. Sci. 19, 447 (1984).

16. Schultz, J. M., Poly. Sci. and Eng. 24, 770 (1984).

17. Freidrich, K. and Fakirov, J. Mat. Sci. 20, 2807 (1985).

18. Bretz, R. W., R. W. Hertzberg and J. A. Manson, J. Mat. Sci. 16, 2070 (1981).

19. Prabhat, K. and J. A. Donovan, Polymer 26, 1963 (1985).

20. Morelli, T. A. and M. T. Takemori, J. Mat. Sci. 19, 385 (1984).

21. Yamini, S. and R. J. Young, J. Mat. Sci. 14, 1609 (1979).

22. Phillips, D. C., J. M. Scott and M. Jones, J. Mat. Sci. 13, 311 (1978).

23. Young, R. J. and P. W. R. Beaumont, J. Mat. Sci. Lett. 11, 776 (1976).

24. Scott, J. M., G. M. Wells and D. C. Phillips, J. Mat. Sci. 15, 1436 (1980).

25. Mathew, N. M. and S. D. De, Polymer 24, 1042 (1983).

26. Eldred, R. J., J. Poly. Sci. Poly. Lett. 10, 391 (1972).

27. Gent, A. and C. T. R. Pulford, J. Mat. Sci. 19, 3612 (1984).

28. Pal, P. K. and S. K. De, J. Appl. Poly. Sci. 28, 659 (1983).

29. Chakraborty, S. K., A. K. Bhowmick, and S. K. De, Rubb. Chem. and Tech. 53, 321 (1980).

30. Zhang, S. W., Rubb. Chem. and Tech. 57, 755 (1984).

31. Schallamach, A., Trans. Inst. Rubb. Ind. 28, 256 (1952).

32. Southern, F. and A. G. Thomas, Rubb. Chem. and Tech. 52, 1008 (1979).

33. Stupak, R. E. and P. R. Stupak, Unpublished, University of Massachusetts, Amherst.

34. Bhowmick, A. K., Rubb. Chem. and Tech. 55, 1055 (1982).

35. Mathew, N. M. and S. K. De, J. Mat. Sci. 18, 515 (1983).

APPLICATIONS OF THE J-INTEGRAL TO FRACTURE OF NON-ELASTIC RUBBER

J.A. DONOVAN, D.J. LEE, AND R.F. LEE
Department of Mechanical Engneering, University of Massachusetts, Amherst, MA 01003.

INTRODUCTION

It is difficult to determine valid fracture characterizing parameters for non-linear, non-elastic materials like carbon black filled, natural rubber. The classic tearing energy approach developed by Rivlin and Thomas (1) must be modified for the energy dissipated by hysteresis (2). The J-integral approach introduced by Rice (3) and initially applied by Begley and Landes (4) to metals and by William (5) to polymers has been shown to yield valid parameters that characterize crack initiation in these non-elastic materials. Oh (6) showed in rubber that the J integral gave the same results as the tearing energy method at deformations less than required to initiate crack growth. The objective of the current study was to develope test procedures based on the J integral concept, and determine the critical J for initiation of crack growth, and evaluate the critical parameters as material properties.

Carbon black filled, natural rubber was chosen because it is a highly dissipative material and a severe test of the validity of the J integral concept. The J integral was evaluated by 1) multiple specimen tests of Mode I (tension) and mixed mode (tension plus shear) and 2) single specimen tests of the effect of carbon black on crack initiation. The results show that the J integral provides a basis for valid and relatively simple evaluation of fracture resistance in highly dissipative elastomers.

J-INTEGRAL CONCEPT

The J-integral on any path Γ surrounding the crack tip is defined as

$$J = \int_{\Gamma} \left(W dy - T \frac{\partial u}{\partial x} \, ds \right) \qquad (1)$$

where W is the strain energy density, T is the traction vector, $\frac{\partial u}{\partial x}$ is the displacement gradient, and s is the arc length (3). It can be represented equally well by

$$J = -\frac{1}{B}\frac{\partial U}{\partial a} \qquad (2)$$

i.e., the negative change in potential energy U per unit thickness B for an incremental change in crack length a. That is, J is proportional to the area between the load-displacement curves of specimens with cracks of length a and a + da, respectively (Fig. 1). For conditions that satisfy linear elastic fracture mechanics $J = (1 - \nu^2)\, K^2/E = G$, where K is the stress intensity, E is the modulus, ν is Poisson's ratio and G is the strain energy release rate. The J-integral may be interpreted in two ways: (a) the intensity of the elastic-plastic deformation and stress field in the crack tip region or (b) the change in energy of the cracked body due to a small extension of the crack.

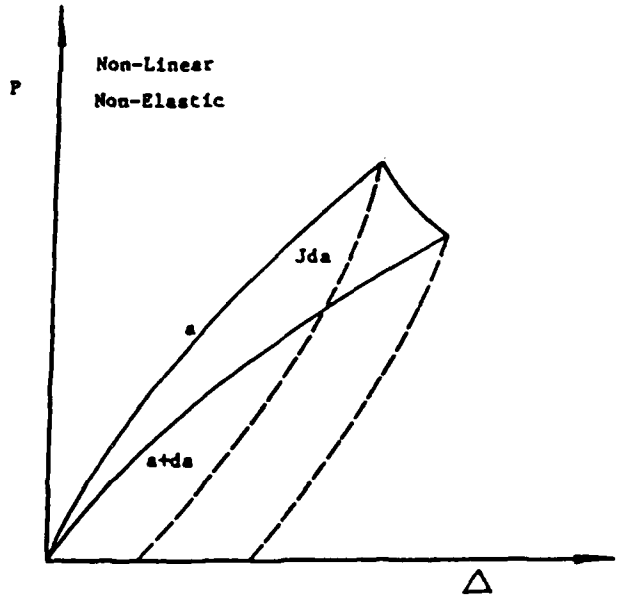

FIGURE 1. Load-displacement curves for specimens with cracks of size a and a+da. The dashed lines represent the un-loading curves.

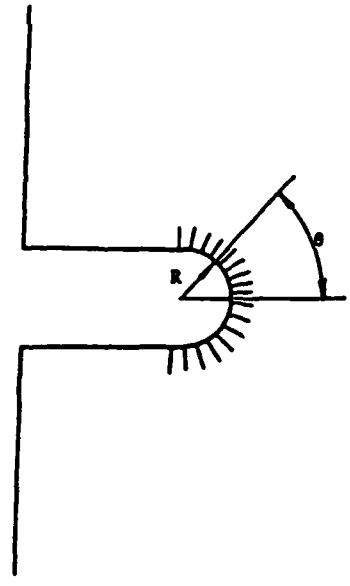

FIGURE 2. The geometry of a blunt notch with fiducial lines for local measurement of extension.

Begley and Landes (4) proposed that the value of J at crack initiation J_c be a fracture criterion and showed it to be a material property for specimens that exhibit large amounts of plasticity before fracture. Hence, J_c can be used to characterize fracture in ductile materials and is known as the ductile fracture toughness, analogous to G_c in linear elastic fracture mechanics. However, since sustained crack growth in ductile materials requires additional energy, the J-integral value for initiation is conservative.

Schapery (7) theoretically justified the use of the J-integral as a failure criterion in non-homogenous, viscoelastic media.

The line integral definition provides an analytical method for evaluating the J-integral and has been shown by Oh (6) to represent the state of stress and strain in elastomers. Rice (8) also showed that if the intergration path was taken along a blunt notch, rather than for a sharp crack,

$$J = \int W \, dy \tag{3}$$

and provided another method, particularly interesting for the study of elastomers. In fact Thomas (9) arrived at the equivalent expression of tearing energy

$$T = R \int W \, d \sin\theta \tag{4}$$

where R is the notch tip radius, W the local strain energy density and θ the angle from the center line of the notch, Figure 2, about 30 years ago.

EXPERIMENTAL PROCEDURE

A natural rubber recipe, compounded by B.F. Goodrich, with carbon black contents of 0, 10, 25 or 40 pph was used for all tests. The multiple specimen results for Mode I and mixed mode loading were done only with 40 pph carbon black, while the results based on the crack tip region were obtained with all four carbon black compositions.

Single edge notched specimens with sharp or blunt notches of different lengths, widths and pre-crack lengths were tested at 21°C and a displacement rate of 1 cm/min. The sharp cracks were made by cutting the rubber with a razor blade; the crack angle (β) varied between 0 and 65° (Fig. 3a). The blunt notches were made by drilling a hole with a sharp hollow circular cutter lubricated with water. Blunt notches with radii 1, 2 and 3 mm were made, then the sides of the notches were cut away with a sharp razor blade (Figure 3b).

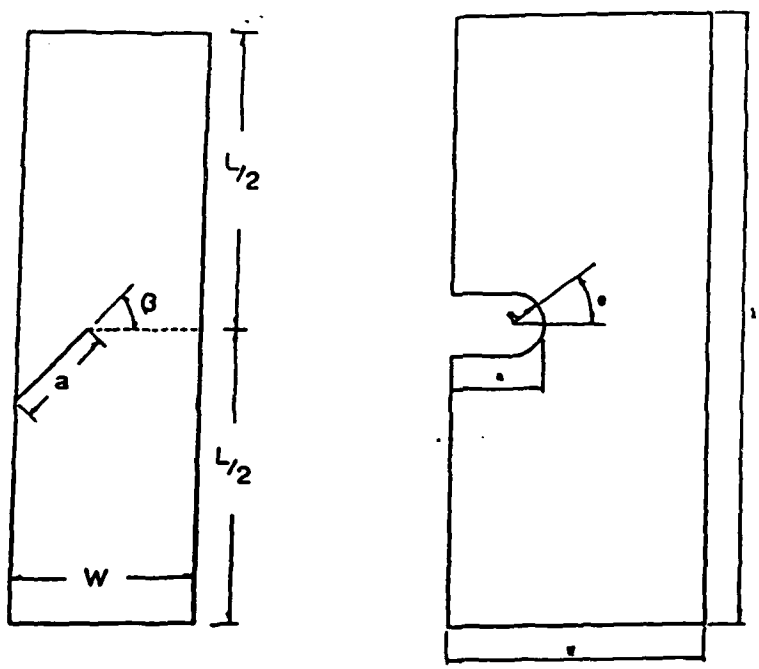

FIGURE 3. The specimen dimensions for a) pre-cracked and b) pre-notched specimen.

The region around the notch tip was coated with white powder so that a series of fine radial lines could be made in the notch tip region. The spacing between the lines was measured with the aid of a 10 x filar eyepiece. Based on these measurements the extension ratio as a function of position was determined and was the basis for calculating the critical J integral at initiation.

The above procedure is not applicable for sharp cracks, therefore J_δ, suggested by results for a Dugdale Zone (8), was defined as

$$J_\delta = \int \sigma d\delta \qquad (5)$$

where σ is the net section stress and δ the crack tip diameter. J_δ was determined and compared to J_θ.

Crack initiation was identified by coating the crack surface with the white powder, as loading increased the region in the crack tip developed a new surface delineated by the white powder was taken as crack initiation in the multiple specimen tests. Crack initiation as defined differenly for the single specimen tests as the first visible sign of peeling. Therefore, the results are consistently higher for the single specimen tests compared to the multiple specimen tests. Additional work is being done to refine identification of the initiation event.

Conventional tensile tests (smooth specimens) to determine stress-extension ratio curves and the stored energy as a function of extension ratio were also measured at 21°C and a displacement rate of 1 cm/min.

RESULTS

Mode I

Initial loading of the pre-cracked specimens (β=0) blunted the razor cut until a crack initiated. Since initiation was relatively easy to observe, the load and extension at initiation were easily determined. Almost immediately after the crack initiated renewed blunting of the crack occurred a the load increased. The initiation event was not apparent on the load-extension curve. Blunting, with little slow stable crack growth, continued with extension until unstable crack growth fractured the specimen.

The area under the load extension curve is the energy stored in the specimen. In the pre-cracked or pre-notched specimens the force-displacement field is non-uniform, therefore the energy density is non-uniform and greatest in the vicinity of the crack tip. The total energy, the area under the load-extension Δ curve, is shown in Figure 4 a a function of pre-crack length for various values of extension. The slope of these curves ($\frac{\partial U}{\partial a}$) gives J and it is shown in Figure 5 as a function of extension. $J(\lambda)$ and extension ratio at initiation are sufficient to determine J at initiation.

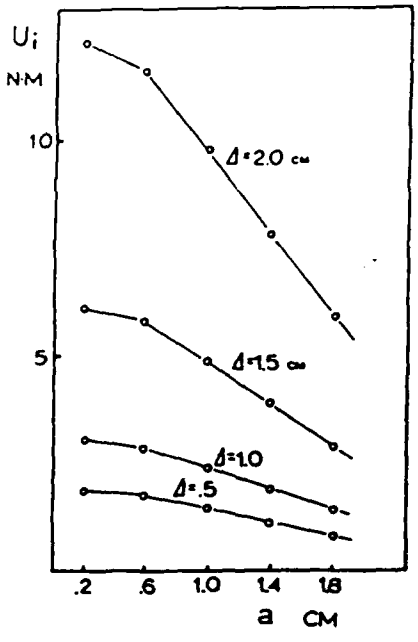

FIGURE 4. Stored energy as a function of pre-crack size at different extensions.

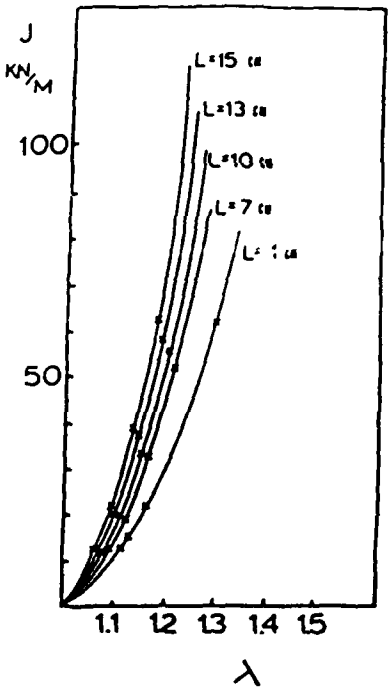

FIGURE 5. The J-integral as a function of extension ratio; the "X" marks the initiation for a specific pre-crack size.

The critical values of J at initiation were determined from Figure 5 for values of the extension at initiation and are shown in Figure 6 as a function of specimen length and pre-crack size. The critical J value is a function of the pre-crack size, but independent of specimen length. However, Figure 7 shows that the critical extension at initiation is a linear function of specimen length and the curves extrapolate to a common intercept, similar to results found by Agarwal et al (10) for composites. These data, therefore, allow the energy release rate to be partitioned between the crack tip region and away from the crack tip.

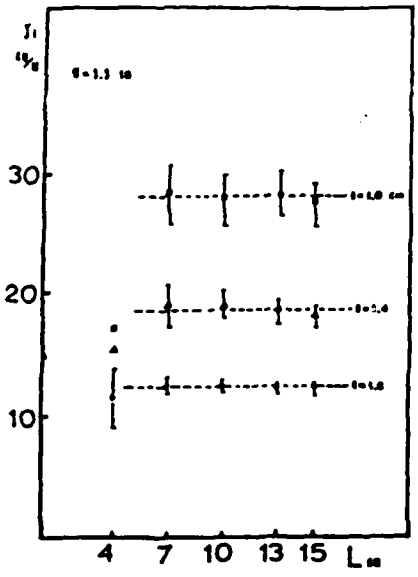

FIGURE 6. Critical J-integral as a function of specimen length and pre-crack size.

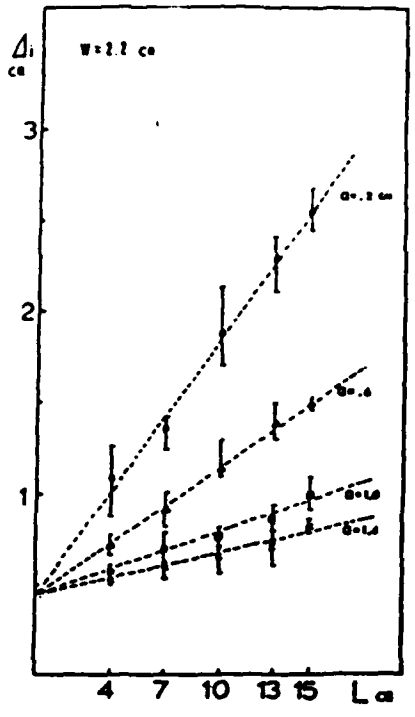

FIGURE 7. Critical extension as a function of specimen length and pre-crack size.

The J value obtained at the critical extension in the hypothetical zero length specimen Δ_o represents the critical energy release rate in the crack tip region to initiate a crack, which is independent of specimen length and crack size. This value was obtained by converting the extension for the hypothetical zero length specimen to the extension ratio for the actual length of the tested specimen $\lambda_o = (\Delta_o + \ell_o)/\ell_o$. With this λ_o the J value representing the critical strain energy release rate in the crack tip region was found from Figure 5 to be 10.8 kN/m for all specimen lengths tested.

The total energy stored in the pre-cracked specimens at initiation as a function of specimen length is shown in Figure 8. These data for a specific pre-crack size can be extrapolated as straight lines to zero specimen length and this energy also can be interpreted as the energy required in the crack tip region to initiate the crack.

Since J is defined as $-\frac{1}{B}\left(\frac{\partial U}{\partial a}\right)$ then the slope of U for ℓ = 0 as a function of pre-crack length would be equivalent to the critical J value for the crack tip region to initiate the crack. These data are shown in Figure 9 and the slope of the line is 12 kN/m virtually the same as obtained from the critical extension at ℓ = 0, and Figure 5.

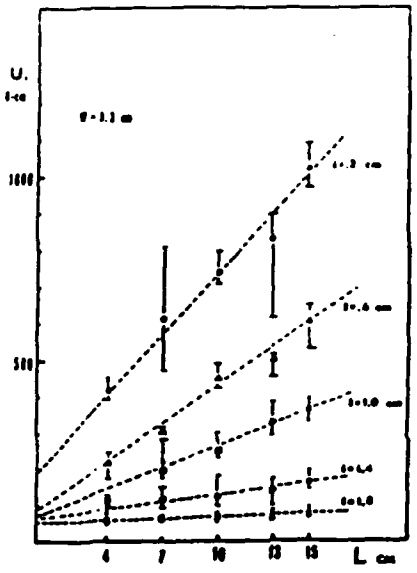

FIGURE 8. Stored energy at initiation as a function of specimen length and pre-crack size.

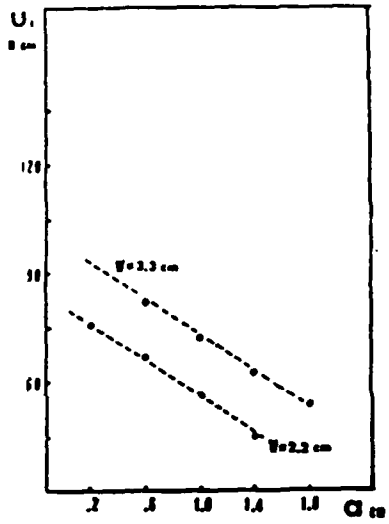

FIGURE 9. Total stored energy at initiation in a "zero" length specimen.

Mixed Mode

The results of the multiple specimen tests to determine the critical conditions for mixed mode loading conditions were analyzed in the same way as the results for Mode I studies. Attempts to measure the critical conditions for pure Mode II were unsuccessful because the specimen buckled due to the loading conditions. The results for the critical J value in the crack tip region as a function of β are shown in Figure 10.

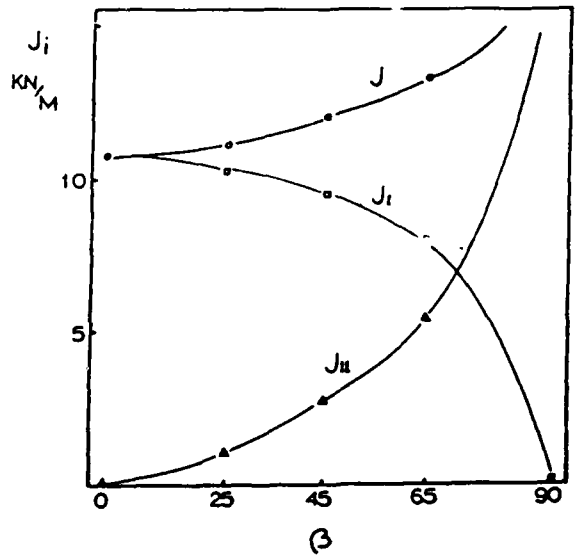

FIGURE 10. Critical J-integral for initiation as a function of crack angle. And, the contribution of J_I and J_{II}.

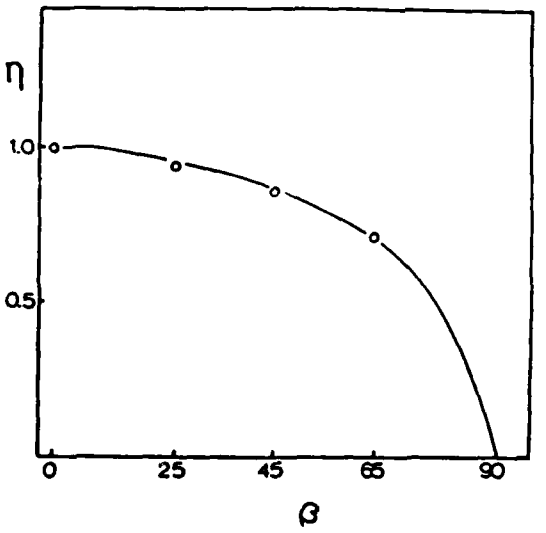

FIGURE 11. The ratio of crack opening displacement in mixed mode to pure Mode I at the critical extension for a "zero" length specimen.

Mode II loading does not cause any crack tip opening, therefore as a means for partitioning the contribution of Mode II to the fracture process the crack opening displacement δ was measured at the critical extension ratio for the zero length specimen as a function of β. The ratio η of crack opening displacement δ for any value of β to $\delta(\beta=0)$ is shown in Figure 11. Based on this experimental result and since it is known that J_I is proportional to δ (3) then

$$J_I = \eta J_{Ic}$$

Ishikawa et al (11) analytically proved that

$$J_{I,II} = J_I + J_{II}$$

then it follows that

$$J_{I,IIc} = \eta J_{Ic} + (\gamma) J_{IIc}$$

where γ is an unspecified proportionality factor. $J_{I,IIc}$ as a function of η is shown in Figure 12 and a linear extrapolation of the data gives the critical J_{II} as 19 kN/m and $\gamma = (1 - \eta)$.

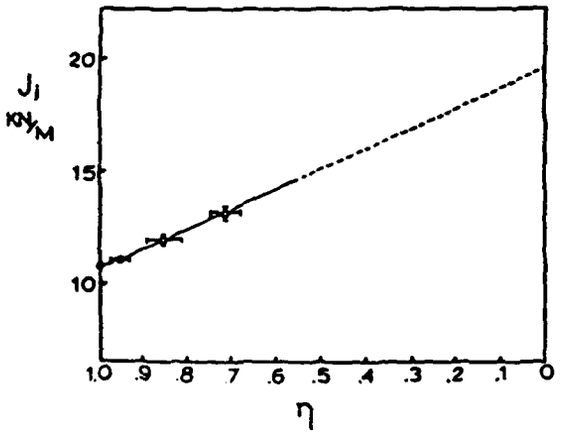

FIGURE 12. Critical mixed mode for J-integral as a function of crack opening displacement ratio.

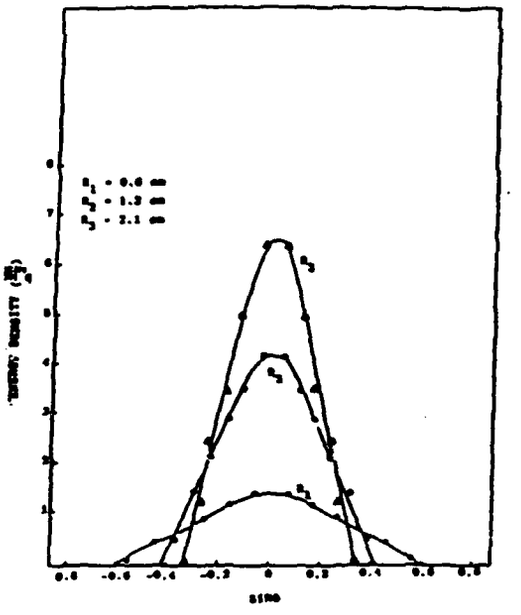

FIGURE 13. Energy density a a function of sinθ for a specimen with an initial radius of 2mm.

Crack Opening

The extension ratio as a function of position along the notch tip for different notch radii were measured, converted to energy density obtained from tensile tests, and are shown in Figure 12 as a function of sin θ for different imposed notch radii. These data were obtained in specimens of different length ℓ, width w, pre-notch radius R_p and pre-crack length a. The data were independent of these variables, except for R_p, within experimental error. The J-integral was then determined according to Equation 4 by intergrating the area under the W-sin θ curve and is shown in Figure 13 as a function of the notch tip radius and shows that it is independent w, ℓ, and a. The J value required for initiation of crack growth from a blunted pre-crack can be obtained by this procedure if the notch radius at initiation is known. Similar data were obtained as a function pre-notch tip radius, specimen geometry and carbon black content.

This procedure is tedious and cannot be applied to sharp cracks. Therefore, the net section stress was measured as a function of crack tip radius and found to be independent of ℓ, w and a (Figure 14). These data were used in Equation 5 to calculate J_δ and are shown in Figure 15. The J_θ was found to be equal to 2.04 times J_δ with a standard deviation of 0.14 for 35 different combinations of ℓ, w, a and carbon black content.

The critical value of J_θ and J_δ were determined by following the above procedures and noting the critical radius at crack initiation; Figure 16 shows J_δ as a function of the pre-notch radius and carbon black content. J_δ is a linear relation of pre-notch radius, including the data obtained for a sharp pre-crack, and also carbon black content increases the critical energy release rate necessary for crack initiation.

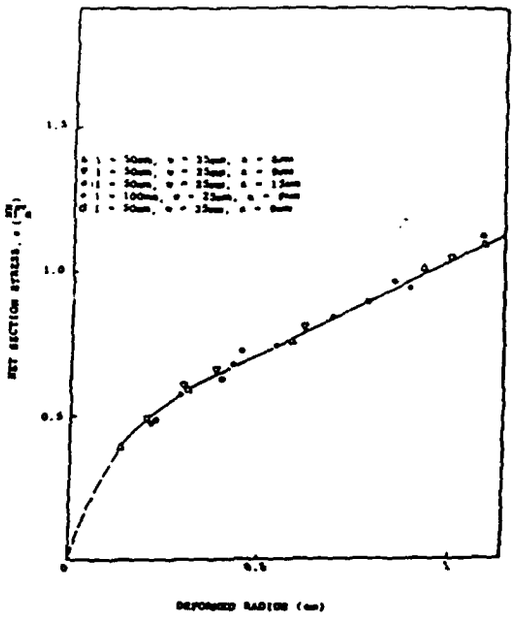

FIGURE 14. Net section stress as a function of crack tip radius in different geometry pre-cracked specimen.

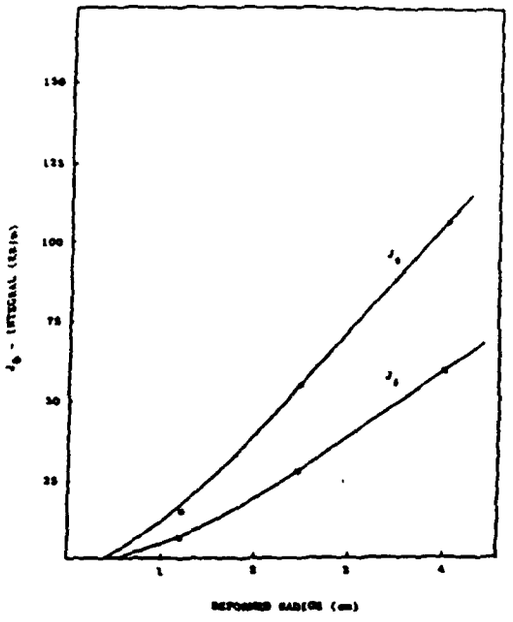

FIGURE 15. J_θ and J_δ as a function of notch radii.

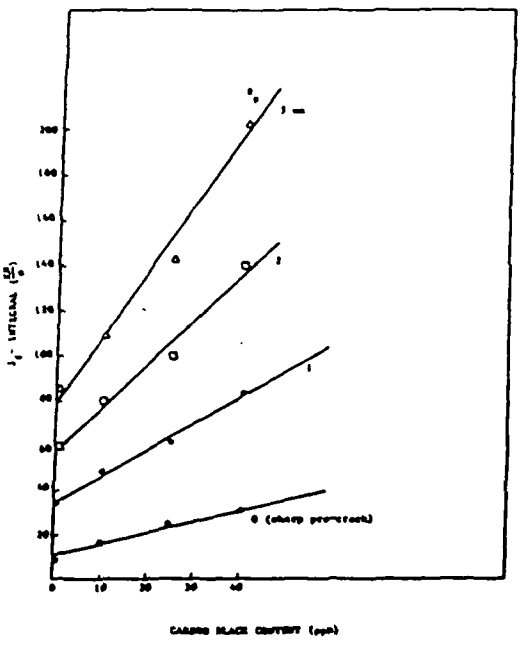

FIGURE 16. J_c at crack initiation as a function of carbon black content for specimen with different pre-notch radii.

DISCUSSION

It has been demonstrated that the J integral describes the critical conditions for crack initiation in carbon black filled, natural rubber, a non-linear, non-elastic material. However, the critical values determined by the multiple specimen method decrease with increasing pre-crack size. But, analysis of the critical extension as a function of crack size and specimen length shows that a unique value of the extension, independent of the crack size and specimen length is obtained for the hypothetical zero length specimen. Calculating the critical J with this value of extension gives a geometry independent material property that is a valid measure of the resistance of the rubber to crack initiation. This critical J is the critical strain energy release rate in the crack tip region for crack initiation. The J value determined by the usual multiple specimen procedure represents the total J required and is not independent of crack size.

The J integral approach also allows the determination of the critical conditions for crack initiation under mixed mode loading conditions. Mixed mode loading may be important for some practical situations, such as wear. By measuring the critical J value as a function of β it was possible to estimate the critical J value for pure Mode II loading as about 18 KN/m. The basis for this prediction involves two assumptions: 1) that the crack opening in mixed mode loading is due to the Mode I contribution alone and 2) that the relationship of $J_{I\,II,c}$ to η is linear over the entire range of η. The first assumption seems realistic, but the second is less certain. However, actual measurements of J_{IIc} don't appear to be possible because of buckling of the specimen, therefore this extrapolated value is believed to be the best approximation available.

The experimental procedures used to determine the critical J values by the multiple specimen procedure are involved and time consuming. However, by considering the net section stress and deflection in the crack tip region it is possible to determine the critical strain energy release rate in the crack tip region from a single specimen test. That is the material property that is a measure of the resistance of the material to crack initiation. It was shown that

$$J_\delta = \int_{\delta_o}^{\delta_i} \sigma \, d\delta$$

equals one half the true J_{IC} value that follows from measurements of the local strain energy density and crack tip diameter as suggested by Thomas (9) and Rice (8). This therefore makes it possible to measure the material property in a highly dissipative material simply by measuring the load and crack tip diameter.

Based on this simple single specimen procedure it was easy to show the linear dependence of the fracture properties on carbon black content. Therefore, this procedure provides an interesting and simple way to study the effect of carbon black on fracture properties.

CONCLUSIONS

It was shown that the critical J integral for crack initiation in carbon black filled, natural rubber is a valid material property (independent of specimen geometry) that describes the materials resistance to crack initiation. Either multiple or single specimen procedures could be used to study the effect of other variables, such as carbon black content, on fracture properties.

ACKNOWLEDGEMENTS

The financial support of the US Army Research Office-Durham and the Transportation System Center, US Department of Transportation of this work is gratefully acknowledged. One of us, R.F. Lee, also appreciates the award of a Cabot Foundation Fellowhip. We would like to thank the B.F. Goodrich Co. for supplying the material.

REFERENCES

1. R.S. Rivlin and A.G. Thomas, "Rupture of Rubber, I. Characteristic Energy for Tearing", J. of Polymer Science, 10, (1953) 291.
2. A. Ahagon, A.N. Gent, H.J. Kim and N. Kumagai, "Fracture Energy of Elastomers in Mode I and Mode III," Rubber Chem. Tech. 48 , (1975) 896,
3. J.R. Rice, "Mathematical Analysis in the Mechanics of Fracture," in Fracture - An Advanced Treatise, 2, Academic Press NY (1968) 191.
4. J.A. Begley and J.D. Landes, "The J-integral as a Fracture Criterion," in Fracture Toughness ASTM STP 514, Phil. (1972) 1.
5. J.M. Hodgkison and J.G. William, "J and G analysis of the Tearing of a Highly Ductile Polymer," J. Mat. Sci. 16 (1981) 50.
6. H.L. Oh, "A Simple Method for Measuring Tearing Energy of Nicked Rubber Strips," Mech. of Crack Growth, ASTM STP 590 (1976) 104.

7. R.A. Schapery, "On the Analysis of Crack Initiatin and Growth in Non-Homogenous Viscoelastic Media," Fracture Mechanics, Am. Math. Soc., SIAM-AMS Proceedings, 12 (1978) 137.
8. J.R. Rice, "A Path Independent Integral and the Approximate Analysis of Strain Concentration by Notches and Cracks," J of Appl. Mech. 35 (1968) 379.
9. A.G. Thomas, "Rupture of Rubber. II. The Srain Concentration at An Incision," J. of Polymer Science," 18 (1955) 177.
10. B.D. Agarwal, B.S. Patro, and P. Kumar, "J Integral as Fracture Criterion for Short Fiber Composites: An Experimental Approach, Eng. Frac. Mech, 19, (1984) 675.
11. H. Ishikawa, H. Kitegawa, and H. Okamura, "J Integral of a Mixed Mode Crack and its Application," ICM 3, 3, Cambridge, England, August (1979).

J-INTEGRAL AND CRACK OPENING DISPLACEMENT AS CRACK INITIATION CRITERIA IN NATURAL RUBBER IN PURE SHEAR AND TENSILE SPECIMENS*

R. F. LEE AND J. A. DONOVAN

DEPARTMENT OF MECHANICAL ENGINEERING, UNIVERSITY OF MASSACHUSETTS, AMHERST, MASSACHUSETTS 01003

INTRODUCTION

To characterize the fracture properties of nonlinear elastic rubber, Rivlin and Thomas[1] showed that the critical strain energy release rate required to advance the crack per unit area, the tearing energy, is

$$T = -\frac{1}{B}\left(\frac{\partial U}{\partial a}\right), \tag{1}$$

where B is the thickness of the specimen, U is the stored energy and a is the crack length. T accurately characterizes the fracture properties of nonlinear elastic rubber[2]. However, if the rubber is nonelastic, exhibiting hysteresis, like carbon-black-filled NR, this approach is suspect[3].

Alternatively, the J-integral satisfactorily characterizes fracture in nonlinear, nonelastic rubbers[4], as it has successfully characterized highly dissipative fracture in ductile metals. The J-integral[5] is defined as

$$J = \int_\Gamma \left(W dy - T\frac{\partial u}{\partial x} ds\right), \tag{2}$$

where W is the strain energy density, T is the traction vector, $\partial u/\partial x$ is the displacement gradient, and s is the arc length. However, several specimens are usually required to determine the critical J-integral for fracture. Consequently, from an engineering point of view, it is desirable to have a single-specimen method which provides a failure-characterizing parameter independent of crack size and specimen geometry, that can be easily obtained.

Previous work[6] discussed two J-integral methods, derived from Equation (2), applied to single-edge notched (SEN) specimens of carbon-black-filled NR. One of them,

$$J_\delta = \int \sigma d\delta, \tag{3}$$

* Based on a paper presented at a meeting of the Rubber Division, American Chemical Society, Atlanta, Georgia, October 7–10, 1986. B.

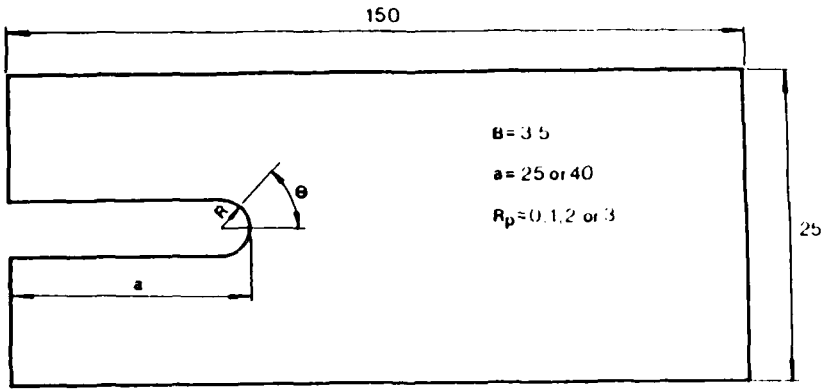

FIG. 1.—Geometry of the pure-shear specimen, (dimensions in mm)

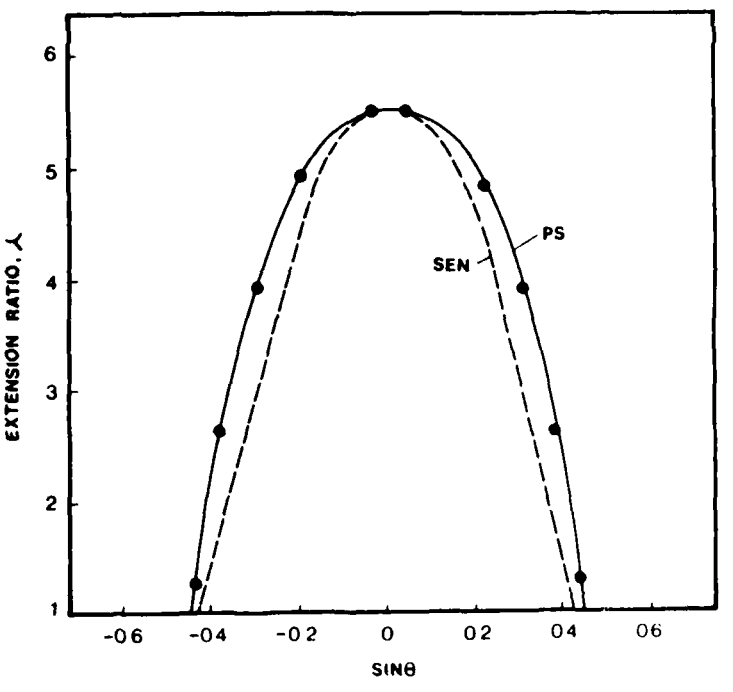

FIG. 2.—Extension ratio as a function of sin θ around a 2 mm prenotch tip for 10 pph NR in pure shear and SEN specimens at crack initiation

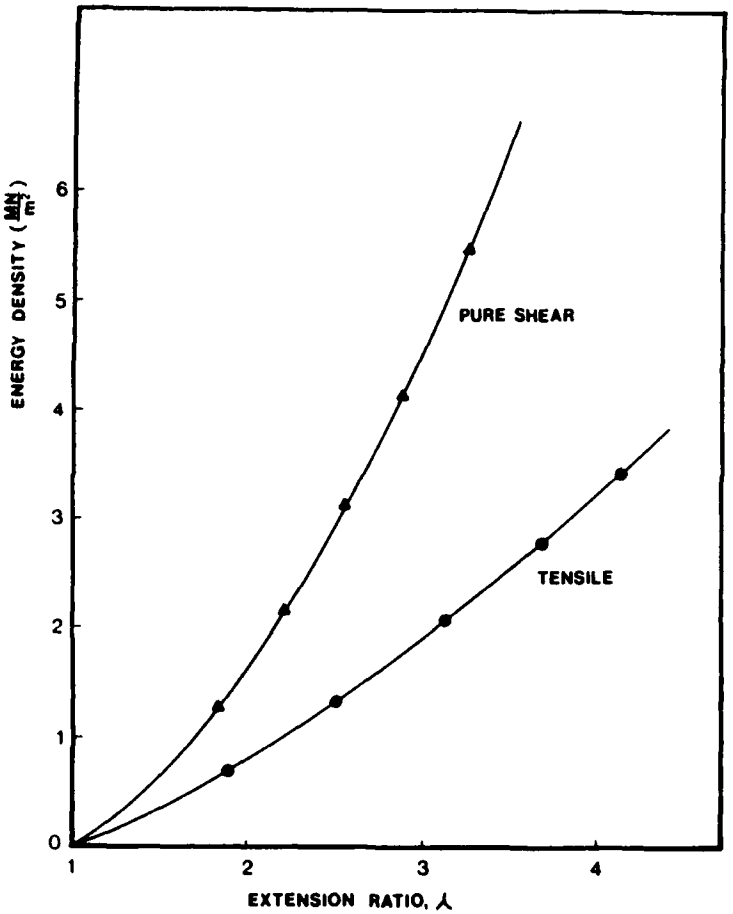

FIG. 3.—Energy density as a function of extension ratio from un-notched tensile and pure-shear specimens.

where σ is the net section stress and δ is the crack opening displacement or crack tip diameter, is experimentally simple to evaluate. For four carbon black levels, J_δ was about one half of

$$J_\theta = R \int W d \sin\theta, \tag{4}$$

where R is the crack tip radius, W is the energy density, and θ is the angle of any element along the notch tip relative to the center line of the crack. Both relations require only a single specimen to characterize crack initiation, and both are independent of crack size and specimen geometry. The critical J-value at crack initiation increased linearly with carbon black content and prenotch radius. It was also found that there is a critical crack opening displacement (crack tip diameter) at which crack initiation occurred. This critical crack tip diameter increased with prenotched radius, but was independent of carbon black content. Furthermore, the mean crack region stress, the ratio of the critical J to the critical radius, increased linearly with carbon black content and was independent of prenotch radius.

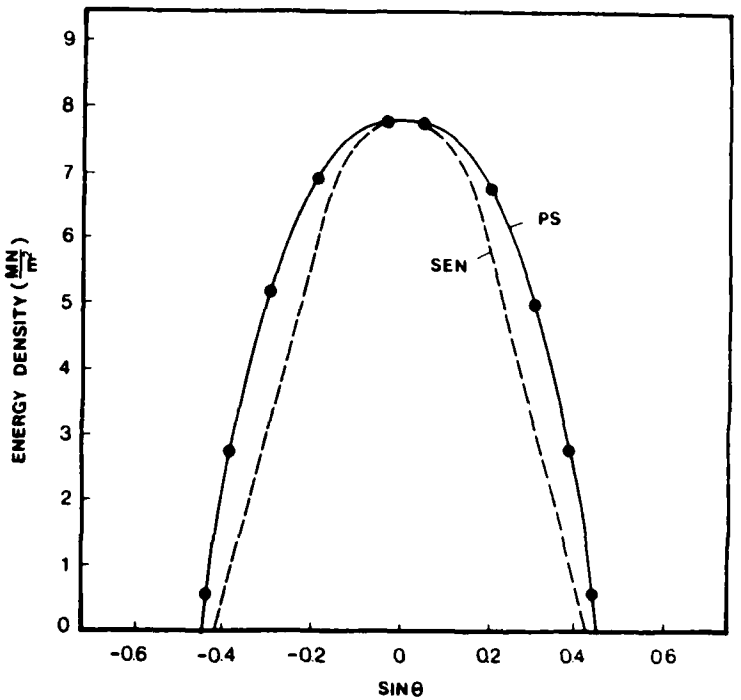

FIG. 4.—Energy density as a function of sin θ around a 2 mm prenotch tip for 10 pph NR in pure shear and SEN specimens at crack initiation.

Fracture data of elastomers have frequently been determined with SEN and pure shear (PS) specimens. For SEN specimens, the tearing energy is approximately

$$T = 2\pi\lambda^{-1/2} W a, \tag{5}$$

where λ is the extension ratio, W is the strain energy density in a tensile specimen at the same λ and a is the crack size[7]. In the PS specimens,

$$T = W h_0, \tag{6}$$

where W is the strain-energy density of an uncracked pure-shear specimen at the applied extension and h_0 is the undeformed specimen height. Therefore, in SEN tensile specimens, the tearing energy, T, increases with crack size, while in pure

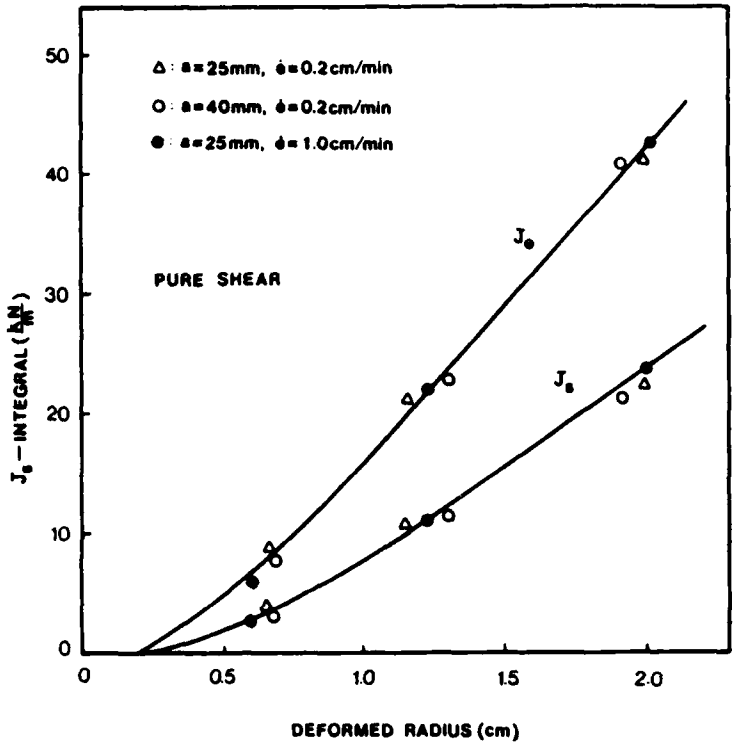

FIG. 5.—Correlation between J_e and J_s as a function of deformed notch tip radius in pure-shear specimens.

shear, specimen T is constant, independent of crack size, but the critical tearing energy, T_c, should be independent of specimen type.

The purpose of this study was to determine, based on the concepts of J-integral and crack opening displacement, the failure criterion of carbon-black-filled NR in pure-shear specimens and to compare the results with those in SEN specimens and with the tearing energy.

EXPERIMENTAL

A NR recipe, compounded by The B F Goodrich Co., with carbon black contents of 0, 10, 25, and 40 pph, and 10% regrind were used for all tests.

PS specimens, shown in Figure 1, with sharp and blunt notches of different prenotch radii and precrack lengths, were tested at 21°C at a displacement rate of 0.2 cm/min; a few specimens were tested at 1 cm/min. The PS dimensions are shown in Figure 1. (Tensile specimens were 25 mm wide with a 100 mm gage

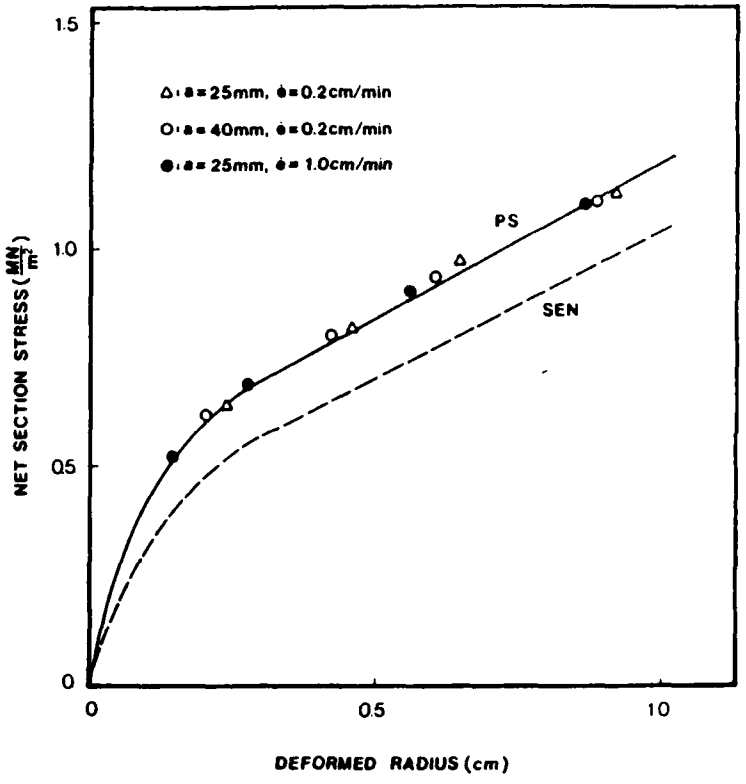

FIG. 6.—Net section stress as a function of deformed crack-tip radius for unfilled NR at various crack sizes in pure shear and SEN tests.

length.) Sharp cracks were made by cutting the rubber with a new razor blade, while the blunt notches were made by drilling a hole with a sharp hollow circle cutter lubricated with water, then the sides of the notches were cut away with a sharp razor blade.

The region around the crack tip was coated with talc, a white powder, so that a series of fine radial lines could be made around the notch tip region. The spacing between the lines around the notch tip was measured with a microscope equipped with a 10× filar eyepiece. Based on these measurements, the extension ratios of all elements around the notch tip as a function of angular position were determined and were the basis for calculating the critical J_e-integral at crack initiation according to Equation (4). J_s was determined by measuring the crack-tip diameter as a function of load for both precracked and prenotched specimens, since J_e is not applicable to precracked specimens.

Crack initiation was identified on the crack surface coated with the white powder when the crack tip developed a new surface delineated by the white powder.

TABLE I

REPRESENTATIVE VALUES OF J_i AND J_s FOR CRACK INITIATION IN NR FOR DIFFERENT CRACK SIZES AND CARBON BLACK CONTENTS IN PURE SHEAR

CB[a], pph	R_p[b], mm	a[c], mm	J_i	J_s	J_i/J_s
0	1	25	57.8	27.8	2.08
0	1	40	51.5	24.5	2.10
0	2	40	70.5	37.8	1.78
10	1	25	74.6	39.5	1.89
10	1	40	69.9	32.7	2.14
10	2	40	103.5	54.0	1.91
25	1	25	97.9	53.2	1.84
25	1	40	93.5	46.3	2.02
25	2	40	194.4	84.2	2.31
40	1	25	163.8	83.2	1.97
40	1	40	175.8	78.5	2.24
40	2	40	245.3	126.5	1.94

[a] Carbon black content.
[b] Precrack radius.
[c] Crack size.

RESULTS

The extension ratio of the elements along the notch tip as a function of angular position relative to the center line was measured and is shown in Figure 2. Then the total stored energy, W, as a function of extension ratio was obtained from tensile tests of uncracked specimens by integrating the area under the stress–strain curve (Figure 3), and used to determine the stored energy as a function of sin θ along the blunted notch (Figure 4). The J-integral, J_i, was calculated with Equation (4) which is the product of the critical notch-tip radius times the area under the W–sin θ curve, and it is shown in Figure 5 as a function of the deformed notch-tip radius. It was independent of crack size and strain rate in the range tested. Similar data were obtained as a function of precrack notch-tip radius, crack size and carbon-black content.

This procedure is tedious and applicable only to prenotched specimens. Therefore, the net section stress was measured as a function of the deformed notch-tip radius and found to be independent of crack size and strain rate in the range 0.2 and 1 cm/min (Figure 6), as was also found in SEN specimens[6]. The area under this curve up to the radius of initiation serves as the basis for calculating J_s, which is one half of J_i as shown in Figure 5 and Table I. The effect of carbon-black content on the net section stress at crack initiation is shown in Figure 7 as a function of crack-tip opening for precracked specimens. Figure 8 shows J_s as a function of deformed crack-tip radius in precracked specimens. Specimens with sharp and notched precracks were tested. Figures 9 and 10 thus show the critical J_s at crack initiation as a function of carbon black and prenotch radius. The critical crack-tip

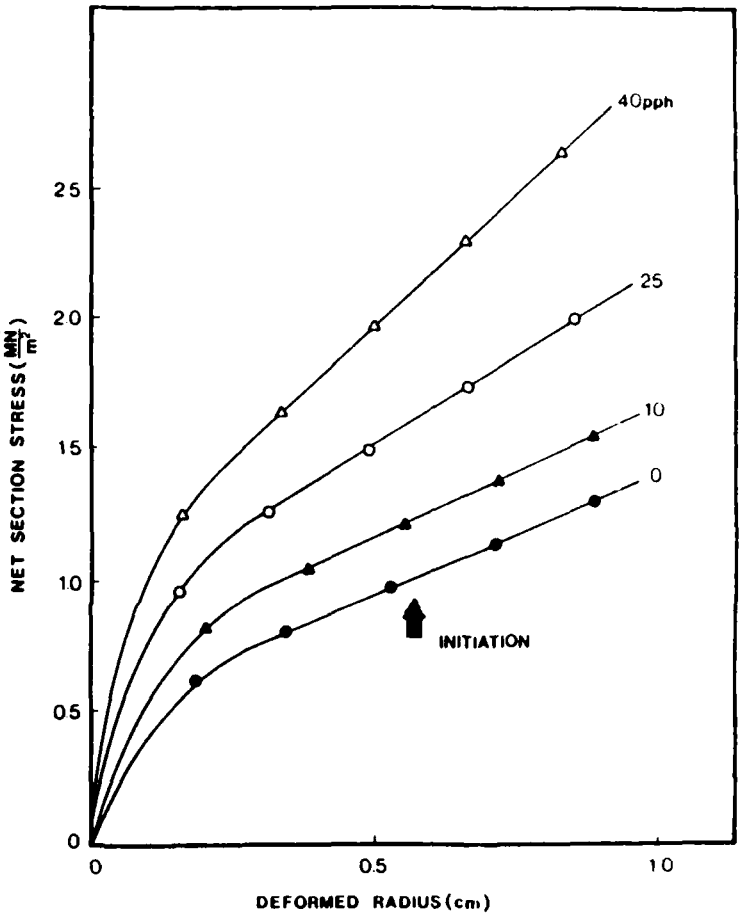

FIG. 7.—Net section stress as a function of deformed crack-tip radius and carbon black content for NR in pure shear

radius at crack initiation depended on the prenotch radius, but not carbon black content, as indicated in Figure 11.

For metals and some thermoplastics[8], the ratio of the critical J-integral over critical crack-opening displacement is proportional to the yield stress. Since the J-integral is an average measure of the stress and strain field in the crack-tip region while the critical radius is a local measure of the strain, their ratio is an average measure of the stress in the crack-tip region required to initiate crack growth. Figures 12 and 13 show that this average crack-region stress increases with carbon black content.

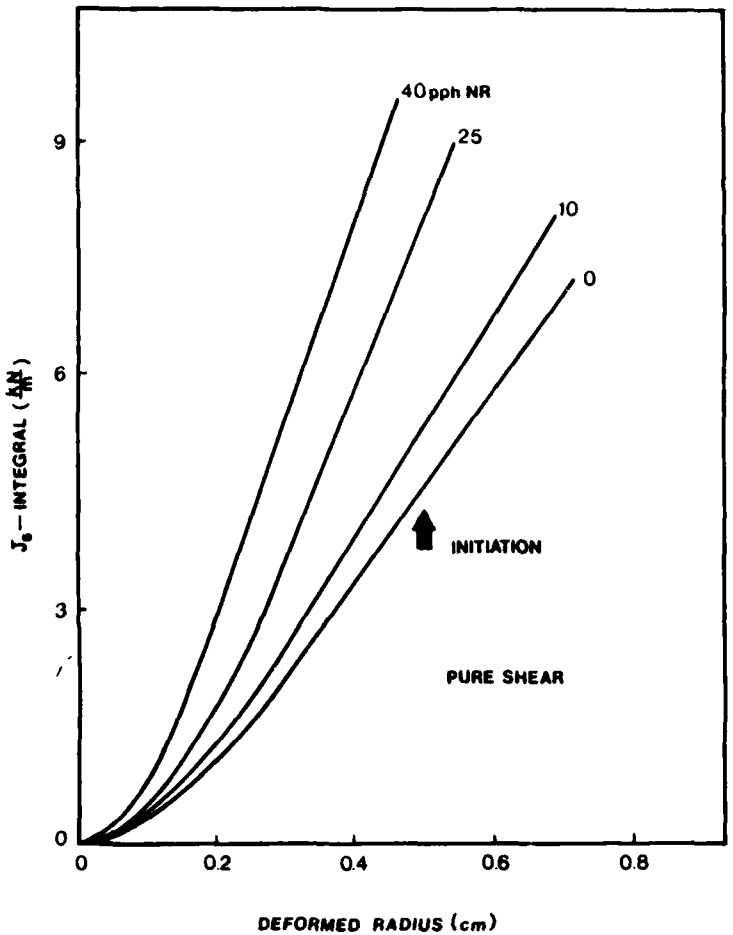

FIG. 8.—J_c as a function of deformed crack-tip radius for NR in pure shear.

To compare the critical J with the classical tearing energy, T was calculated. For elastomers which show marked energy dissipation, the appropriate value for W in the tearing-energy equation is smaller than the energy expended in deforming the material to the point of crack initiation[5]. Therefore, the strain energy, W, available for crack initiation was taken as the area under the force-deformation curve on retraction from the deformed state. After this correction was made, the tearing energy for SEN specimens calculated according to Equation (5) from previously published data[6], and the tearing energy for pure shear tests obtained from Equation (6) differed from the J-values, as shown in Table II. Also, the critical T for SEN specimens (only specimens with a = 6 mm satisfy Thomas' recommendations) was

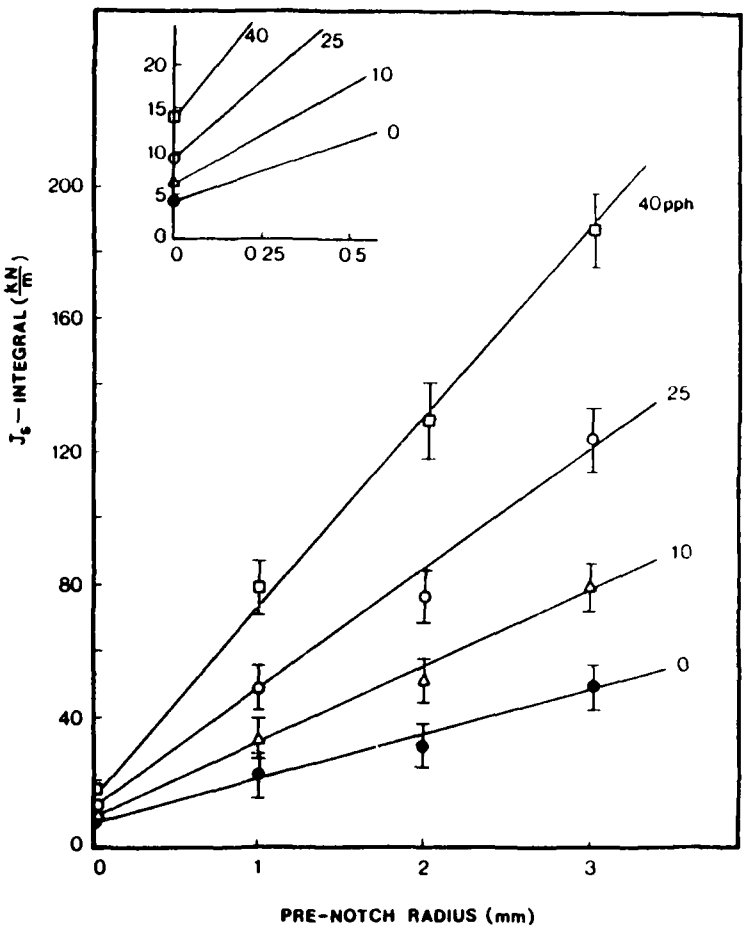

FIG. 9.—J_c at crack initiation as a function of prenotch radius and carbon black content.

a function of specimen geometry and crack size, but T for PS specimens was independent. As discussed, the J-integral is crack-size and specimen-geometry independent in SEN tests as well as in PS tests. However, both the J-integral and T differed for SEN and pure-shear tests.

DISCUSSION

The J-integral for crack initiation from a blunt notch [Equation (4)] can be derived from Rice's definition of the J-integral[6] and is equivalent to that originally proposed by Thomas[9]. A small error exists in the calculated J-value, since the

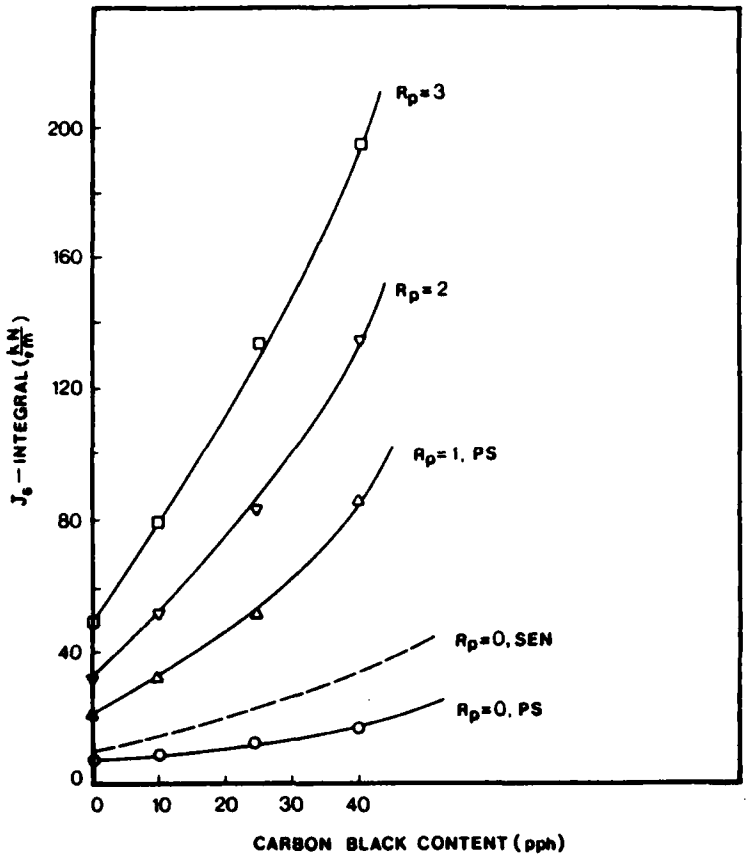

FIG. 10.—J_δ at crack initiation as a function of carbon black and prenotch radius.

strain-energy density was obtained from uniaxial extension data, but a biaxial state of stress exists in the crack-tip region. This is considered to be small, since the critical radius is large and the notch-tip elements are predominately in uniaxial extension.

The calculation of J_δ, which requires the measurement of the crack-tip opening as a function of stress, is a simple, efficient method to characterize the conditions for crack initiation. In addition, this procedure is valid for sharp precracks. Moreover, the correlation of the true J_δ value with J_δ from Figure 5 and Table I is about a factor of two. This simple procedure, as a result, seems to be valid to characterize the critical condition for crack initiation of a highly dissipative rubber, and it requires only one specimen.

Comparing PS with SEN specimen results[6] shows that the critical J-integral at crack initiation for PS specimens is usually smaller than those of SEN specimens,

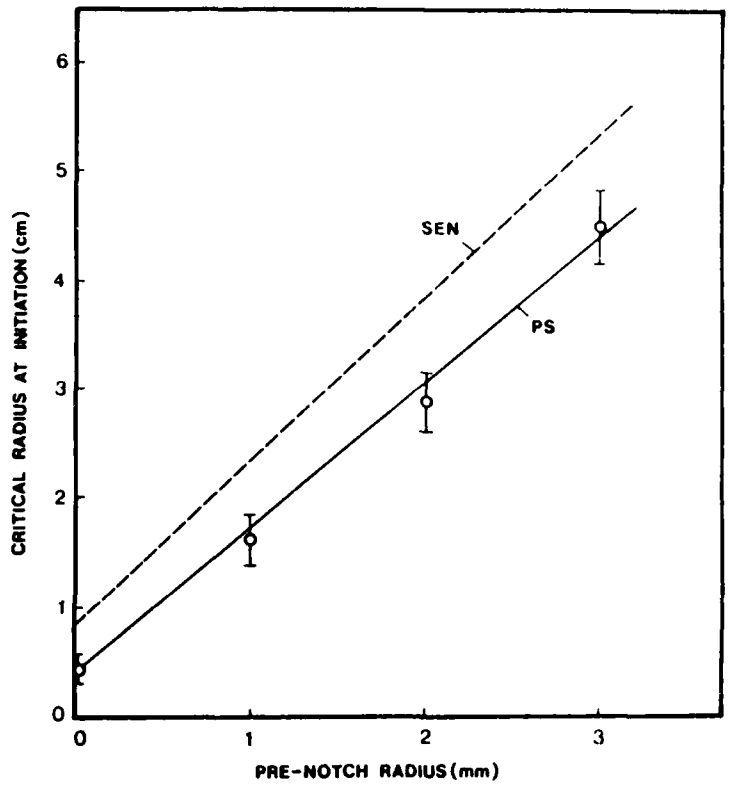

FIG. 11.—Critical radius at crack initiation as a function of prenotch radius in SEN and pure-shear specimens.

especially for specimens with sharp precracks. Also the critical crack-tip radius at crack initiation for PS is less than that for SEN specimens (Figure 11). But, the average J_δ/R at crack initiation for SEN specimens is smaller than for PS specimens, as in Figure 13. However, for PS specimens they increase linearly with carbon-black content, and are independent of prenotch radius, similar to SEN specimens.

These differences are possibly due to different stress-induced microstructures and stress–strain fields in the crack-tip region of the two types of specimens. The stress–strain field in the region far from the crack-tip in the PS specimen is more biaxial than in the SEN specimen. This biaxial state of strain will induce different morphologies than will a uniaxial strain and the reduced fracture resistance may be related to this effect. From the fracture mechanics point of view, both SEN and PS specimens are in Mode I loading; that is, crack-opening mode. However, fracture mechanics theory does not describe the state of stress and molecular arrangement in the crack-tip region in a highly dissipative material like carbon-black-filled NR. The understanding of these differences requires additional work.

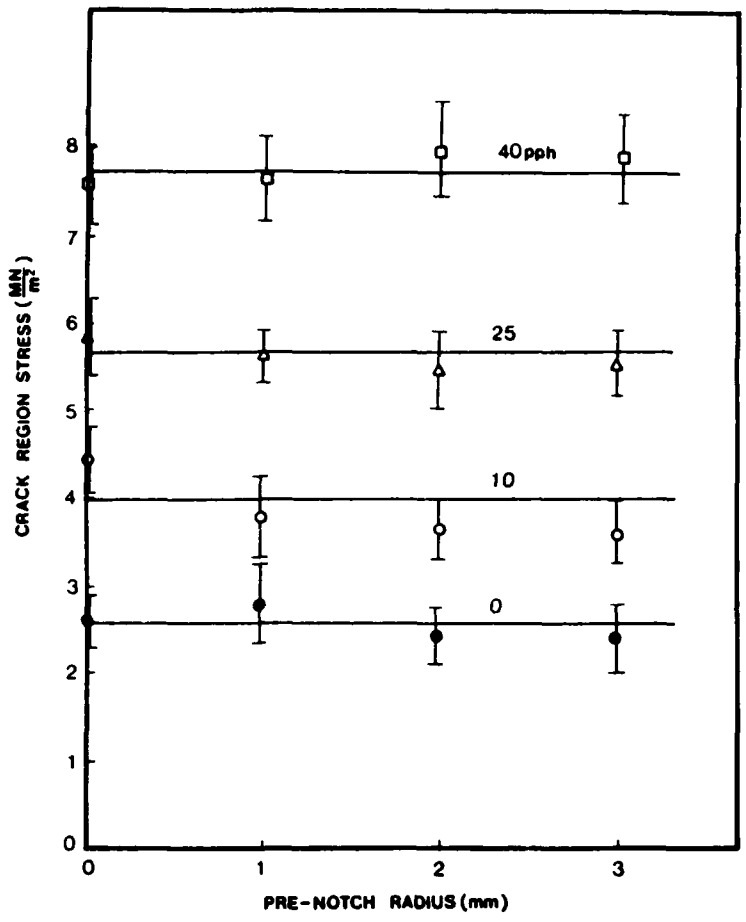

FIG. 12.—Crack region stress, J_s/R, as a function of prenotch radius and carbon black content in pure-shear specimens.

The critical J-values obtained in this study from local crack-tip measurements are significantly higher than those obtained by the energy-rate interpretation of J[4]. The origins of these differences are presumed to arise from the relative contributions of the local and remote crack-tip processes; the molecular and fracture mechanics aspects of these differences are being investigated.

In summary, it was found that for nonelastic carbon-black-filled NR, both T and J at crack initiation obtained from SEN and PS tests differred, but both were crack-size independent in PS. However, for SEN tests, only J was independent of crack size and specimen geometry. These results suggest that the J-integral has

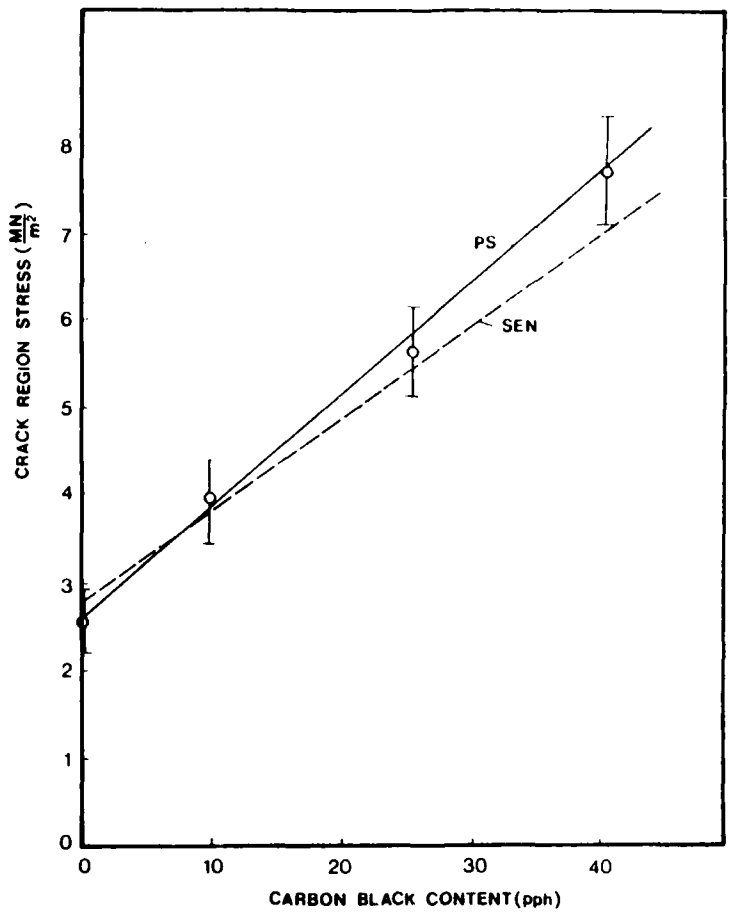

FIG. 13.—Crack region stress as a function of carbon black content in SEN and PS specimens

merit as a failure criterion for rubber, but understanding its dependence on specimen type and testing procedure requires more work.

CONCLUSIONS

For PS and SEN specimens:

1) J_s (one half J_0) can be determined from one specimen and is independent of crack size and specimen geometry.

2) J and T at initiation differed.

3) J at initiation increased with carbon black content, but the critical crack tip radius did not.

TABLE II

$2J_s$ AND T FOR PURE SHEAR AND SEN TESTS FOR PRECRACKED SPECIMENS[a]

CB, pph	*a*, mm	$2J_s$, kN	T_{ps}, kN/m	*l*, mm	*WS*, mm	*a*, mm	$2J_s$, kN/m	T_{sen}, kN/m
0	15	10.31	12.73	50	25	15	21.74	13.43
				50	25	6	19.68	12.96
0	25	11.61	11.89	50	35	12	18.71	10.78
				50	35	22	19.53	22.31
0	40	10.41	12.65	100	25	15	20.73	26.11
				100	25	6	22.64	22.84
10	25	14.75	13.63	50	25	15	30.68	13.36
10	40	13.29	13.73	50	25	6	33.44	10.88
				50	25	15	46.54	16.58
25	25	17.88	12.59	50	25	6	44.74	12.66
				100	25	15	47.06	11.71
25	40	19.35	14.51	100	25	9	49.37	12.84
40	25	26.73	15.37	50	25	12	63.28	21.46
40	40	27.06	17.46	50	25	6	57.89	17.00

[a] *CB*, carbon black content; T_{ps}, tearing energy of pure shear specimens; T_{sen}, tearing energy of SEN tensile specimens; *l*, tensile specimen length; *W*, tensile specimen width; *a*, crack size.

ACKNOWLEDGMENT

The financial support of the U.S. Army Research Office in Durham and the Cabot Foundation is gratefully acknowledged and appreciated. We would also like to thank Dr. S. Parhizgar and The B F Goodrich Co. for supplying the materials.

REFERENCES

[1] R. S. Rivlin and A. G. Thomas, *J. Polym. Sci.* **10**, 291 (1953).
[2] H. W. Greensmith and A. G. Thomas, *J. Polym. Sci.* **18**, 198 (1955).
[3] A. Ahagon, A. N. Gent, H. J. Kim, and Y. Kumagai, RUBBER CHEM. TECHNOL. **48**, 897 (1975).
[4] D. J. Lee and J. A. Donovan, *Theor. Appl. Fract. Mechanics* **4**, 137 (1985).
[5] *J. R. Rice, J. Appl. Mech.* **35**, 379 (1968).
[6] R. F. Lee and J. A. Donovan, RUBBER CHEM. TECHNOL. **59**, 787 (1986).
[7] H. W. Greensmith, *J. Appl. Polym. Sci.* **7**, 993 (1963).
[8] S. Hashemi and J. G. Williams, *Polym. Sci. Eng.* **26**, 76 (1986).
[9] A. G. Thomas, *J. Polym. Sci.* **18**, 177 (1955).

Reprinted from RUBBER CHEMISTRY AND TECHNOLOGY,
Vol. 60, No. 5, November-December 1987
Printed in U. S. A.

EFFECT OF CARBON BLACK ON THE *J*-INTEGRAL AND STRAIN ENERGY IN THE CRACK TIP REGION IN A VULCANIZED NATURAL RUBBER*

H. LIU, R. F. LEE, AND J. A. DONOVAN

MECHANICAL ENGINEERING DEPARTMENT, UNIVERSITY OF MASSACHUSETTS AT AMHERST, AMHERST, MASSACHUSETTS 01003

INTRODUCTION

Since 1953, the tearing energy theory developed by Thomas and Rivlin[1] has been used to characterize the fracture properties of nonlinear, elastic elastomers; *i.e.* crack initiation occurs when the strain energy release rate reaches a critical value, T_c. However, the application of the tearing energy theory raised several concerns: 1) Tearing energy equations for single-edge notched (SEN), pure shear (PS) and trousers specimens have been simplified to make this theory easy to apply. But for specimens with more complicated geometry, the experiments and calculations are usually intractable. 2) Tearing energy theory assumes an elastic material, but technologically important elastomers, like carbon-black (CB)-filled natural rubber (NR), are nonelastic materials that dissipate energy during extension due to viscous deformation and strain-induced crystallization. Because of this, it has been suggested that T should be adjusted for this hystersis[2]. Also, to account for dissipation of energy, Andrews[3] described the crack growth process in nonelastic materials by an energy-loss function. 3) In strain crystallizing elastomers, the material strength is enhanced by the crystals, while the crystallinity is stress or strain state dependent. This may affect the geometry independence of the critical tearing energy, a requirement for a valid fracture characterizing parameter.

The *J*-integral theory was first proposed by Rice[4] in 1968 to characterize the stress and strain field in the crack tip for nonlinear materials of infinitesimal elasticity. For perfect elastic materials, the *J*-integral value is path independent and equal to G, the Griffith strain-energy release rate, and T. Path independence was shown for elastic–plastic material except very close to the crack tip in the region affected by the blunted tip[5,6].

Chang[7] subsequently verified Rice's theory and mathematically showed that the *J*-integral for highly deformable materials had the same form as Rice's equation, and the *J*-integral was related to the tearing energy. Oh[8] measured the *J*-integral values along the outer edges of a single-edge notched specimen and obtained the same result as obtained from the calculation of the tearing energy. Since CB-filled NR is nonlinear and nonelastic and significant energy is

* Presented at a meeting of the Rubber Division, American Chemical Society, Montreal, Quebec, Canada, May 26–29, 1987. G.

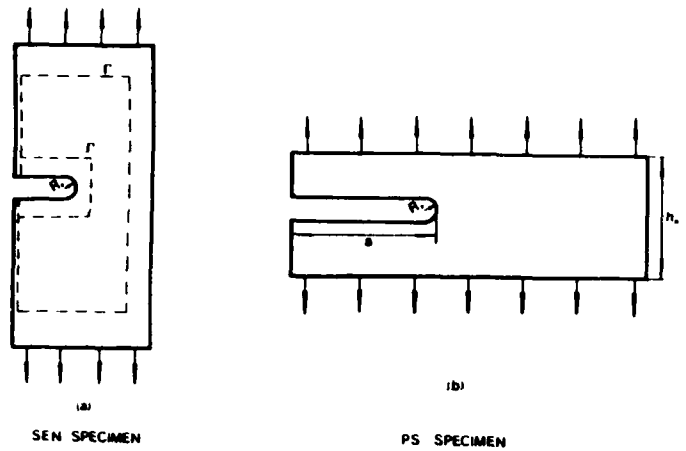

FIG. 1.—Geometry of the single edge notched specimen and pure-shear specimen

dissipated during deformation, especially around the crack tip where strain-induced crystallization occurs, the path independence of the J-integral might be affected.

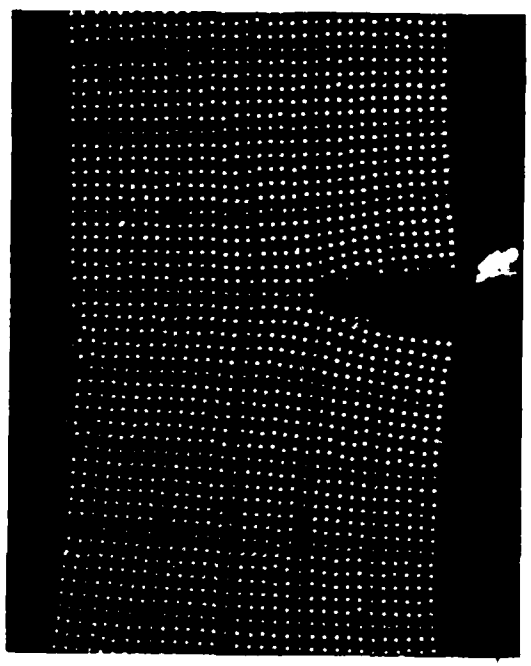

FIG. 2.—Photograph of deformed crack-tip region in a SEN.

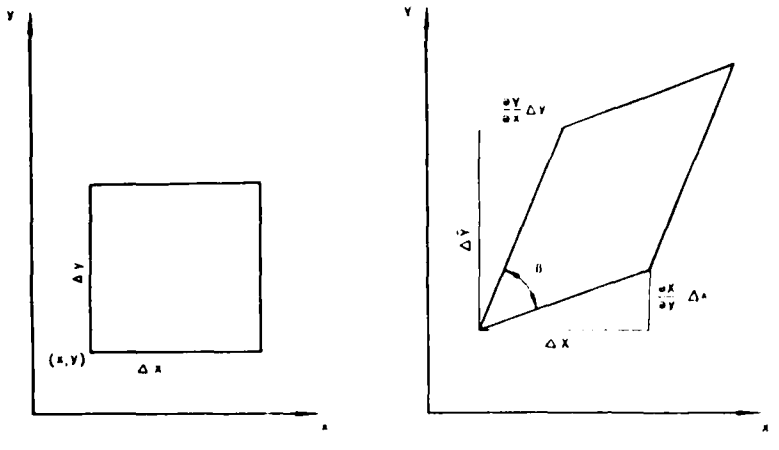

FIG. 3.—Schematic showing the dot coordinates of one element (a) before deformation and (b) after deformation

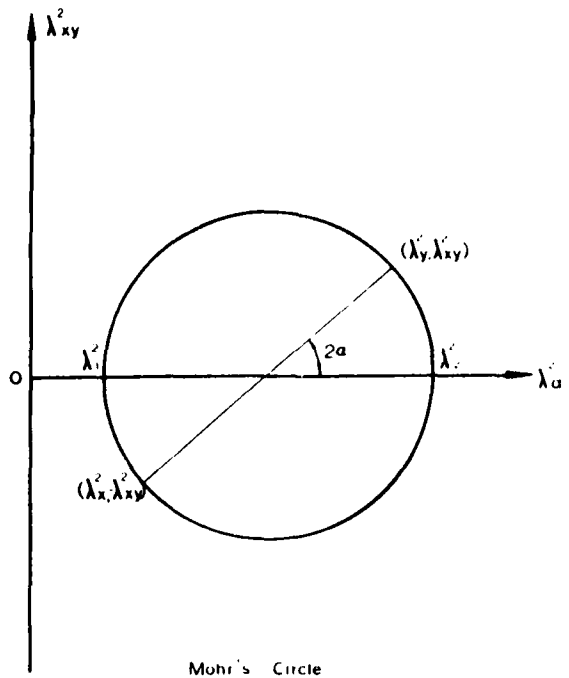

FIG. 4.—Mohr's circle for finite deformation

This paper presents the experimental results of measuring J, according to · line integral definition, and the strain energy along different paths in the ick tip region, and compares the critical J-integral and tearing-energy values single-edge notched and pure shear specimens as a function of CB content.

TEARING ENERGY AND J-INTEGRAL THEORY

J-integral and tearing energy are both defined as the energy released when rack advances unit area.

$$T_c = J_c = -\frac{1}{t}\left(\frac{\partial U}{\partial a}\right), \tag{1}$$

ere t is the thickness of the specimen, U is the energy stored in the specimen, s the crack length and T_c or J_c is the critical energy release rate at crack tiation. In general, several specimens are required to determine the critical lue in Equation (1).

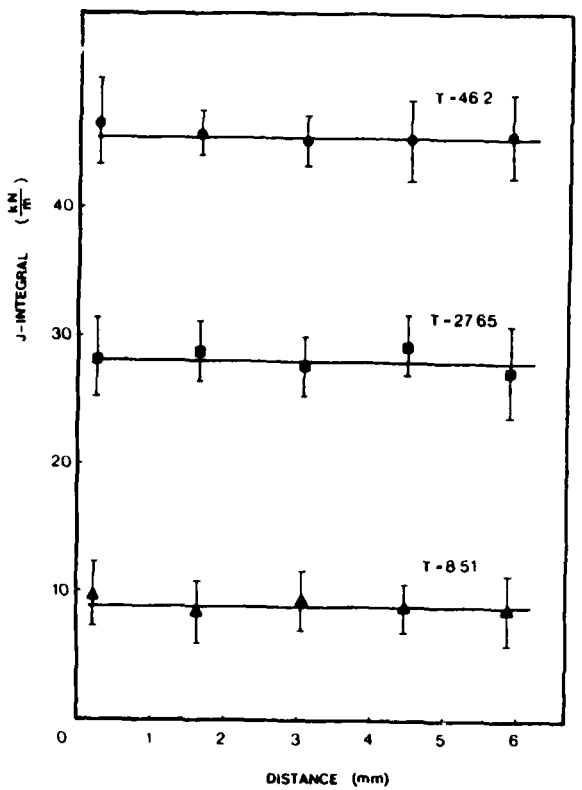

Fig. 5 —J-integral as a function of the distance from the crack tip at different extensions.

Thomas simplified the general expression for several types of specimens so that T could be easily determined. T for a SEN specimen, shown in Figure 1 (a), is given by

$$T = 2K(\lambda)Wa, \tag{2}$$

where W is the stored strain energy density in the specimen far away from the crack tip, $K(\lambda)$ is a proportionality factor dependent on the extension ratio λ, and a is the crack length. Equation (1) can only be used if a is small compared to the specimen width, so that most of the specimen is in simple tension.

For the PS specimen, shown in Figure 1 (b), the equation for the tearing energy is

$$T = Wh_o, \tag{3}$$

where W is the energy density in the pure-shear region of the PS specimen, h_o is the specimen height in the undeformed state. Since Equation (3) is not an explicit function of crack length, it is easier to calculate the tearing energy for a PS specimen than for a SEN specimen.

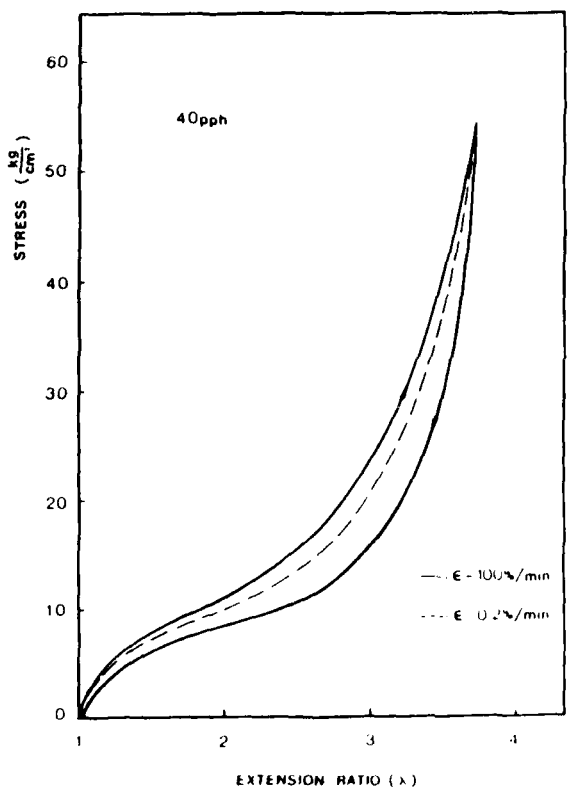

Fig. 6 —Stress vs. extension ratio for 40 pph NR in simple tension [illegible]

The *J*-integral is also defined as

$$J = \int_\Gamma W dy - \bar{T} \cdot \frac{\partial \bar{u}}{\partial x} ds, \qquad (4)$$

here Γ is any path enclosing the crack tip, W is the strain energy density on Γ, is the traction vector per unit area of the undeformed surface defined as T_i $\sigma_{ij} n_j$, where $\bar{n}$ is the normal vector of the path and σ_{ij} is the engineering ress, s is the arc length of the undeformed path, and $\bar{u}$ is the displacement ector. By taking special integral paths to eliminate T, as Oh did, Equation (3) n be simplified so that the integration becomes easier.

EXPERIMENTAL PROCEDURES

A NR recipe, compounded by BF Goodrich with HAF carbon black contents 0, 10, 25, and 40 pph, and 10% regrind were used for all tests.

The rubber specimen was 3 mm thick. Sharp cracks and prenotches of fferent prenotch radii were cut with a razor blade or hole cutter as shown in

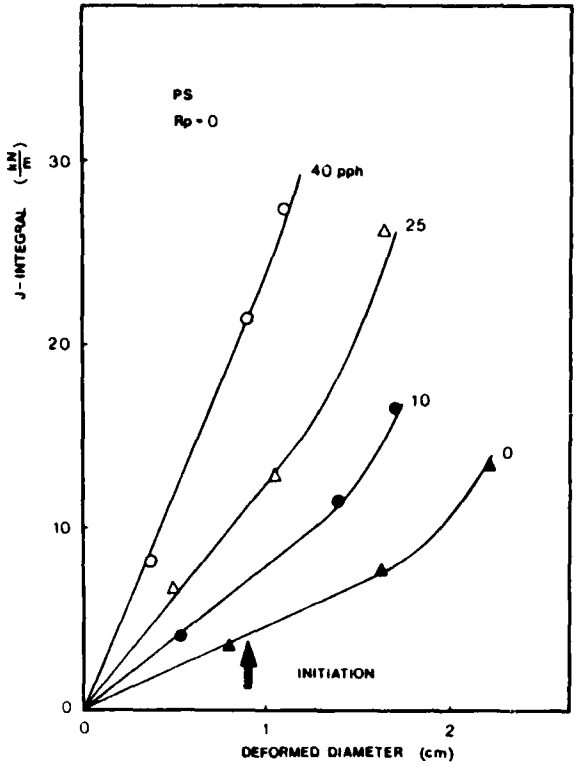

FIG. 7 —*J*-integral as a function of deformed notch-tip diameter in sharp crack PS specimen.

Figure 1. The SEN specimens were 25 mm wide and 100 mm long with crack lengths of about 6 mm; the PS specimens were 150 mm wide and 25 mm high with crack lengths of about 30 mm. White dots, made by Chartpak Transfer Lettering Co., with a density of 144 points/cm^2 were pressed onto the specimen before deformation. The specimens were tested at an extension rate of 0.1 mm at 21°C.

Photographs of the dots were taken before and after deformation with a camera equipped with a macrolens so that the displacement of the white dots on the specimens could be recorded for analysis; a typical photo of a deformed crack tip region is shown in Figure 2.

The crack surface was coated with white powder (talc), and crack initiation was defined as when the crack tip developed a new surface delineated by the white powder.

To measure the *J*-integral, the displacement of each dot on the selected path around the crack tip must be determined. This was done by establishing a cartesian coordinate system fixed in space, then the coordinates of each dot on the specimen before and after deformation were assigned as (x, y) and (X, Y)

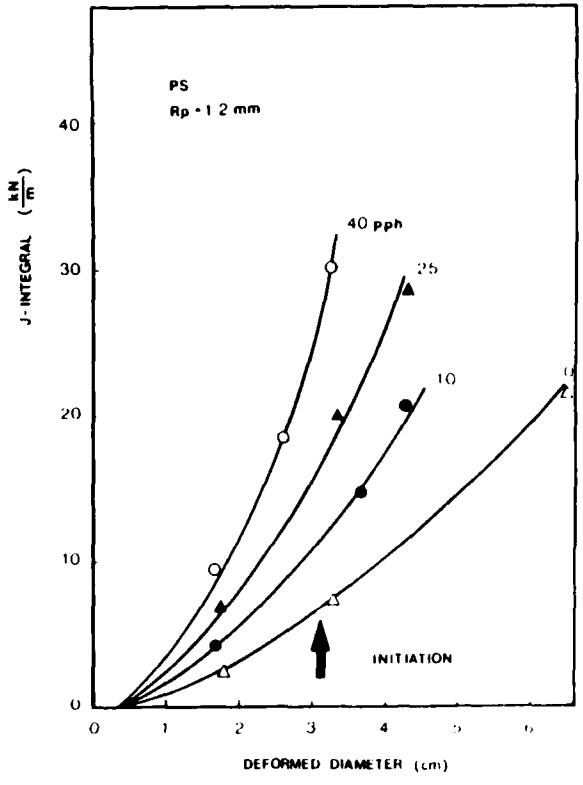

FIG. 8 —*J*-integral as a function of deformed notch-tip diameter in prenotched PS specimen.

espectively. Since large deformations were involved in the rubber specimens, he extension ratio, $\lambda = l/l_0$, was computed from the measured coordinates ccording to large deformation theory[9]:

$$\lambda_x^2 = \left(\frac{\partial X}{\partial x}\right)^2 + \left(\frac{\partial Y}{\partial x}\right)^2,$$

$$\lambda_y^2 = \left(\frac{\partial Y}{\partial y}\right)^2 + \left(\frac{\partial X}{\partial y}\right)^2,$$

$$\lambda_{xy}^2 = \lambda_x \lambda_y \cos \beta,$$

where λ_x, λ_y are the extension ratios in the x and y directions, λ_{xy} is the shear atio, and β is the angle of the element after deformation as shown in Figure 3. Mohr's circle for large deformations, as shown in Figure 4, was used to transorm the extension ratios into the two principle extension ratios λ_1, λ_2, and hen $\lambda_1\lambda_2 = \lambda_3^{-1}$.

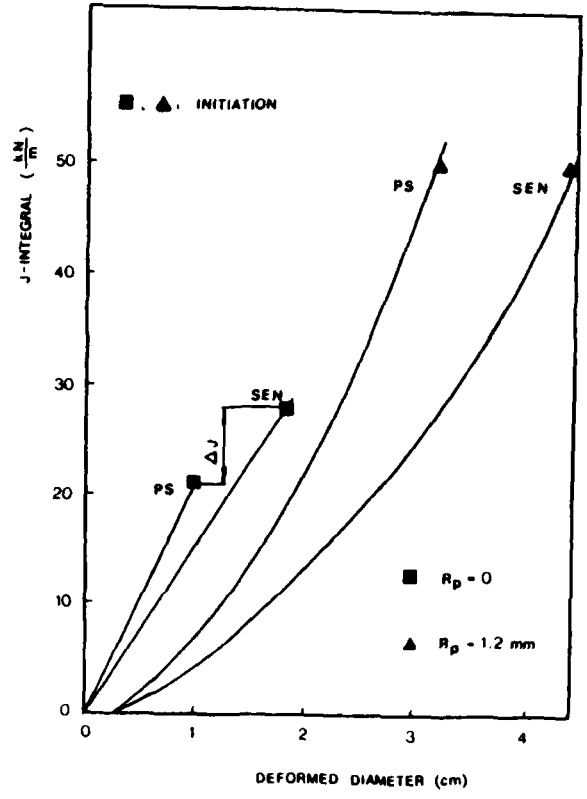

FIG. 9 —*J*-integral as a function of deformed crack-tip radius in precracked and prenotched SEN and PS specimens.

The energy density was calculated from the displacements with Tschoegl's equation[10]:

$$W = C_1(I_1 - 3) + C_2(I_2 - 3) + C_3(I_1 - 3)(I_2 - 3) + C_4(I_1 - 3)^2 (I_2 - 3), \quad (5)$$

where C_1, C_2, C_3, and C_4 are constants determined by curve fitting to stress extension ratio data, I_1 and I_2 are the extension ratio invariants:

$$I_1 = \lambda_1^2 + \lambda_2^2 + \lambda_3^2,$$

$$I_2 = \lambda_1^{-2} + \lambda_2^{-2} + \lambda_3^{-2}.$$

The engineering stresses are given by

$$\sigma_1 = \frac{\partial W}{\partial \lambda_1}, \qquad \sigma_2 = \frac{\partial W}{\partial \lambda_2}.$$

A Fortran program was written to calculate the strain, stress, energy density, and *J*-integral values from the data in the deformed and undeformed

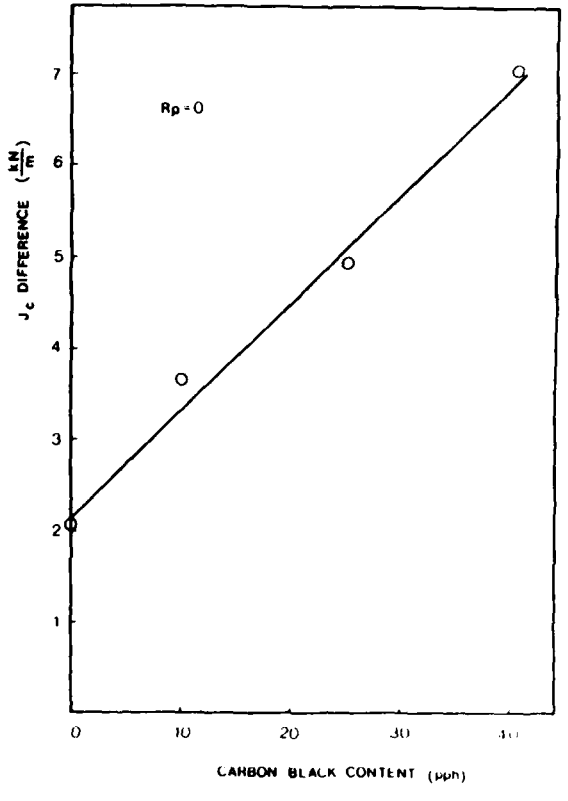

FIG. 10 —The difference in J_c between SEN and PS as a function of carbon black content

positions. The *J*-integral was determined on undeformed coordinates following Rivlin and Shelby for finite strain[11].

RESULTS AND DISCUSSION

J-INTEGRAL PATH INDEPENDENCE

The *J*-integral was computed along several paths around the crack tip as shown in Figure 1 (a). The results show that the average *J*-integral value is path independent over the test piece as shown in Figure 5, although there is scatter up to 30%, which decreases with *J*, probably due to errors in measuring the coordinates of the dots.

CB-filled NR is a nonelastic material, in which strain energy is dissipated primarily by viscous deformation and strain-induced crystallization. However, since the stress–strain behavior is not very sensitive to the strain rate around 100%/min as shown in Figure 6, the effect of the viscous losses on *J* was neglected. Similar to the effect of plastic deformation in metals, it seems that the strain-induced crystallization does not affect the path independence.

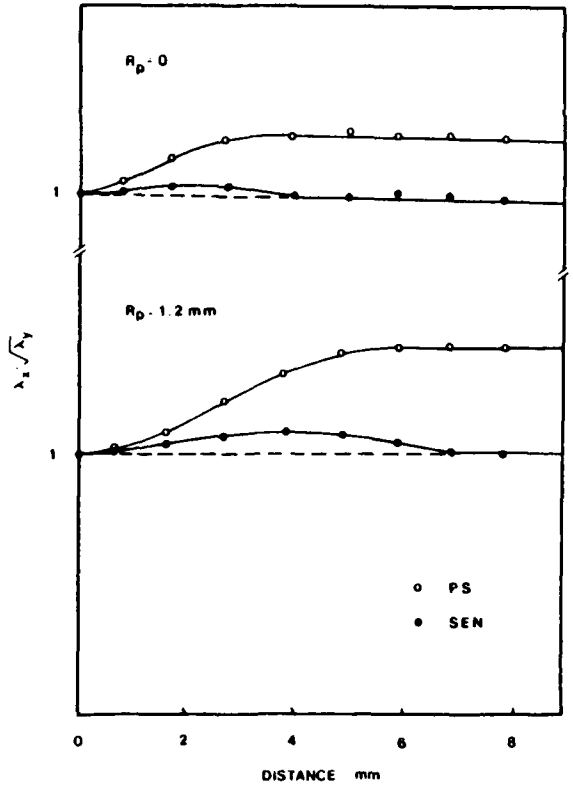

FIG. 11 — The biaxial strain distribution as a function of distance from the crack tip.

The tearing energy in pure shear was also determined from Equation (3) and was equal to *J*. This supports the theoretical result by Chang[7] and the earlier experiments by Oh[8], which showed that the *J*-integral and tearing energy are equivalent. Thus, due to the characteristics of path independence, the critical *J*-integral could be determined by integrating any path around the crack tip.

CRITICAL *J*-VALUE AT INITIATION

The *J*-integral value during the deformation was plotted against the deformed crack-tip diameter δ for precracked (Figure 7) and prenotched PS specimens (Figure 8). There seems to be a linear relationship between *J* and the deformed crack-tip diameter for precracked specimens before crack initiation, but after initiation, the *J* value increases rapidly until rupture.

The critical tearing energy and *J* at initiation increased with CB content, but the critical diameter at initiation was about the same for the same prenotch radii and was in agreement with previous work[12]. The constant notch-tip radius at initiation suggests that the failure of the NR is strain controlled, due

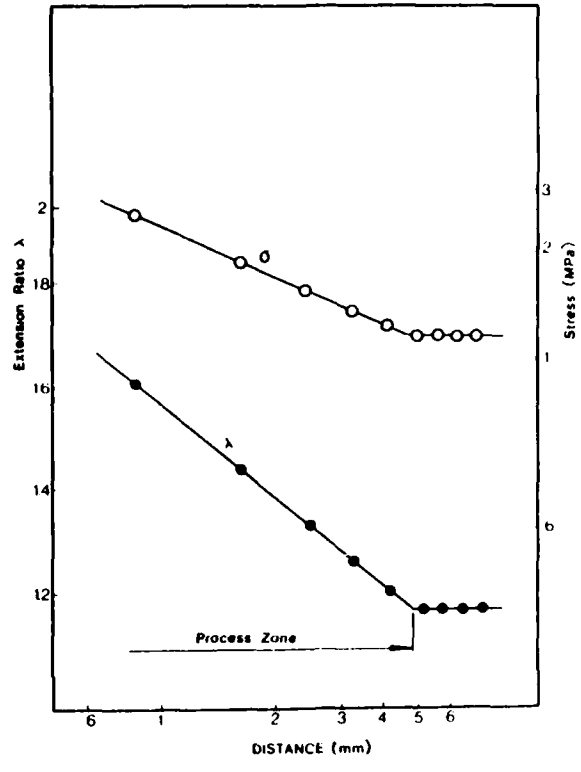

FIG. 12 — Stress and strain as a function of distance from the crack tip.

the breaking of molecular bonds and is not affected by the addition of CB. hat is, the CB is NR increases the energy necessary to deform the crack or otch tip to the critical extent. This agrees with Lake and Thomas' theory[13] of a ommon threshold tearing energy for fatigue and other experimental sults[14,15].

The dependence of J on the deformed radius differs for SEN and PS specimens as shown in Figure 9. The differences are not unexpected considering the ifferent stress state in the two specimens. But for prenotched specimens, the ritical J at initiation is the same in SEN and PS specimens in spite of the naller critical crack-tip radius of PS. For precracked specimens, J_c is smaller PS than in SEN specimens, and the difference increases with CB as shown in igure 10.

For simple extension, $\lambda_1 \cdot \sqrt{\lambda_2} = 1$, where λ_2 is the simple extension ratio. lowever, if the stress state is biaxial, $\lambda_1 \cdot \sqrt{\lambda_2} > 1$. Figure 11 shows $(\lambda_1 \cdot \sqrt{\lambda_2})$ as a unction of r, the distance from the crack tip, for PS and SEN of precracked pecimens. The strain state at the crack tip is in simple extension in both PS and EN specimens, but the stress state in front of the crack tip of the PS specimens

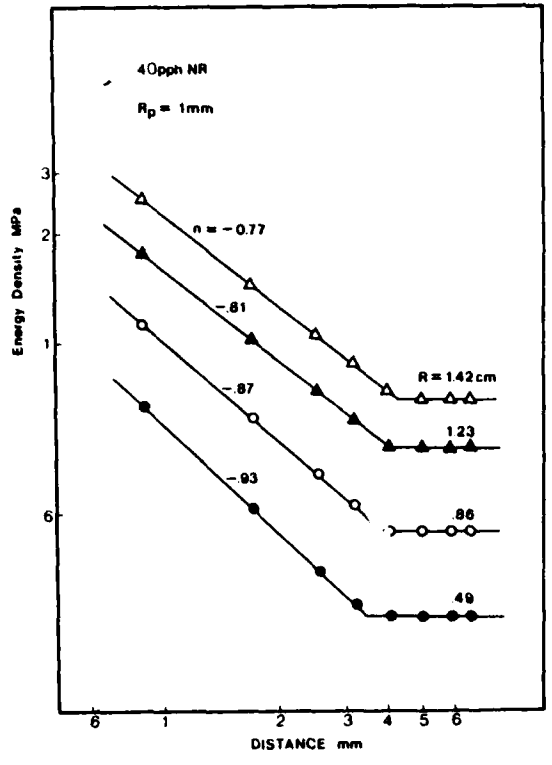

FIG. 13 —Strain energy as a function of distance from the crack tip.

is more biaxial than in the SEN specimens. Since strain-induced crystallization is more difficult in a biaxial state of stress[16], therefore, the energy dissipation is less in PS and the critical J-integral in PS is smaller than in the SEN specimens. The strain state is less biaxial at the crack tip in prenotched than in precracked PS specimens (Figure 11), which explains the same J_c for different prenotched specimens.

STRAIN ENERGY IN CRACK TIP REGION

The strain, stress and energy density are shown on log-log plots in Figures 12 and 13. The stress and energy density were determined from the strain and Tschoegl's equation. All these parameters decrease linearly on the log-log plot until they become constant; the intersection of these regions defines the process zone—the region in which strain, stress, and energy density are being determined by the crack or notch.

Classic linear elastic theory predicts that the strain and stress in this region would vary as $r^{-1/2}$ and the energy density as r^{-1}. All three parameters deviate

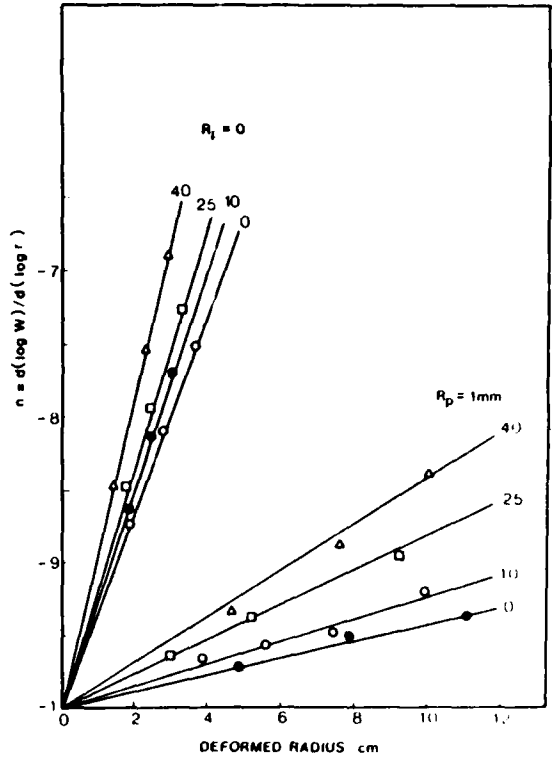

FIG. 14 — n as a function of CB content and deformed crack tip radius.

rom these relations, which differ also from results of Andrews[17] at much loser distances to the crack tip in NR.

The slope, n, of log W *vs.* log r in the process zone increased with applied J, vhich is proportional to the deformed radius and with CB content as shown in 'igure 14, showing that CB increases n in precracked specimens as well as in)renotched specimens. From fracture mechanics theory, it has been sug- ;ested[18,19] t'.at W varies as r^{-1}; this was not found in CB-filled NR. Figure 14 :hows that for both the precracked and the prenotched specimens, the data ·xtrapolate to −1 for an ideally sharp crack with a deformed radius of zero. 'his suggests that the deviation of n from −1 is due to the extensive blunting :hat occurs at the crack tip in rubber during deformation.

CB also affects the process zone size at comparable values of applied J as shown in Figures 15 and 16, in which the zone size increases with J and CB. This supports the suggestion of Stacer, Yanyo and Kelley[20] that CB increases the volume of the anisotropic zone at the crack tip.

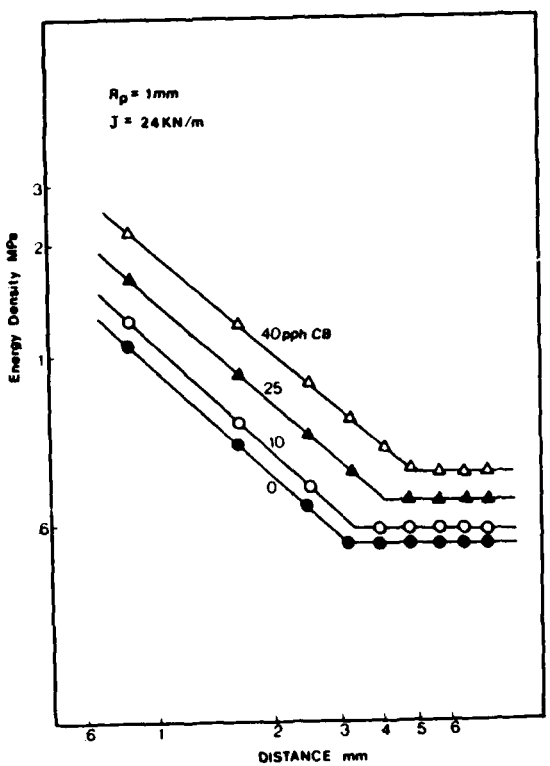

FIG. 15.—Energy density as a function of distance from the crack tip at the same applied J for different CB content.

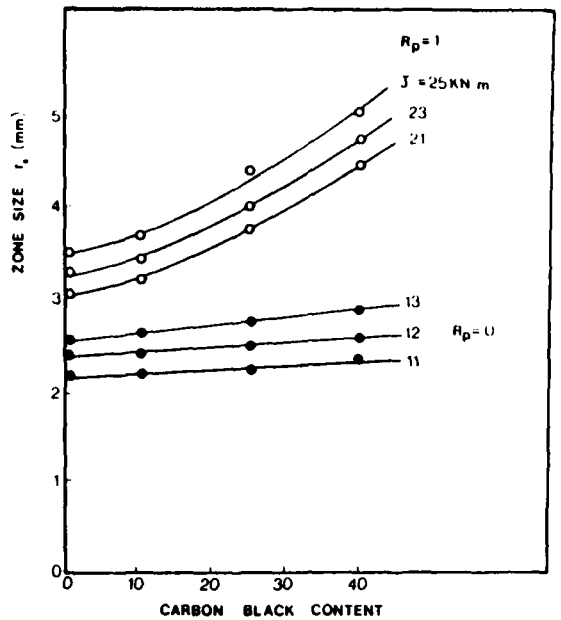

FIG. 16.—Process-zone size as a function of CB content and applied J

Comparison of W as a function of r in precracked SEN and PS specimens (Figure 17) at the same applied J shows that the process zone is smaller in the PS specimen, which correlates with the lower value of J_c in precracked PS specimens. This means that the energy absorbed in the process zone is a major contribution to the fracture resistance of the rubber.

CB REINFORCEMENT

The results just discussed show that CB increases the size and the energy density of the process zone, but not the local crack-tip strain at which crack initiation occurs. Thus it appears that the critical condition for crack initiation at the crack tip is strain controlled, and CB increases the energy required to achieve this. Related studies by x-ray diffraction and differential scanning calorimetry[21,22] shows that CB increases the strain-induced crystallization of NR in general and at the crack tip, and this is a significant sink for energy and a source of fracture resistance.

CONCLUSIONS

1) The J-integral is path independent in both PS and SEN specimens and equals the tearing energy.

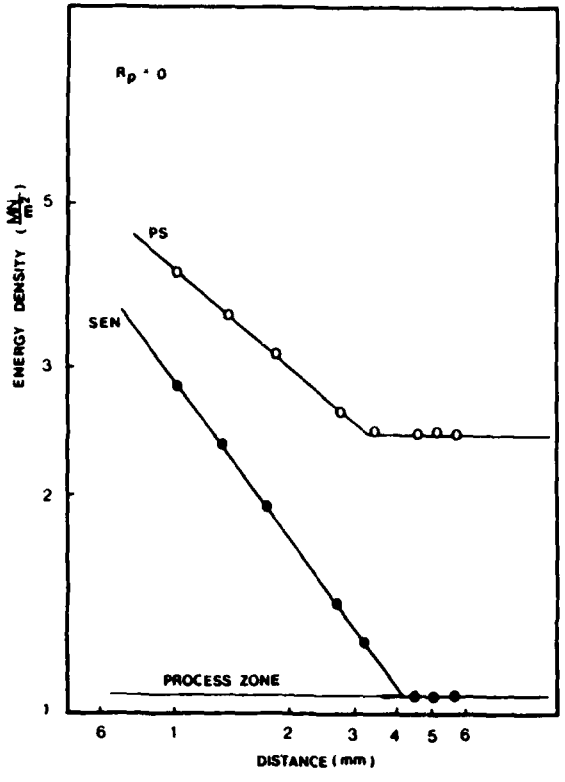

FIG. 17.—Energy density as a function of distance from the crack tip at intiation for PS and SEN specimens.

2) The critical *J*-integral at initiation is less in PS specimens than in SEN specimens, because the greater biaxial stress in PS restricts the process zone.

3) At initiation, the crack-tip radius, proportional to the local strain, is independent of CB.

4) The energy density within and the size of the process zone near the crack tip increase with CB; these are major contributions to CB reinforcement.

ACKNOWLEDGMENT

The financial support of the U.S. Army Research Office—Durham and the Cabot Foundation is gratefully acknowledged and appreciated. We would also like to thank Dr. S. Parhizgar and the BF Goodrich Co. for supplying the materials.

REFERENCES

[1] R. S. Rivlin and A. G. Thomas, *J. Polym. Sci.* **10**, 291 (1953).
[2] A. Ahagon, A. N. Gent, H. J. Kim, and Y. Kumagai, RUBBER CHEM. TECHNOL. **48**, 897 (1975).

[3] E. H. Andrews and E. W. Billington, *J. Mat. Sci.* **11**, 1354 (1976).
[4] J. R. Rice, *J. Appl. Mech.* **35**, 379 (1986).
[5] B. N. Leis and Akram Zahoor, *ASTM Spec. Tech. Publ.* **n700**, 65 (1980).
[6] R. M. McMeeking, *J. Mech. Phys. Solids* **25**, 357 (1977).
[7] S. J. Chang, *Z. Angew. Math. Phys.* **23**, 149 (1972).
[8] H. L. Oh, *ASTM Spec. Tech. Publ.* **n590**, 104 (1976).
[9] J. G. Williams, "Stress Analysis of Polymers," 2nd Edition, Halsted Press New York, 1980.
[10] N. W. Tschoegl, *J. Polym. Sci. Part A-1*, **9**, 1959 (1971).
[11] J. D. Eshelby, *Solid State Phys.* **3**, 79 (1956).
[12] R. F. Lee and J. A. Donovan, RUBBER CHEM. TECHNOL. **59**, 787 (1986).
[13] G. J. Lake and A. G. Thomas, *Proc. Roy. Soc. London, Ser. A* **300**, 108 (1967).
[14] G. J. Lake and P. B. Lindley, *J. Appl. Poly. Sci.* **9**, 1233 (1965).
[15] A. Ahagon and A. N. Gent, *J. Polym. Sci., Polym. Phys. Ed.* **13**, 1903 (1975).
[16] Yu. S. Zuyev, *Polymer Sci. USSR* **21**, 1315 (1980).
[17] E. H. Andrews, *Proc. R. Soc. London* **A227**, 562 (1964).
[18] J. R. Rice and G. F. Rosengren, *J. Mech. Phys. Solids* **16**, 1 (1968).
[19] J. Hutchinson, *J. Mech. Phys. Solids* **16**, 337 (1968).
[20] R. G. Stacer, L. C. Yanyo, and F. N. Kelly, RUBBER CHEM. TECHNOL. **58**, 421 (1985).
[21] D. J. Lee and J. A. Donovan, RUBBER CHEM. TECHNOL. **60**, 910 (1987).
[22] R. F. Lee and J. A. Donovan, unpublished results.

MICROSTRUCTURAL CHANGES IN THE CRACK TIP REGION OF CARBON-BLACK-FILLED NATURAL RUBBER*

D. J. LEE AND J. A. DONOVAN

MECHANICAL ENGINEERING DEPARTMENT, UNIVERSITY OF MASSACHUSETTS, AMHERST, MASSACHUSETTS 01003

INTRODUCTION

The reinforcement of rubber by carbon black (CB) is well known, and extensive research has been done to understand the phenomenon[1], but, the mechanism is not well understood. CB improves the fracture, fatigue, and wear resistance of rubber and, thus, CB probably affects the resistance of the rubber to crack growth. Understanding the fracture properties and CB reinforcement depends on understanding the microscopic as well as macroscopic aspects of rubber fracture. This study shows that CB increases the amount of strain-induced crystallization in the crack tip region, and suggests that in natural rubber (NR) this contributes significantly to crack growth resistance.

In rubber it is not sufficient to describe the effect of a notch or crack as a stress concentrator, because the stress concentration affects the molecular arrangement. In CB-filled NR the CB also orients with the stress field[2]. These stress-induced rearrangements create a crack tip region that has anisotropic mechanical properties which have been suggested as the reason for knotty tearing[3]. In the case of NR, because strain can induce crystallization (SIC), the crack tip region should be crystallized. SIC is an efficient process to dissipate strain energy and increase the fracture resistance. One study of the effect of CB on fracture properties by Glucklich and Landel[4] concluded that the energy density in the crack tip region determined the fracture resistance rather than the general energy stored in the specimen. While Stacer, Yanyo, and Kelley[5] have suggested that CB reinforces the crack tip by facilitating the development of an anisotropic structure over a larger volume. The results of this study show that CB expands the crack tip crystallization zone and increases the crystallinity.

EXPERIMENTAL PROCEDURES

MATERIALS

Materials used for this study were BFGoodrich NR compounds with 10 pph reclaim, and 0, 10, 25, and 40 pph HAF carbon black. Single-edge notch speci-

* Presented at a meeting of the Rubber Division, American Chemical Society, Montreal, Quebec, Canada, May 26-29, 1987. G.

mens were cut from 30 × 25 × 0.33 cm sheets. Precracks were made by cutting with a new razor blade. Specimens were loaded in tension on a special load frame and held with serrated grips to prevent slippage during testing. All tests were performed at room temperature.

X-RAY SYSTEM

8 keV monochromatic x rays with a wavelength (λ) of 1 nm were used for the diffraction experiments at the Cornell High Energy Synchrotron Source (CHESS). The x-ray beam had an approximate intensity of 2×10^{10} photons $mm^{-2}\ s^{-1}$ and was focused to 0.3 mm diameter with a pinhole collimator. Real time x-ray patterns could be obtained because of the high x-ray intensity.

The detector system consisted of a transmission ZnS (Ag) fluorescent screen coupled by fiber optics to a 40 mm diameter, 3-stage Varo image intensifier. The scattering pattern was recorded on video tape with 525 lines/frame and 30 frame per s. After the beam was focused in front of the crack tip, the specimen was moved relative to the beam, 1 or 2 mm to map the x-ray pattern in the crack tip region. Less than 4 s were used to obtain the x-ray pattern at each position

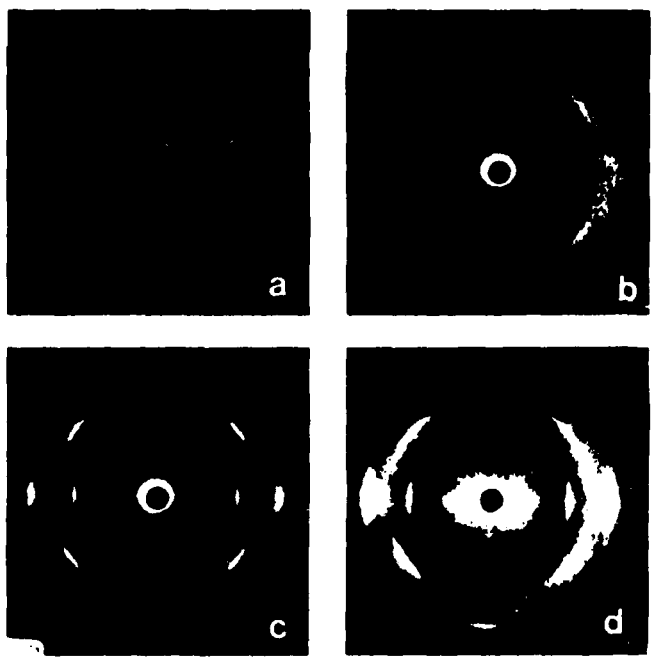

FIG. 1.—X-ray patterns showing the effect of extension and CB on the SIC at room temperature: (a) unfilled rubber without stretching ($\lambda = 1.0$), (b) unfilled rubber with $\lambda = 4.0$, (c) 10 pph CB-filled rubber with $\lambda = 4.0$, and (d) 25 pph CB-filled rubber with $\lambda = 4.0$

DIGITIZING SYSTEM AND ANALYSIS

Selected scattering patterns were digitized with a Micro Works Digisector Model DS-65A installed in an Apple IIe computer. This system could resolve 256 × 256 picture elements (pixels) and provide up to 64 levels of grey scale. The center of the beam and other geometric factors were determined by calibration with x-ray patterns from polystyrene and poplyethylene specimens. Then the diffraction pattern was divided into the upper and lower halves for digitizing because of computer limits. Also, the apparent recorded intensity on specific portions of the screen were corrected for the nonlinearity in detection system, background scatter, noise, etc. The digitized data were analyzed with a Vax-Cluster Engineering Computer.

MEASUREMENT OF CRYSTALLINITY

The digitized data, which give the x-ray intensity as a function of position, were analyzed by the method of Dumbleton and Bowles[6], which calculates the percent crystallinity (X_c) from the scattered intensity from the amorphous phase according to

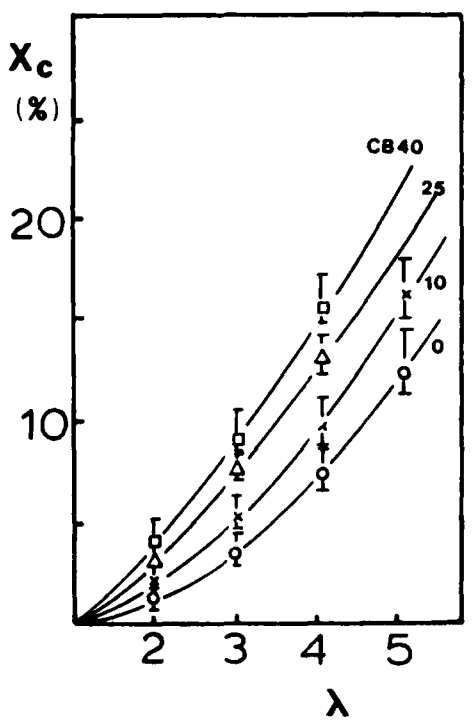

Fig. 2 — Degree of crystallinity (%) as a function of carbon black and extension ratio (λ).

$$X_c = \left[1 - \frac{I(s)}{I'(s)}\right] \times 100,$$

where $I(s)$ is the scattered intensity from the amorphous phase in the semi crystalline material and $I'(s)$ is the scattered intensity from the completely amorphous material. Also, more than half of these results were checked by the more comprehensive Ruland method[7], corrected for the stress induced uniaxial orientation[8]. The results did not differ significantly.

The crystalline orientation factor was not determined, but qualitative interpretation of the diffraction patterns suggests very high crystalline alignment with the stress axis[9].

MOLECULAR ORIENTATION IN AMORPHOUS PHASE

The orientation of the amorphous molecules was obtained from the anisotropy of the amorphous peak at $s = (22\ \text{pm})^{-1}$, where $s = 2\lambda^{-1} \sin\theta$, by the method of Hermans and Platzek[10] for uniaxially oriented materials, and the crystalline component was removed by the extrapolation technique of Mitchell[11].

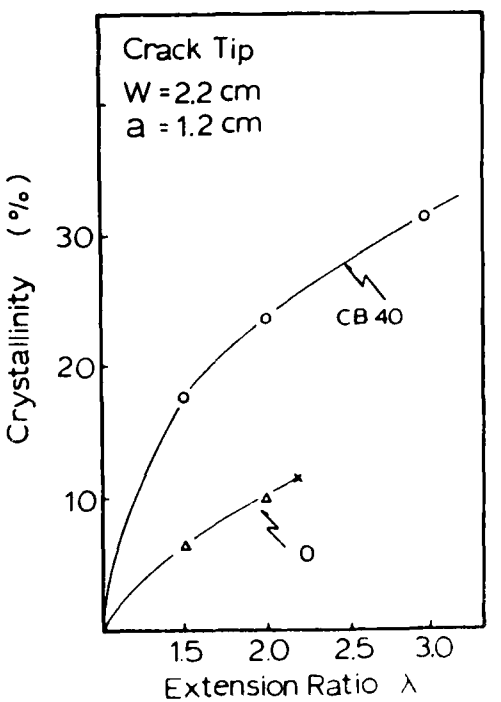

Fig. 3 — Degree of crystallinity (X_c) at the crack tip as a function of carbon black and extension ratio

RESULTS AND DISCUSSION

CRYSTALLINITY

Transmission x-ray patterns, shown in Figure 1, show qualitatively the effect of CB and extension on the degree of crystallinity. In the unstretched condition for all CB levels, there was only an amorphous halo, but in the stretched condition, a discrete diffraction pattern developed, whose intensity increased with CB content, indicating the formation of strain-induced crystals which were apparently facilitated by the CB.

To quantify the effect of extension and CB on the formation of SIC, two approaches were used: diffractometer studies for tensile specimens and digitizing of the x-ray patterns from the crack tip region. Both extension and CB increase the percentage of SIC in uniformly strained, uncracked specimens, Figure 2.

These results agree in general with the previously reported work of Gehman and Field[2] and Mitchell[11], but differ in detail at low extension ratios. For the rubber recipes used in this study, SIC appeared after small strains ($\lambda \approx 2$), while in the previously published work[9], unfilled rubber required an extension ratio of about 3.0 before SIC was detected. The reasons for this difference are not known.

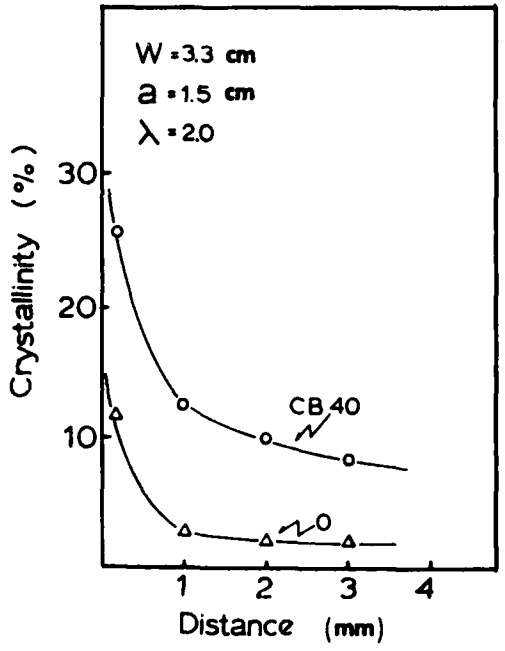

FIG. 4.—Crystallinity (X_c) as a function of distance from crack tip in unfilled and 40 pph carbon-black-filled rubber at $\lambda = 2.0$.

From the x-ray patterns obtained from the region at the crack tip, *i.e.*, the 0.3 mm x-ray beam was focused just ahead of the crack tip, the percent crystallinity was greater in CB-filled material and increased as the sample was stretched as shown in Figure 3. Therefore, at comparable crack tip conditions the degree of crystallization was significantly greater due to the presence of CB, similar to the results obtained with uniaxial strained specimens.

By moving the specimen relative to the X-ray beam, it was possible to measure the percent crystallinity, X_c, as a function of distance from the crack tip. Figure 4 shows the decrease in X_c with distance from the crack tip in a specific specimen when the extension ratio was 2.0.

Because a crack or a notch concentrates the stress and strain at the notch, Figure 5 is a log–log plot of X_c as a function of r, distance from the crack tip. Far from the crack tip, X_c is constant and increases with the CB content. Close to the crack tip, X_c decreases with r. The intersection of the constant X_c region with the increasing region can be used to define the size of a highly crystallized zone (r_z) or process zone. Figure 6 shows that the size of the process zone increases with global extension of the specimen. This process zone is analogous to the plastic zone commonly observed in metals at the tip of stressed cracks

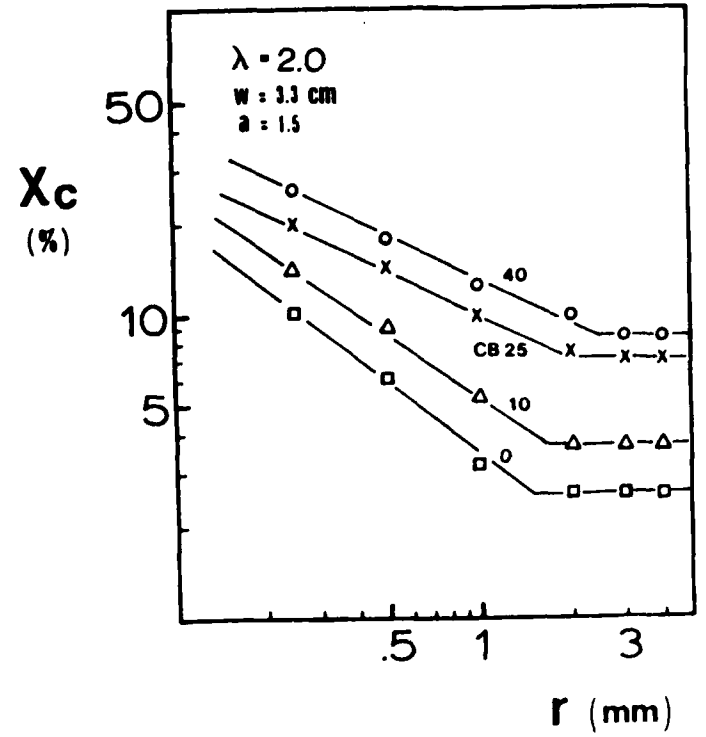

FIG. 5.—Log–log plot of crystallinity (X_c) as a function of distance (r) from the crack tip.

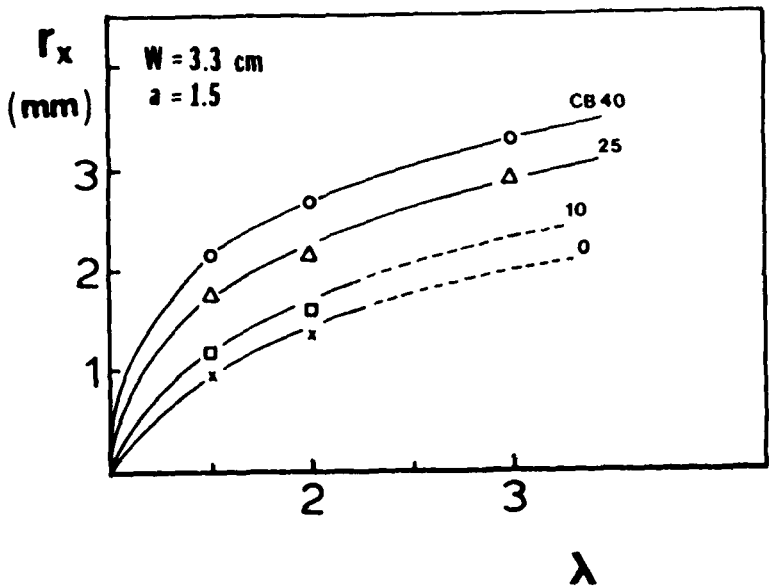

Fig. 6.—Highly crystallized zone (r_x) as a function of CB and extension ratio (λ).

ne difference, however, is that, in metals, the plastic zone is not reversible, it if the stress is removed from the cracked NR, the crystals melt. The crys-llization and melting process may not be truly time independent, but with the ility to do real time experiments at CHESS, the time dependence at room mperature was not detectable within 20 min.

In the crack tip region, the stress and strain vary with distance from the ack tip, therefore, neither are appropriate parameters to describe the stress d strain field; the appropriate parameter, as has been shown convincingly r linear elastic materials, is G, the strain energy release rate or the stress tensity factor k which is related to G. In nonlinear elastic materials, Thomas d coworkers 30 years ago suggested the tearing energy, T, which is similar to but for nonlinear elastic materials. Or, because of concerns about inelastic havior the J-integral, which we have shown by evaluating its line integral is uivalent to T[13]. However, following conventional experimental determina-n of T and J based on the energy rate interpretation, there may be some fferences[14]. Nevertheless, the appropriate parameter to describe the state of ress and strain around a crack is T or J, therefore, it is appropriate to replot gure 6 for data obtained at similar applied J, the crack driving force, instead the same global extension ratio. This is done in Figure 7. The appearance is nilar to Figure 6, but comparison of the process zone size, r_x, in the different 3 rubbers shows that the size of the highly crystallized zone at the crack tip creases with CB at the same crack driving force.

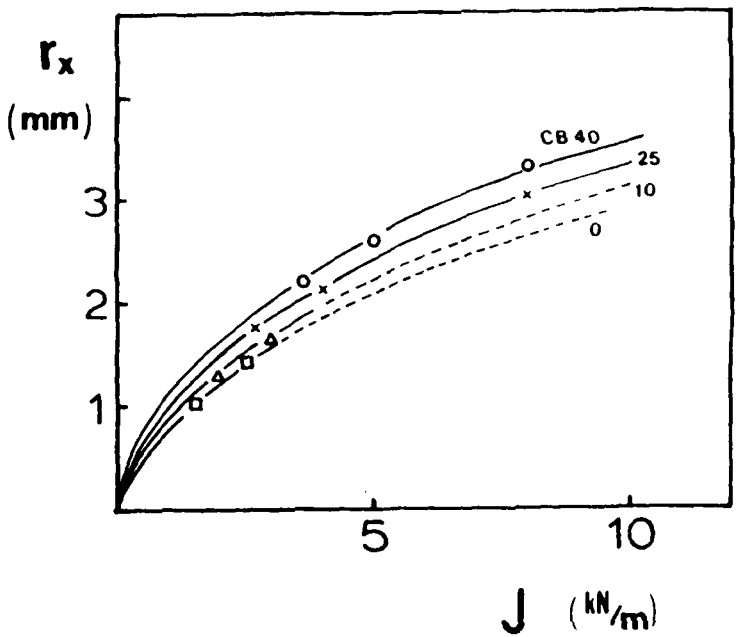

Fig. 7.—Highly crystallized zone (r_x) as a function of CB and J-values

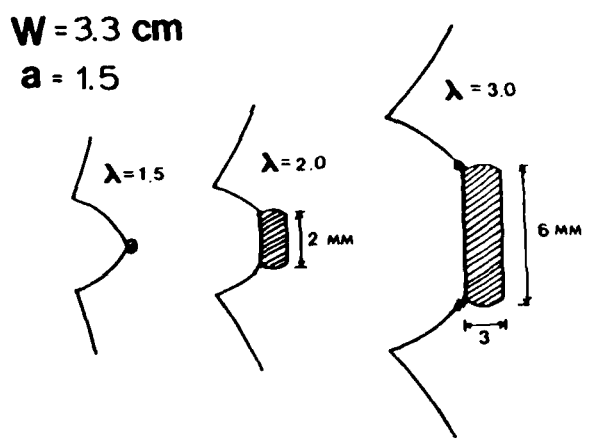

Fig. 8. Schematic of the highly crystallized zone size at the crack tip and crack blunting with increased extension

The effect of the crack driving force, J, on the size of the process zone is shown in Figure 7. This graph was obtained by correlating r_x with data that determined J as a function of λ, the extension ratio[14]. Thus, at comparable crack driving forces, the process zone increases with CB. Since the volume of this zone is proportional to the energy dissipated by crystallization in the crack tip region, the fracture resistance increases. CB not only increases the process zone volume, but also the extent of crystallization, which accounts for the higher strain-energy density in the process zone[13].

The dependence of the extent of crystallinity of distance from the crack tip in the process zone (Figure 5) depended on the CB level and the extent of overall strain. The slope of these curves varied between −1 and −0.5, which is similar to the variation of the strain-energy density and appears to be related to the degree of crack tip blunting[13].

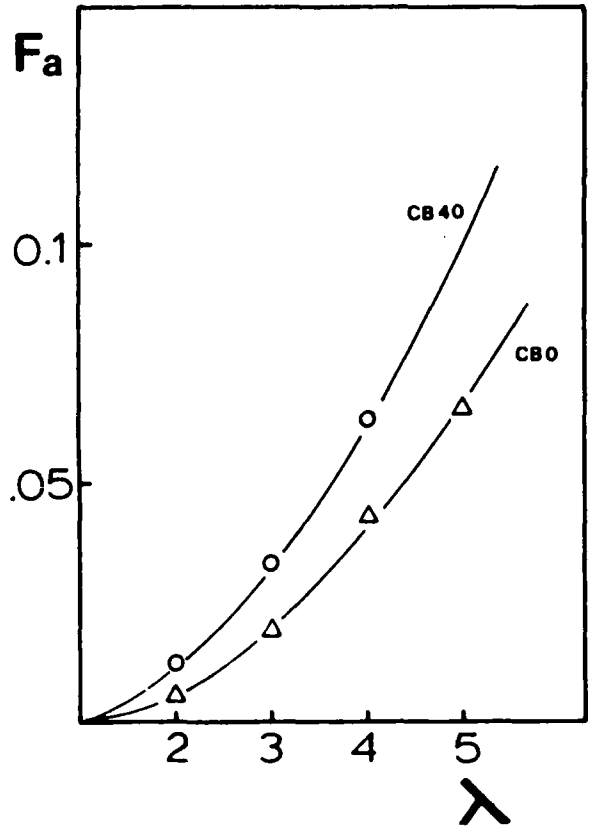

FIG. 9.—Molecular orientation (F_a) of noncrystalline component as a function of carbon black and extension ratio.

Figure 8 shows the approximate shape of the highly crystallized zone at the crack tip before crack initiation. Since this rubber does not fail catastrophically at initiation, but the crack tip region blunts, and based on qualitative interpretation of the diffraction patterns the shape of the highly crystallized zone is as shown in Figure 8, the highly crystallized zone also blunts.

AMORPHOUS ORIENTATION

As well as causing crystallization, the stress–strain fields cause the amorphous molecules to become less randomly oriented. F_a, the molecular orientation factor, from the x-ray data, increased with extension, and CB facilitated the orientation in a tensile specimen (Figure 9), and at the crack tip (Figure 10). However, in the tensile specimen, the orientation appears to increase with CB and extension ratio, but at the crack tip, F_a is nearly constant for CB contents greater than or equal to 10 pph. There is a difference in stress state between a

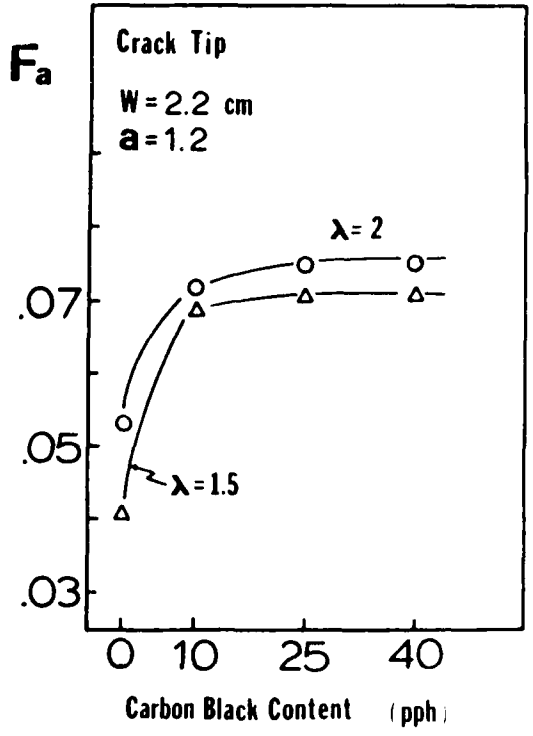

FIG. 10.—Molecular orientation (F_a) of noncrystalline component at the crack tip as a function of carbon black and extension ratio.

tensile specimen and at the crack tip: the tensile specimen is uniaxially stressed, while the crack region just in front of the crack surface is in a state of biaxial stress. The net effect of the state of stress on the orientation factor is not known but may contribute to its apparent saturation. Also, the coordinated orientation of the CB and molecules in the crack tip stress field could tend to reach a limiting value.

The CB-assisted orientation of the amorphous molecules could help explain the effect of CB on the SIC, in the sense that the greater the orientation, the easier should be crystallization.

The variation of F_a with distance from the crack tip shown in Figure 11, suggests that there is a common value about 0.02 mm in front of the crack that is independent of the crack driving force (which is proportional to λ). This maximum value of F_a is similar to what Mitchell[11] found in unfilled NR at an extension ratio of about seven.

CARBON BLACK REINFORCEMENT

The effect of CB content on the stress-extension ratio curve is shown in Figure 12, which shows the well-known increase in modulus and the energy required for deformation (the area under the curve) with CB. CB also increases

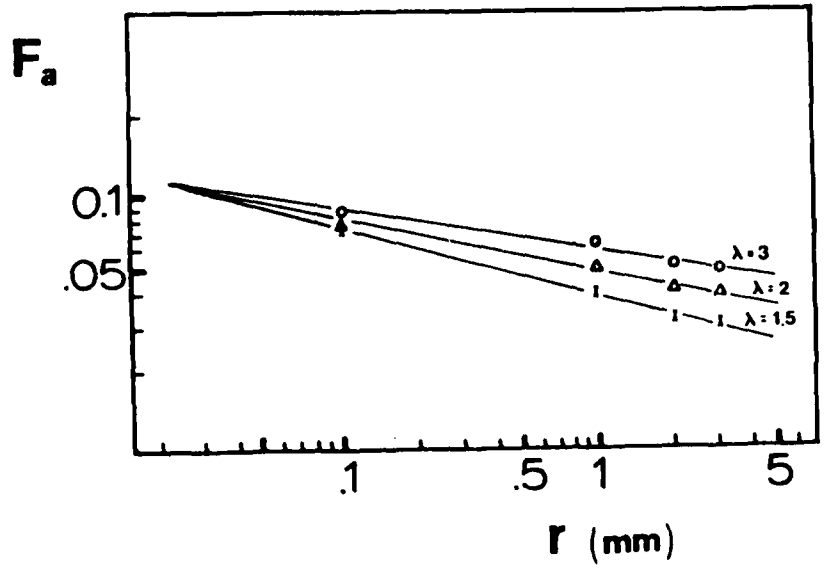

Fig. 11.—Log-log plot of molecular orientation (F_a) of noncrystalline component at the crack tip as a function of carbon black and extension ratio

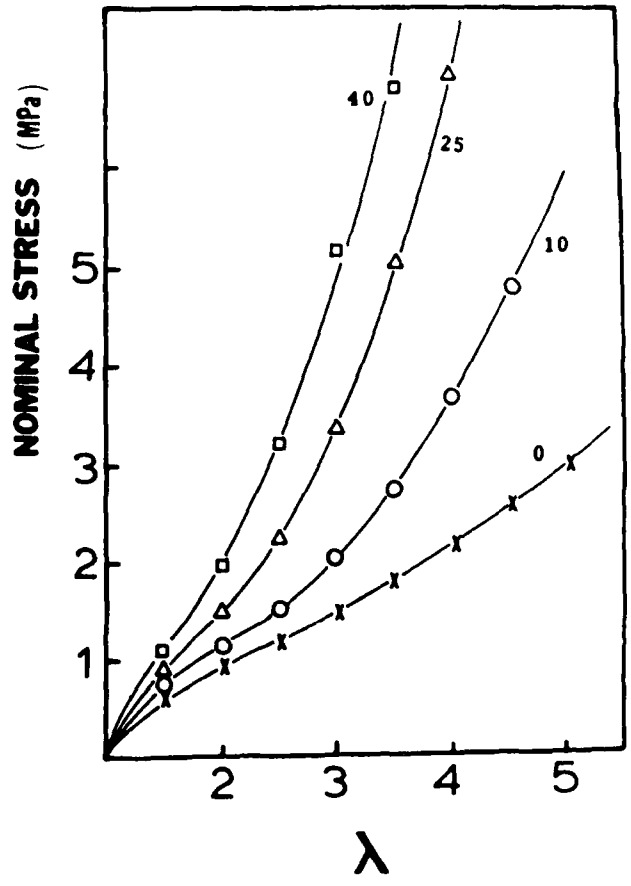

Fig. 12.—Stress-extension ratio curves for different carbon black content

the critical J for crack initiation and ultimate rupture from precracked specimens, Figure 13[1]. The results of this study suggest that an apparently overlooked effect of CB on the extent of crystallization, originally reported by Gehman and Field[12], makes a major contribution to crack initiation and rupture resistance by increasing the extent of crystallinity and increasing the size of the crystallized zone at comparable crack driving forces. SIC absorbs deformation energy in proportion to the amount of transformation, therefore CB allows more energy to be dissipated through the transformation. Hence, CB-filled rubber requires more energy to establish the critical conditions in the crack tip. Both the increase in percent crystallinity and the increase in size of the crystallized zone increase the energy required for initiation or rupture.

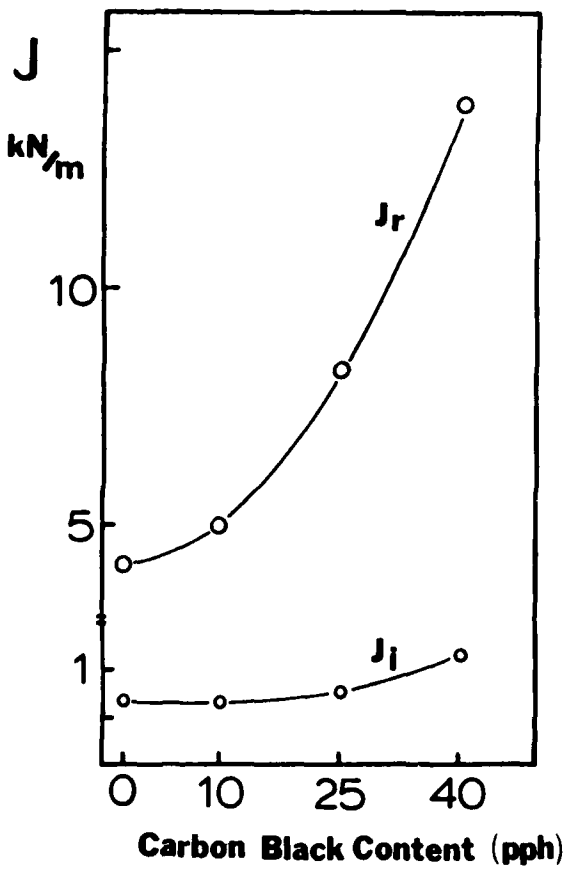

FIG. 13.—Critical *J*-values for initiation and final rupture as a function of carbon black content.

CONCLUSIONS

CB facilitates strain-induced crystallization and increases the size of the crystallized zone at the stressed crack tip. Both effects are major reinforcement mechanisms that increase the fracture resistance of CB-reinforced NR.

ACKNOWLEDGMENTS

The financial support of the U.S. Army Research Office—Durham is gratefully acknowledged and appreciated. Also, we would like to thank Dr. S. Parkizgar of the BFGoodrich Co. for the materials, and Prof. E. J. Kramer and Dr. M. H. Ree for their help at CHESS.

REFERENCES

[1] A. C. Patel and W. A. Brown, *Rubber World* **194**(1), 20 (1986).
[2] A. E. Medalia, *Rubber World* **168**(5), 49 (1973).
[3] L. Mullins, "Effects of Fillers in Rubber" in "Chemistry and Physics of Rubber-like Substances," L. Bateman, Ed., MacLaren & Sons, Ltd., London,, John Wiley & Sons, New York, 1963, chap. 11, p 301.
[4] J. Glucklich and R. F. Landel, *J. Appl. Polym. Sci.* **20**, 121 (1976).
[5] R. G. Stacer, L. C. Yanyo, and F. N. Kelly, RUBBER CHEM. TECHNOL. **58**, 421 (1985).
[6] J. H. Dumbleton and B. B. Bowles, *J. Polym. Sci., Part A* **2 4**, 951 (1966).
[7] W. Ruland, *Acta Crystallogr* **14**, 1180 (1961).
[8] C. R. Desper and R. S. Stein, *J. Polym. Sci., Part B* **5**, 893 (1967).
[9] L. E. Alexander, S. Ohlberg, and G. R. Taylor, *J. Appl. Phys.* **26**, 1068 (1955).
[10] P. H. Hermans and P. Platzek, *Kolloid Z.* **88**, 68 (1939).
[11] G. R. Mitchell, *Polym. J.* **25**, 1562 (1984).
[12] S. D. Gehman and J. E. Field, RUBBER CHEM. TECHNOL. **14**, 85 (1941).
[13] H. Liu, R. F. Lee, and J. A. Donovan, RUBBER CHEM. TECHNOL. **60**, 893 (1987).
[14] D. J. Lee and J. A. Donovan, *Int. J. Fract.*, **34**, 41 (1987).

International Journal of Fracture 34: 41-55 (1987)
© Martinus Nijhoff Publishers, Dordrecht - Printed in the Netherlands

Mixed mode I and II fracture of carbon black filled natural rubber

D.J. LEE and J.A. DONOVAN
Mechanical Engineering, University of Massachusetts, Amherst, MA 01003, USA

Received 13 June 1986; accepted in revised form 20 March 1987

Abstract. The J-integral was used to characterize initiation and rapid fracture under mixed mode loading conditions in carbon black filled natural rubber. The total critical J was geometry dependent, but the J analysis partitions the energy into that needed locally in the crack tip region and in the bulk. The critical conditions for pure mode II loading could not be determined because of buckling of the specimen; however, values obtained by extrapolation show J_{IIc} to be about twice J_{Ic}. The relation

$$\frac{J_I}{J_{Ic}} + \frac{J_{II}}{J_{IIc}} = 1$$

describes the failure conditions under mixed mode loading conditions.

1. Introduction

Mixed mode crack growth is due to the superposition of two or three loading modes: I-tension, II-shear and III-torsion. Most experimental fracture research has been concerned with mode I loading since this is the most common mode for crack propagation. But, initiation and propagation of cracks in, practical situations can be mixed mode; consequently, mixed mode crack initiation and growth has recently received considerable analytical and experimental study [1–5].

Two practical examples of where mixed mode crack growth may be important are in Suh's [6] delamination theory of wear and Champ, Southern and Thomas's [7] theory for abrasive wear of rubber. Both recognize the relevance of a fracture mechanics description for the complex processes. However, it is believed that abrasive wear could be due to mixed mode crack growth rather than only mode I, especially in the case of viscoelastic materials like rubber. Despite the practical importance for wear and fracture of rubber products, there appears to be no information available on the behavior of rubbers under such conditions.

For rubber the fracture properties are strongly influenced by stress induced orientation of the molecular chains in the material. Since the crack tip stress field for each loading mode differs, the stress induced molecular and filler orientation creates different anisotropic crack tip zones. This anisotropy is expected to affect fracture, fatigue and wear properties. For example, Gent and Kim [8] showed that the tearing energy in mode I was half that in mode III. Also, they showed a significant effect of pre-stretching on fracture properties of carbon filled rubber, and concluded that the change in fracture energy was due to deformation induced changes in microstructure.

These stress induced microstructural changes may lead to anisotropic mechanical properties in the crack tip region that depend on the stress state and hence the loading mode. Data on

these changes in microstructure and fracture properties as a function of loading mode are needed for better understanding of fracture and reinforcement in rubber and its relation to failure and wear processes.

In a previous paper [9], it was shown that the J-integral concept can characterize the initiation and final rupture of rubber. The definition of the J-integral is exactly the same as the definition of the tearing energy, T

$$J = T = -\frac{1}{B}\frac{dU}{da} \tag{1}$$

where B is the thickness of the specimen, dU is the energy released when the crack is increased by da. And, for linear elastic materials both are equivalent to Griffith's failure criterion, and can be interpreted as the energy required to form new fracture surfaces. The tearing energy has successfully characterized non-linear elastic rubbers [10, 11], but for non-elastic rubbers the critical tearing energy depends on specimen geometry [12, 13].

The J-integral for initiation in non-elastic rubber also depends on specimen geometry [9], but it was possible to separate the energy required to deform the bulk of the specimen and that required to form the new surfaces. This separation of energy was based on the experimental observation that the extension at initiation for different sized cracks as a function of specimen length had a common intercept at zero length and therefore, was independent of specimen geometry. This extension was taken as a local characterization of crack initiation and related only to the energy required to form the new crack surfaces. The remaining energy was interpreted as absorbed into the bulk of the specimen. This analysis was similar to that used by Agarwal et al. [14] in their application of the J-integral to composites.

The J-integral can be separated into components for the mixed mode problem [15]; Ishikawa et al. [16] proposed an analytical method for separating mode I and II such that $J = J_I + J_{II}$, when both J_I and J_{II} are path independent integrals in a two-dimensional linear elastic deformation field. For a non-linear elastic body, J_I and J_{II} may be interpreted as the crack extension force under pure mode I or pure mode II deformation respectively [17].

The objective of this study was to evaluate the fracture properties of a commercial carbon black filled natural rubber under mixed mode loading conditions by using the previously established J-integral analysis.

2. Material

The material used for this study was B.F. Goodrich compound number 17170, natural rubber with 10 pph reclaim, 40 pph HAF carbon black. Test specimens were cut from 30 cm × 25 cm × 0.33 cm sheets with a cutting mold.

3. Experimental procedures

Single edge notch specimens (Fig. 1) of different lengths (l), widths (ω), pre-crack sizes (a) and angles (β) were tested to determined J values for initiation and final rupture. All

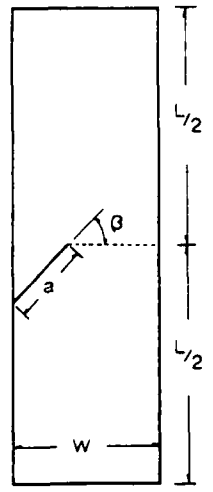

Fig. 1. Specimen geometry and associated dimensions.

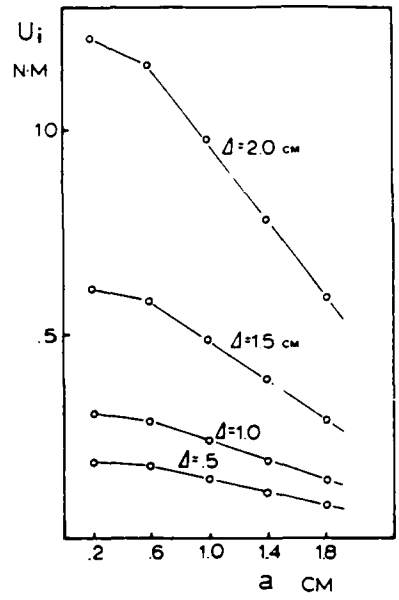

Fig. 2. Stored energy as a function of pre-crack size at different extensions.

Table 1.. Specimen dimensions

Length (cm)	Width (cm)	Pre-crack length (acos β) (cm) (see Fig. 1)
4	1.1	0.2
7	2.2	0.6
10	3.3	1.0
13	4.4	1.4
16		1.8

possible combinations of the dimensions of the specimens were tested and the dimensions are given in Table 1. Preliminary tests showed that the rubber sheets were isotropic. The data reported are average values for more than three tests of each geometry. The tests were done at room temperature and at an extension rate of 1 cm/min in an Instron tensile machine with serrated grips to prevent slipping.

Pre-cracks were made by cutting the rubber along one edge with a new razor blade. The surfaces of the pre-crack were coated with a water based white ink (Wite-out®). After the ink dried the excess was removed to aid identification of crack initiation. Crack initiation was easily identified by observation of the crack tip region at a magnification of 10×.

The test method for determination of the critical J at initation or rupture was based on the energy rate interpretation of J [18] given by (1). The total energy U, the area under the load-extension curve, is shown in Fig. 2 as a function of pre-crack length at various values of extension Δ. The slope of these curves (dU/da) is proportional to J and is shown in Fig. 3 for specimens with different lengths as a function of extension (3a) and extension ratio (3b).

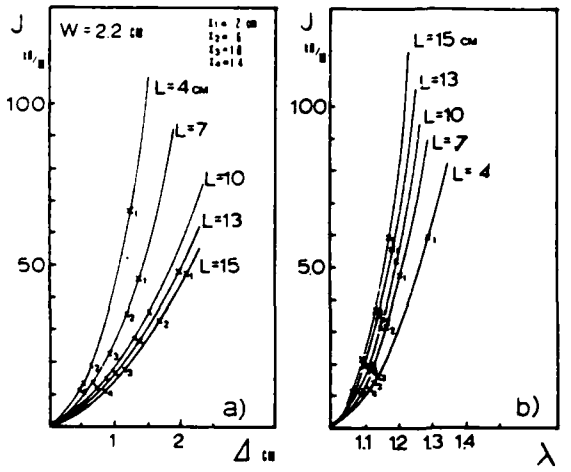

Fig. 3. J-integral for initiation as a function of (a) extension and (b) extension ratio for different length specimens.

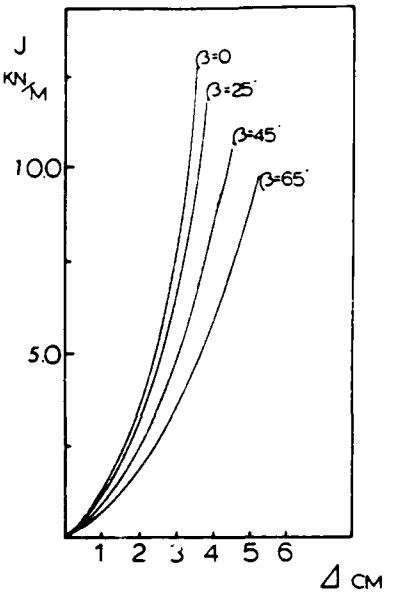

Fig. 4. J-integral as a function of extension for different pre-crack angles (β).

4. Results

Initial loading of the pre-cracked specimen slightly blunts the razor cut until a crack initiates. The initiation event was not apparent on the load-extension curve, but the load and extension at initiation were easily correlated by visual observation of the crack tip. Blunting, with little stable crack growth, continued with extension until unstable crack growth fractured the specimen. In general, the extent of slow crack growth increased as the pre-crack angle (β) increased. Moreover, visual observation of initiation clearly showed that the loading mode affects initiation because the crack opening displacement and crack tip region differed significantly with pre-crack angle (β). However, visually final rupture appeared as if due to only mode I loading.

The total J value was a function of the specimen length (Fig. 3), and of the pre-crack angle (Fig. 4). The critical values of J at initiation and rupture were determined from Fig. 4 for values of extension at initiation (J_i) or rupture (J_r) as a function of pre-crack angle. J and J_r were independent of the specimen length, but depended on β and the pre-crack size (Figs. 5 and 6). Therefore, one of the conditions for a valid fracture characterizing parameter (that the parameter be independent of geometry, including pre-crack size) is apparently not satisfied.

However, the critical extension at initiation or rupture was a linear function of specimen length and the data for different pre-crack sizes extrapolated to a common intercept. Representative results are shown in Fig. 7 for initiation ($\beta = 65$) and for rupture in Fig. 8 ($\beta = 45$). Similar results were obtained for pure mode I loading [9]. Δ_i or Δ_r is the total extension required to initiate or rupture a specimen, respectively. Some of this deformation occurs in the crack tip region and some of it occurs remote from the crack tip; a greater

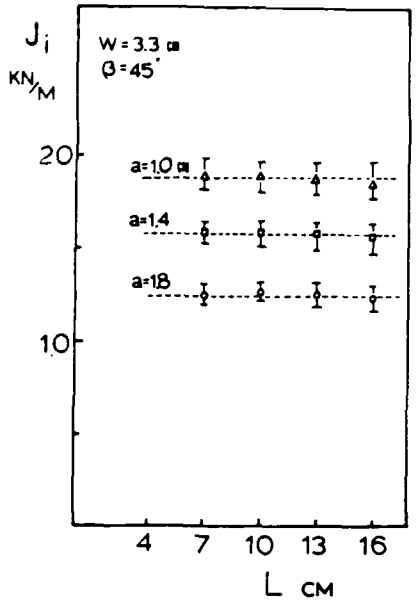

Fig. 5. *J*-integral for initiation as a function of specimen length and pre-crack size.

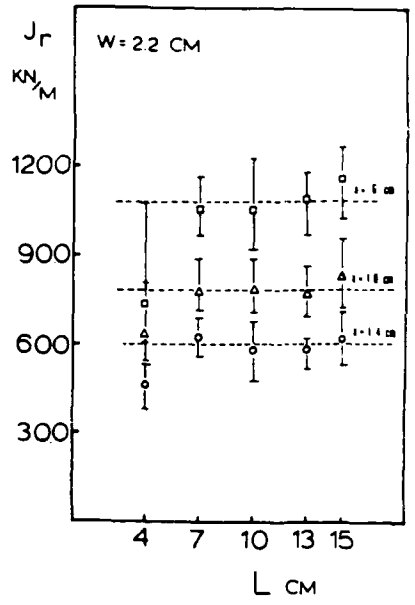

Fig. 6. *J*-integral for rupture as a function of specimen length and pre-crack size.

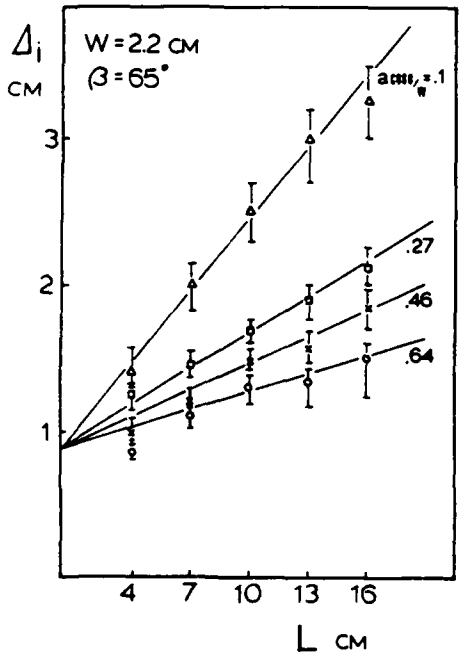

Fig. 7. Critical extension for initiation as a function of specimen length and pre-crack size (acos β/w).

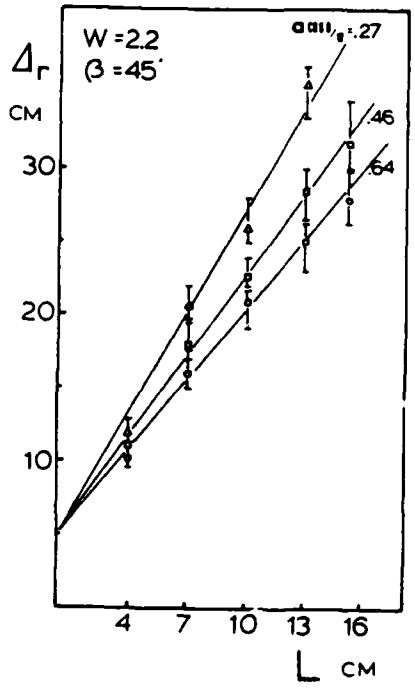

Fig. 8. Critical extension for rupture as a function of specimen length and pre-crack size (acos β/w).

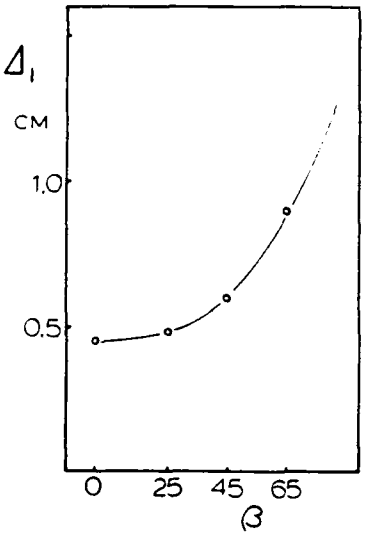

Fig. 9. Critical extension at initiation in a "zero" length specimen as a function of pre-crack angle (β).

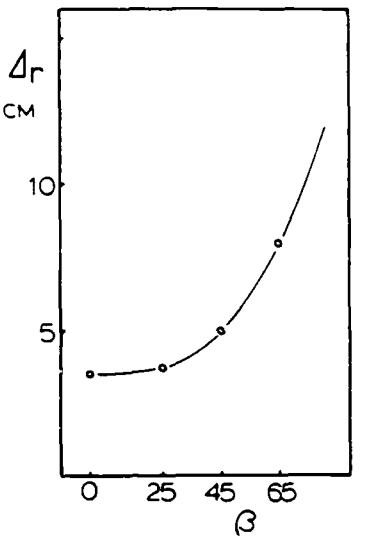

Fig. 10. Critical extension at rupture in a "zero" length specimen as a function of pre-crack angle (β).

percentage of the deformation occurs away from the crack tip in longer specimens. But, the intercept represents the displacement that must occur in the crack tip region. Extrapolation of the total displacement to zero length allows separation of the crack tip displacement due to deformation in the crack tip region to initiate crack growth or fracture the specimen from that which occurs in the bulk of the specimen. This critical extension for a zero length specimen is a characteristic of an isolated crack including its crack tip region, but not the bulk of a cracked specimen.

The critical extension for the zero length specimen for initiation and rupture are shown in Fig. 9 and Fig. 10 respectively as a function of β. The J-value obtained at the critical extension in the hypothetical zero length specimen represents the critical energy release rate in the crack tip region to initiate a crack or to fracture the specimen under the given conditions independent of specimen length. These values from Fig. 5 are shown in Fig. 11 for initiation and in Fig. 12 for final rupture as a function of crack angle. The values were obtained by converting the extension for the hypothetical zero length specimen to the extension ratio for the actual length of the tested specimen $\lambda_0 = (\Delta + l_0)/l_0$. With this λ_0, the J value representing the critical strain energy release rate in the crack tip region was found for all specimen lengths tested. The additional energy is stored in the specimen away from the crack tip region. That is the total J value is not geometry independent, but the material property that characterizes the initiation can be determined by extrapolation of the critical extension to a specimen of zero length.

The total energy $U(a)$ stored in the pre-crack specimen at initiation as a function of crack length is shown in Fig. 13. These data for a specific pre-crack size can be extrapolated as straight lines to a zero length specimen and this energy also can be interpreted as the energy required in the crack tip region to initiate the crack. These data are shown in Fig. 14 as a function of (a/w); since J is defined as $-1/B\ (\mathrm{d}U/\mathrm{d}a)$ then the slope of U for $l = 0$ as a function of pre-crack length would be equivalent to the critical J-values for the crack tip

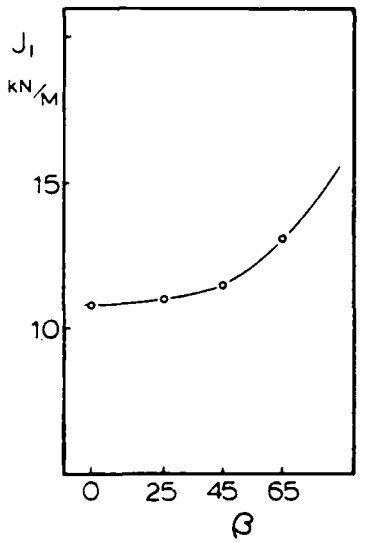

Fig. 11. Critical J values for the crack tip region to initiate the crack as a function of pre-crack angle (β).

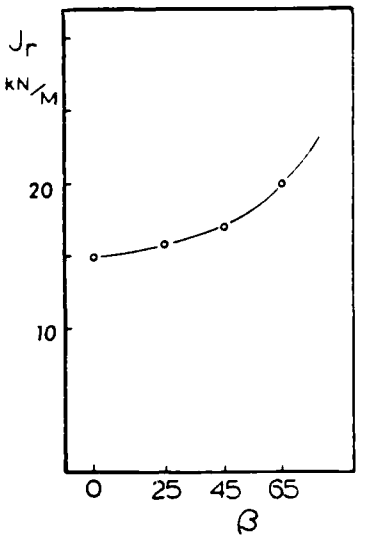

Fig. 12. Critical J values for the crack tip region to rupture the specimen as a function of pre-crack angle (β).

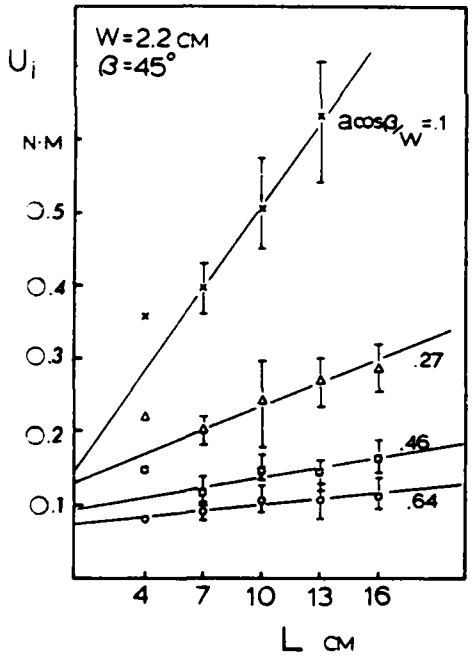

Fig. 13. Total stored energy as a function of specimen length and pre-crack size (acos β/w) for $\beta = 45°$.

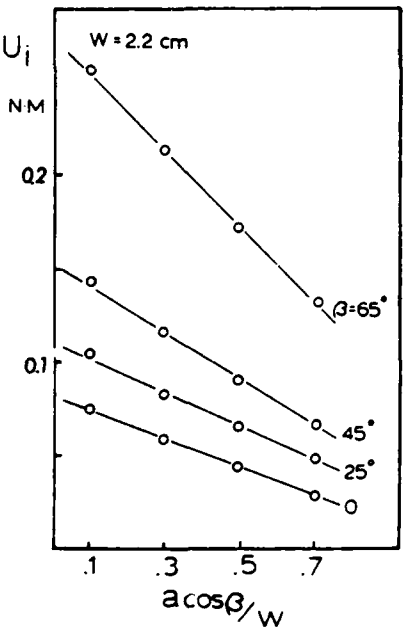

Fig. 14. Total stored energy at initiation in a "zero" length specimen as a function of pre-crack angle (β).

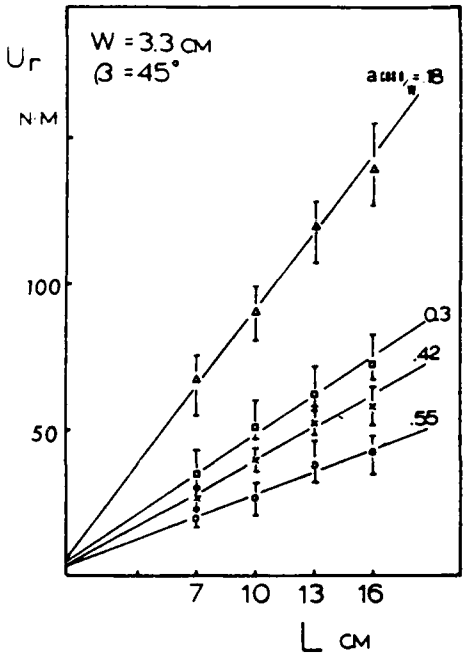

Fig. 15. Total stored energy at rupture as a function of specimen length and pre-crack size for $\beta = 45$ deg.

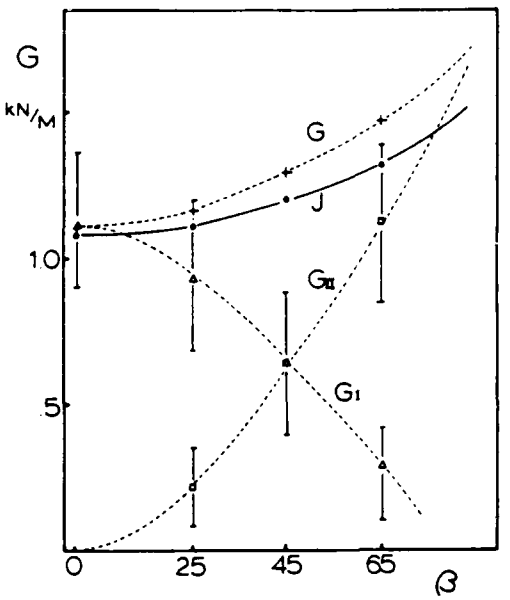

Fig. 16. The calculated strain energy release rate (G) at initiation as function of pre-crack angle (β) for comparison with measured critical J values.

Table 2. J for initiation as a function of crack angle (kN/m)

Analysis\angle	$\beta = 0$	$\beta = 25$	$\beta = 45$	$\beta = 65$
Displacement	1.08 ± 0.02	1.11 ± 0.03	1.20 ± 0.03	1.32 ± 0.05
Energy	1.0 ± 0.05	1.15 ± 0.05	1.25 ± 0.1	1.35 ± 0.15

Table 3. J for rupture as a function of crack angle (kN/M)

Analysis\angle	$\beta = 0$	$\beta = 25$	$\beta = 45$	$\beta = 65$
Displacement	15.0 ± 0.5	16.0 ± 0.5	17.5 ± 1.5	20.0 ± 1.5
Energy	17.5 ± 2	19.5 ± 3	21.5 ± 4	26.5 ± 6

region at each angle (β) to initiate the crack. The derived values are listed in Table 2 and are comparable to data from the displacement analysis (Fig. 12). Therefore, both methods of analyzing the data give approximately the same values for critical energy release in the crack tip region as a function of β. These values of J can be interpreted as the material property that characterizes the materials' resistance to initiating crack growth under combined loading (I + II) conditions.

Similar to the case of initiation, the total energy stored in the specimen at fracture is plotted as a function of specimen length in Fig. 15 for $\beta = 45$. The data at zero length give approximately the same values for J as the analysis based on displacement and are as shown in Table III. Also, this J-integral analysis provides a measure of the energy required to rapidly propagate a crack that is a function of the specimen length, but again this total

energy can be partitioned into that required in the crack tip region as independent of the specimen geometry and that stored away from the crack tip.

5. Discussion

The results clearly show that the presence of a mode II component increases the critical J required for initiation and final rupture, and this implies a difference in fracture properties, which probably are associated with microstructural changes. X-ray diffraction data obtained at the Cornell High Energy Synchrotron Source of the crack tip region show that the extent of crystallinity and orientation greatly differ for pure mode I and mixed mode loading [19].

It was not possible to measure J_{IIc} experimentally because a center cracked specimen with the crack parallel to the load or other pure mode II specimens buckled extensively. But J_{IIc} is of engineering interest and may be relevant to wear of rubbery materials, therefore estimates of J_{IIc} were obtained from the analyses that follow.

6. Initiation

The increase in J_c for initiation with β can be separated into J_I and J_{II} components according to two approaches:

(1) Compliance

Assume that the critical J for initiation is equivalent to the critical strain energy release rate (G) for linear elastic materials which is independent of crack length and specimen geometry then [20, 21]

$$G = G_I + G_{II}.$$

Also, G does not depend on the loading system and is related to the compliance C by

$$G = \frac{P^2}{2B}\frac{\partial C}{\partial a}$$

where P is the load, B the thickness and C is Δ/P of the cracked specimen.

From the geometry of the loading specimen the mode I and II components of the load are:

$$P_I = P\cos\beta \quad \text{and} \quad P_{II} = P\sin\beta.$$

Therefore,

$$G_I = G(\beta)\cos^2\beta \quad \text{and} \quad G_{II} = G(\beta)\sin^2\beta.$$

In order to calculate $G(\beta)$ the compliance of the rubber samples was calculated from the critical displacement and the corresponding load as a function of β and a. Based on these

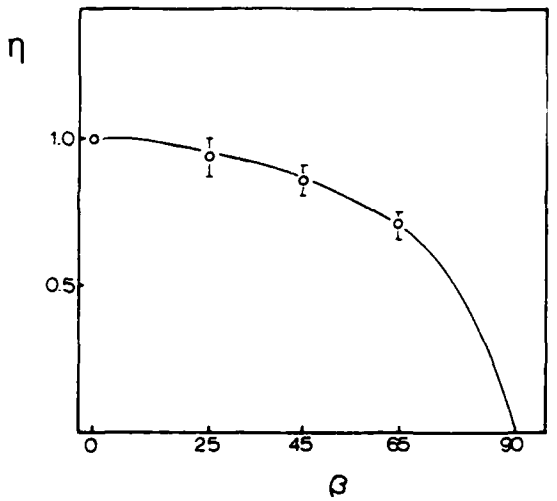

Fig. 17. The ratio of crack opening displacement in mixed mode to pure mode I at the critical extension for a "zero" length specimen.

assumptions, the components of G and the total G are compared to the measured critical $J(\beta)$ in Fig. 16. The derived values of G show a large amount of scatter, but the similarity of the β dependence of G and J supports the analysis.

But because of the non-linear viscoelastic deformation of the rubber, the compliance calculation is certainly only approximate. Therefore another approximation was analyzed.

(2) Crack Opening Displacement (COD)

It is well established that J_I is proportional to the COD (δ) [22]. Since mode I loading tends to open the crack and mode II does not, any crack opening can be attributed to mode I loading. Therefore, the components of J can be derived if δ is known at the critical displacement for initiation for the hypothetical zero length specimen as a function of β for all specimen lengths, widths and crack sizes. δ decreased with β and was a function of specimen length and width, but a common curve was attained by plotting η, the ratio of $\delta_{I,II}$ to δ_{IC} (Fig. 17), that was independent of geometry; based on these experimental results and since it is known that J_I is proportional to δ then

$$J_I = \eta J_{Ic}.$$

Ishikawa et al. [16] analytically showed that

$$J_{I,II} = J_I + J_{II}$$

then it follows that

$$J_{I,IIc} = \eta J_{Ic} + \kappa J_{IIc}$$

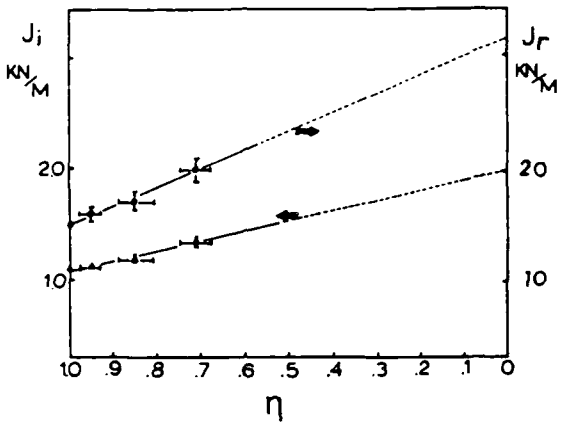

Fig. 18. Critical J values at initiation and rupture for mixed mode as a function of crack opening displacement ratio (η).

where κ is an unspecific proportionality factor. $J_{I,II}$ as a function of η is shown in Fig. 18 and a linear extrapolation of the data gives the critical J_{IIc} as 1.9 kN/m and $\kappa = (1 - \eta)$.

Failure criterion for a crack under combined loading has been expressed in terms of the stress intensity factor in the following form

$$\left(\frac{K_I}{K_{Ic}}\right)^a + \left(\frac{K_I}{K_{Ic}}\right)^b = 1$$

where a and b are constants. Values of a and b reported in the literature for different materials range from one to two [23–25].

Since J_{Ic} and J_{IIc} also are material constants an analogous failure criterion could be

$$\left(\frac{J_I}{J_{Ic}}\right)^a + \left(\frac{J_{II}}{J_{IIc}}\right)^b = 1.$$

To determine the form of this function the derived data are shown in Fig. 19 showing that a and b equal to one is a reasonable fit.

7. Fracture

After initation of crack growth, the crack tip blunts with limited crack growth by peeling of surface layers. The extent of peeling was limited, but increased with increasing β and decreasing a. Eventually, rapid crack propagation occurred at an angle to the original crack. The propagation angle depended on the original crack length and pre-crack angles; in general, the propagation angle is smaller for long pre-cracks and small pre-crack angles (β).

In specimens with long cracks, ten percent of cracks propagated in two steps. Also, for short cracks and large β, final rupture conditions were more scattered. This is believed to be due to the large difference between the total J and that required in the crack tip region as pre-crack size decreases (acos $\beta/w < 0.5$). Figure 7 shows that J_r depends on the initial crack size (acos β/w), but is independent of specimen length similar to the situation for initiation. The critical J_r increases more than 30 percent for β increasing from 0 to 65 deg (Fig. 13).

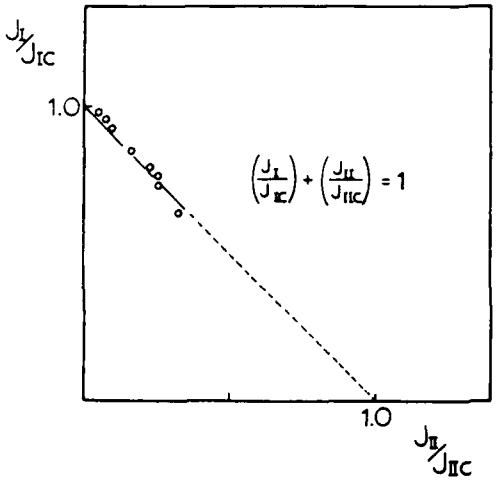

Fig. 19. Empirical fracture criteria relationship for mixed mode.

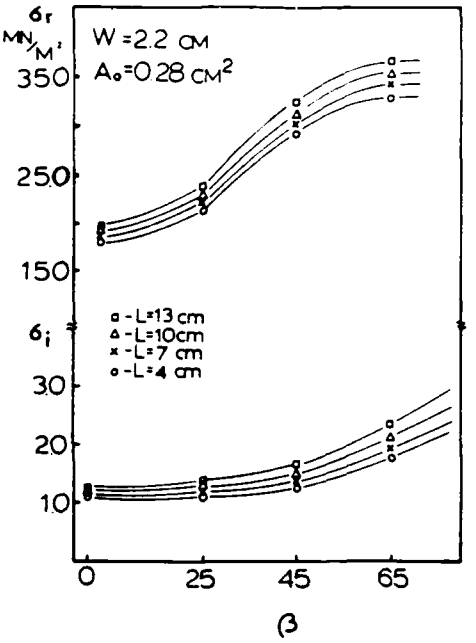

Fig. 20. Nominal stress for initiation and rupture based on area of un-cracked ligament.

It is interesting to note that although blunting is so severe that the pre-cracked specimen appears like a conventional tensile specimen the net section stress at rupture is a strong function of β (Fig. 20). This is further evidence that the presence of an angled crack influences the ultimate properties and that stress is not the appropriate characterizing parameter.

Also, it was impossible to separate the contributions of mode I and mode II for rupture because it was not possible to compute the compliance nor measure the COD because of the large amount of non-linear deformation. However, $J_{I,II}$ at rupture plotted as a function of the crack opening ratio at initation appears linear (Fig. 18) and suggests that the ratio of J_{II} to J_I is about 1.6.

8. Fractography

The fracture surfaces in the limited slow crack growth region were similar at all values of β (Fig. 21). But, for the fracture surfaces formed during rapid crack growth, although not uniform, the density of tear ridges increased with β (as is shown in Fig. 22). These observations concur with the general relation of increasing surface roughness with increasing toughness.

9. Conclusions

Application of the J integral concept to mixed mode crack growth in carbon black filled natural rubber was able to partition the contribution of each mode to crack initiation. By

Fig. 21. Fracture surface in slow crack growth region, (× 40).

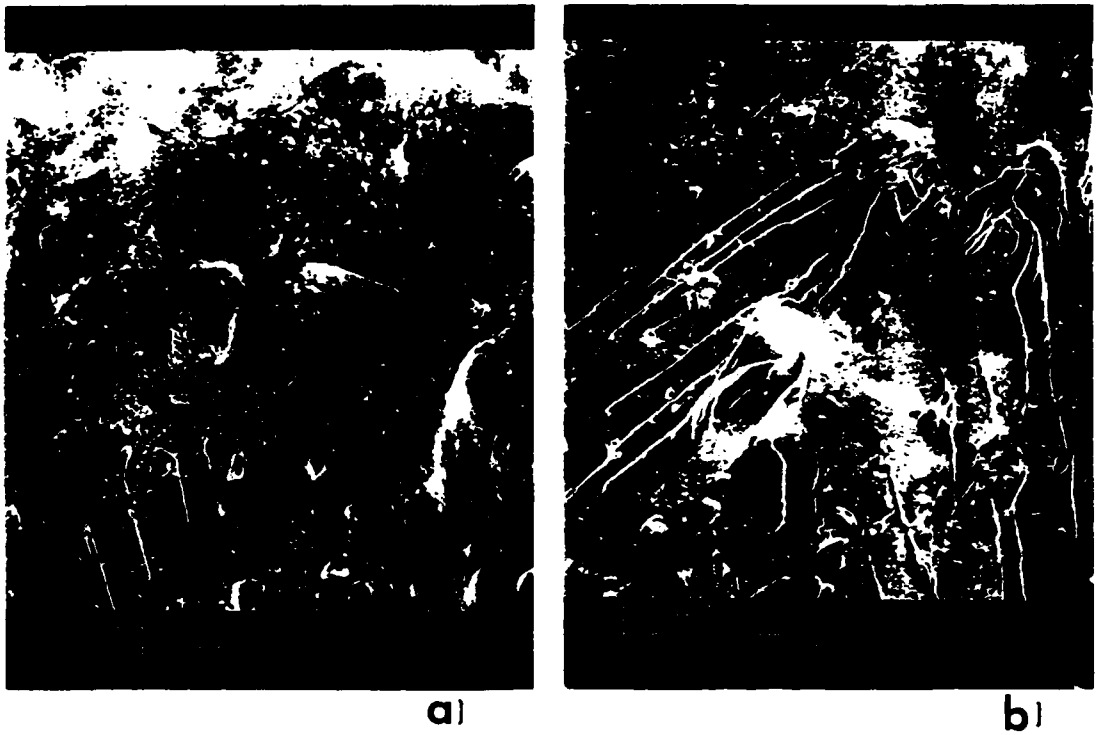

Fig. 22. Fracture surfaces during rapid crack growth for (a) pure mode I (b) mixed mode I & II, (× 40).

extrapolation, based on crack opening displacement, J_{IIc} for initiation was about twice J_{Ic}. This is due to the difference in stress induced structure in the crack tip region. For rupture the ratio of J_{IIc}/J_{Ic} was about 1.6. However, the basis for the extrapolation is not as well founded as for initiation.

As a criterion for crack initiation the relationship

$$\left(\frac{J_I}{J_{Ic}}\right) + \left(\frac{J_{II}}{J_{IIc}}\right) = 1$$

was found to describe the data.

In general the fracture surface roughness increased with the pre-crack angle in agreement with the increase in toughness with pre-crack angle.

Acknowledgements

The financial support of the US Army Research Office (Durham) is gratefully acknowledged and appreciated. Also, we would like to thank Dr S. Parkizgar of B.F. Goodrich Co. for the materials.

References

1. G.C. Sih, *International Journal of Fracture* 10 (1974) 305–321.
2. P.D. Ewing, J.L. Swedlow and J.G. Williams, *International Journal of Fracture* 12 (1976) 85–93.
3. K.J. Chang, *Engineering Fracture Mechanics* 14 (1981) 125–142.
4. S.K. Maiti and R.A. Smith, *International Journal of Fracture* 23 (1983) 281–295 and 24 (1984) 5–22.
5. P.S. Theocaris and H.P. Andrianopoulous, *Journal of Applied Mechanics* 49 (1982) 81–86.
6. N.P. Suh, in *Fundamentals of Friction and Wear of Material*, D.A. Rigney (ed.), ASTM (1981) 43–71.
7. D.H. Champ, E. Southern and A.G. Thomas, in *Advance in Polymer Friction Wear*, L.H. Lee (ed.), Plenum Press (1974) 133–144.
8. A.N. Gent and H.J. Kim, *Rubber Chemistry and Technology* 51 (1978) 35–41.
9. D.J. Lee and J.A. Donovan, *Theoretical and Applied Fracture Mechanics* 4 (1985) 137–147.
10. A.G. Thomas, *Journal of Applied Polymer Science.*, 3 (1960) 168–174.
11. H.W. Greensmith and A.G. Thomas, *Journal of Polymer Science* 18 (1955) 189–200.
12. R.G. Stacer, L.C. Yanyo and F.N. Kelly, *Rubber Chemistry Technology* 58 (1985) 421–435.
13. M.L. Studebaker and J.R. Beatty, *Science and Technology of Rubber*, F. Eirich (ed.) Academic Press, N.Y. (1978) 367–418.
14. B.D. Agarwal, B.S. Patro and P. Kumar, *Engineering Fracture Mechanics* 19 (1984) 675–684.
15. B. Cotterell and Y.W. Mai, *International Journal of Fracture* 20 (1982) 243–250.
16. H. Ishikawa, H. Kitagawa and H. Okamura, in *Proceedings ICM3*, Cambridge, 3, R.J. Miller and R.F. Smith (eds), Pergamon Press, London (1979) 447–455.
17. B. Budiansky and J.R. Rice, *Journal of Applied Mechanics* 40 (1973) 201–203.
18. J.R. Rice, in *Fracture – An Advanced Treatise*, 2, Academic Press, NY (1968) 191–311.
19. D.J. Lee and J.A. Donovan, to be published.
20. G.C. Sih and H. Liebowitz, in *Fracture, An Advanced Treatise*, 2, Academic Press, NY (1968) Chapter 2.
21. E.F. Rybicki and M.F. Kanninen, *Engineering Fracture Mechanics* 9 (1977) 931–938.
22. J.R. Rice, *Journal of Applied Mechanics* 35 379–386.
23. R.C. Shah, *Fracture Analysis*, ASTM STP 560 (1974) 29–52.
24. H. Awaji and S. Sato, *Journal of Engineering Materials and Technology*. 100 (1978) 175–182.
25. E.M. Wu, *Journal of Applied Mechanics* 34 (1967) 967–974.

JOURNAL OF MATERIALS SCIENCE 23 (1988) 2230-2242

Fractal analysis of rubber wear surfaces and debris

P. R. STUPAK, J. A. DONOVAN
Mechanical Engineering, University of Massachusetts, Amherst, Massachusetts 01003, USA

The wear surface and debris of three rubber compounds (NR, PBD and NR/PBD/SBR), worn on a modified blade abrader, were fractal. The fractal dimension of the wear surface was: (1) limited to a finite range, and if the wear mechanism remained the same; (2) independent of the wear load; and (3) the basis for creating a master fractal plot by a shift factor that (4) decreased linearly with wear load. The fractal dimension of wear was determined on the basis of profilometer traces and showed that the wear load affected the scale of the wear process. The fractal dimension of the debris also increased with the wear load and is thought to be a function of the agglomeration mechanism during wear.

1. Introduction

To appreciate the practical nature of rubber wear, one need only consider that an estimated 430 Gg of rubber are lost through tyre wear in the United States annually [1]. Past advances in rubber wear properties were achieved chiefly through empirical relations and expensive road testing [2]. But, diminishing resources and increased competition require future improvements to be gained by a more effective method based on the understanding of the mechanisms of wear. This undertaking is difficult because of the complexity of the wear phenomenon which currently is thought to include tensile, fatigue, mechanochemical, thermochemical, and oxidative processes [3]. However, lasting evidence of these processes is found through the examination of the remaining wear surfaces and debris.

1.1. Rubber wear

For example, the overt signs of wear for many rubber compounds are surface roughening and the formation of small particles known as primary wear debris. Wear is due to frictional forces between an asperity and the rubber surface causing the rupture of primary molecular bonds [4]. Continued wear in one direction results in the formation of ridges perpendicular to the direction of motion. Eventually the pattern of ridges attain a steady state size and spacing, and the wear rate is constant. A microscopic survey of worn tyre tread by Smith and Veith [5] reported that the easily visible pattern consisted of several levels of even smaller ridges upon magnification. This process of ridge formation was originally recognized by Shallamach [6] as being fatigue dominated. Later, Thomas [7] and Southern and Thomas [8] supported this view by developing a fatigue model of steady state wear based on fracture mechanics concepts. More recently, however, Gent and Pulford [2] and Zhang [9] have shown that wear involves tensile failure and chemical effects as well as fatigue.

However, the dry wear mode described above does not occur in all materials at all times. When certain compounds are worn under mild conditions, reactive species generated by the rupture of rubber molecules react with oxygen in the atmosphere to form a degraded product. This is called oily mode wear because a thin oily film eventually covers the surface and reduces the rate of wear [2]. Ridges which may have been present initially are rounded and the complex surface altered [9].

In the past, studies [2, 8, 9] of rubber wear topography have shown that the spacing between ridges and the size of the wear debris are proportional to the applied frictional force under dry wear conditions. An improved method of surface and debris analysis which distinguishes wear mechanisms and correlates with wear properties would be useful in helping select rubber compounds for service. To this end, this study analysed profilometry traces of worn surfaces and boundary profiles of wear debris by fractal concepts. Fractal plots correlated with wear mechanism, wear rate and frictional work.

1.2. Fractal geometry

Fractal analysis, created by Mandelbrot [10], can be thought of as a tool which produces a quantitative description of an otherwise indescribably rugged line or surface. The essence of fractal analysis is: the length (or area) of an irregular line (or surface) depends on the size of the measuring device. Small measuring devices resolve finer details than larger, thereby give greater length (or area) measurements. A graphical representation of log length (L) of a mathematical fractal curve against log measuring unit size (R) yields a straight line described by the relation

$$L \propto R^{(1-D)} \tag{1}$$

where D is the fractal dimension. For example, a smooth line gives a constant length for all measuring unit lengths; the resulting fractal dimension equals the Euclidian dimension of one for a line. However, D for

0022-2461/88 $03.00 + .12

an irregular line is greater than one and increases with increasing roughness to a limit of two.

An analogous expression for complex surfaces produces fractal dimensions ranging from the Euclidean $D = 2$ to $D = 3$.

The length estimate continually increases because a mathematically fractal object posesses self-similarity. That is, every large irregularity is composed of smaller irregularities. Mathematical fractals possess self-similarity at all length scales, but natural fractal objects are always limited by upper and lower bounds [10].

Applications of fractal geometry have ranged from interpreting the irregular nature of clouds [11] to the description of Brownian motion [10]. Recently, several authors have determined the fractal dimensions of metal fracture surfaces. In a study by Mandelbrot *et al.* [12], of 300 grade maraging steel as a function of heat treatment, the fracture surfaces were first nickel plated and then polished parallel to the fracture plane in several stages. Each stage revealed a set of irregular "islands" of the underlying steel. The relation of the island area, A, to its perimeter, P, for many islands was

$$P \propto A^{(D/2)} \tag{2}$$

and D decreased with the impact energy required to fracture the specimen; a result which appears counter-intuitive [13].

Two other investigations [13, 14] determined D by applying Equation 1 to micrographs of polished vertical sections of the metal fracture surfaces. The study by Underwood and Banerji [14] showed that fracture surfaces are generally self-similar over only a limited range of scale.

2. Wear testing

2.1. Experimental methods

Wear testing was performed with a modified blade abrader [7, 9]. Wear proceeds by forcing a rigid stationary razor blade into the circumferential surface of a rotating rubber wheel. The stiff cantilever beam holding the blade was instrumented with strain gauges to record the transverse frictional forces generated during wear.

Three rubber compounds (Table I) were tested under frictional forces ranging from 650 to 2150 N per metre of wheel width, which corresponds to a frictional work input of 650 to 2150 J per square metre of nominal wheel surface area. All compounds were tested at 25° C and a tangential velocity of 33 mm sec^{-1} to minimize the effect of frictional heating on the wear rate. In addition, wear measurements were made only after each sample formed a steady state wear pattern. A nylon brush continually removed wear particles during testing. The wear rate was determined from rubber weight loss, testing time, r.p.m., compound density, and was expressed as the decrease in the radial wheel thickness per revolution. After testing, the specimens and collected debris were stored in a desiccator to prevent absorption of moisture and oxidation.

TABLE I Compound formulations

Formulation	NR compound	Blend compound	PBD compound
NR	100	0.33	0.0
PBD	0.0	0.33	100.0
SBR	0.0	0.33	0.0
Zinc oxide	4.0		4.0
Steric acid	2.0		2.0
Black, N110	45.0		45.0
Agerite Resin D	0.5		0.5
Agerite White	0.5		0.5
Anozite 2	3.0		3.0
Sulphur	2.5		2.0
Stanocure	0.8		1.5
Cure (min/°F)	25/300		20/300

2.2. Results and discussion

The radial wear rate as a function of frictional work input is shown in Fig. 1 for the three compounds. The data conform to the same relation found in experiments by Thomas [7], Gent [2], and Zhang [9]

$$W = AF^n \tag{3}$$

where W is the radial wear rate, F the applied frictional work input, and A and n are material parameters and are listed in Table II.

The least wear resistant material was the natural rubber (NR) compound. All NR samples tested developed steady state wear patterns and produced non-adhering particulate debris indicative of the dry wear mode. The ridge height, spacing, and debris size increased with increasing frictional work input (Fig. 2).

The natural rubber, polybutadiene, and styrene butadiene blend compound (NR, PBD, and SBR Blend) ranked second. Samples run at work inputs greater than 1100 J m^{-2} formed steady state ridges similar in size to the NR material, but produced strongly adhering rolls of debris. Brushing would not remove the debris so the testing was periodically interrupted to pull the particles from the surface with tweezers. At work inputs below 1100 J m^{-2}, ridge formation associated with dry wear occurred initially, but soon transformed into the oily wear mode. A dark, oily film formed, rounding the existing ridges and decreasing the wear rate to an unmeasurably low level (Fig. 3).

The PBD compound wore in the dry mode only and was the most abrasion resistant material. The scale of the ridges and the debris were much finer than the other compounds. As with the other dry wear samples, the pattern height, spacing, and debris size increased with increasing frictional work input (Fig. 4).

3. Profilometry

3.1. Experimental details

A traversing Clevite Surfanalyser 150 profilometer recorded surface roughness profiles in the rotation direction. For each compound, traces were made of samples worn at several different frictional work inputs. Traces were obtained at five or six locations around the wheel circumference to develop a statistical representation of the surface. The forward and reverse trace of each location was recorded for

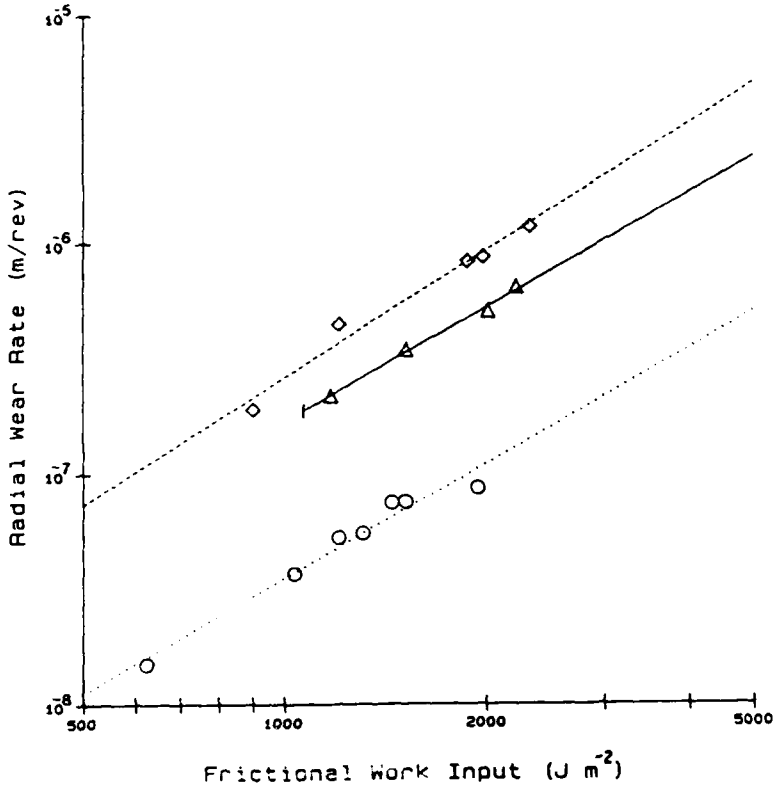

Figure 1 Radial wear rate as a function of frictional work input (△) Blend, (◇) NR, (○) PBD

analysis to include differences of roughness observed by the stylus deforming some of the thin ridge tips. Additionally, a vertical to horizontal enhancement of ten to one was used in all cases. The amplification of the roughness allowed more accurate analysis because even very small features became measurable. The total circumferential trace length for each sample was approximately 3 cm. The ability of the profilometer to form a consistent detailed surface representation over such a large distance was the reason for its use in this study. A microscopic survey of surface cross-sections at the same resolution, while giving a more exact surface description, would require a prohibitive number of micrographs.

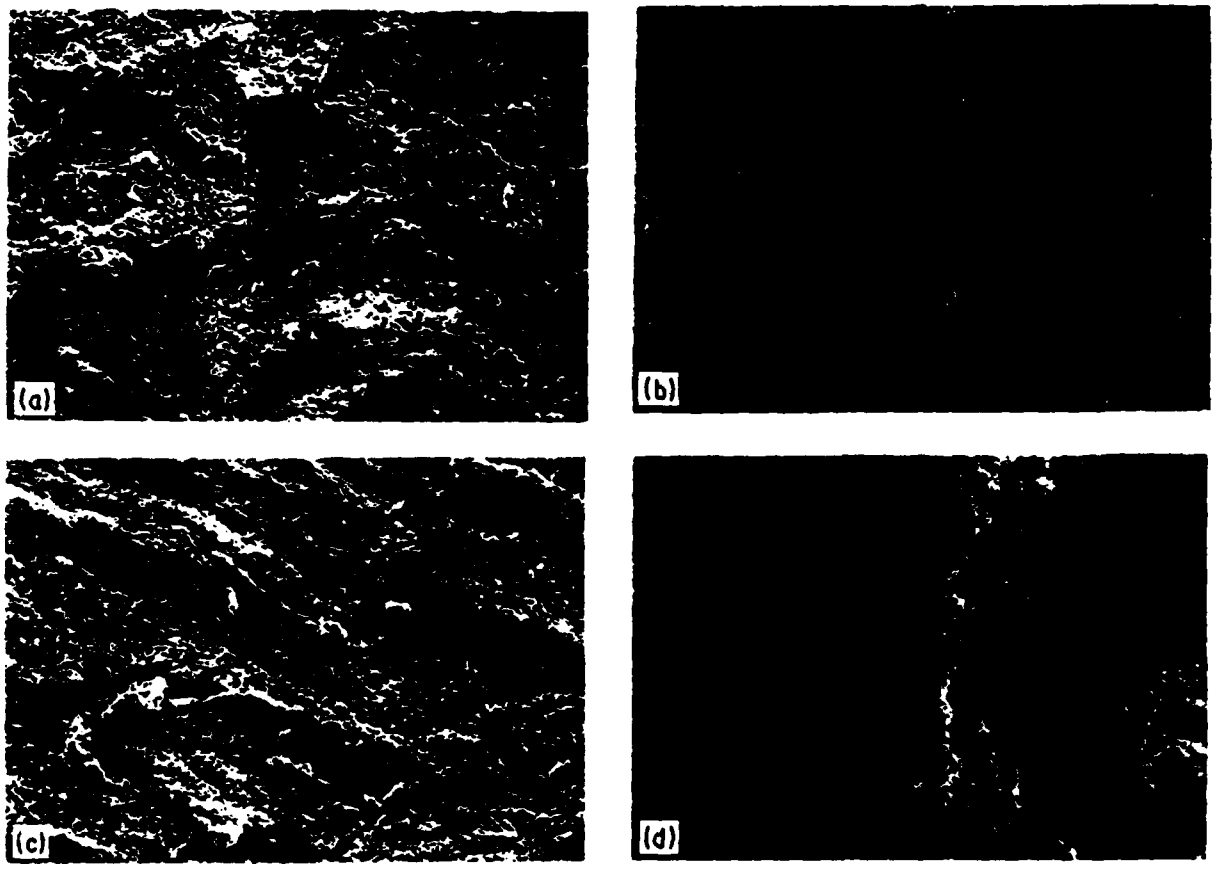

Figure 2 Natural rubber wear surfaces and debris as a function of frictional work input. (a, b) 2000 J m^{-2}, (c, d) 1350 J m^{-2}, (e, f) 690 J m^{-2}

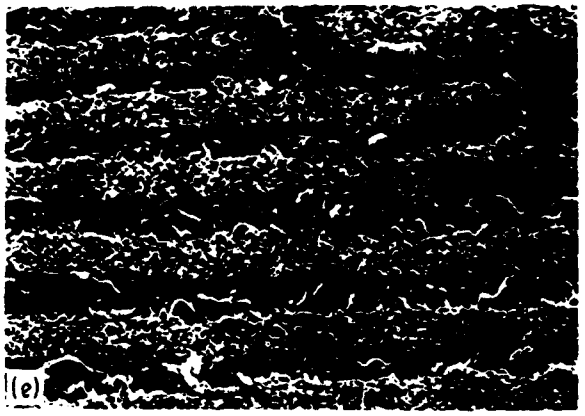

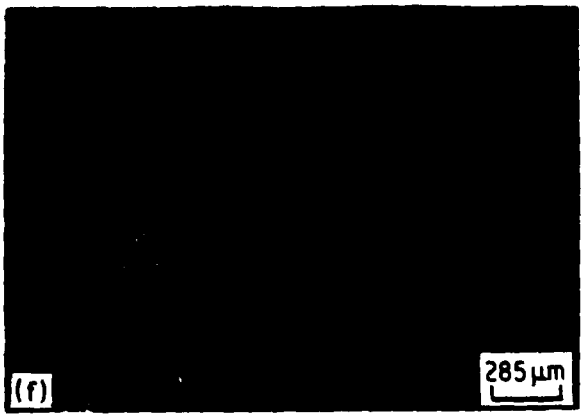

Figure 2 Continued.

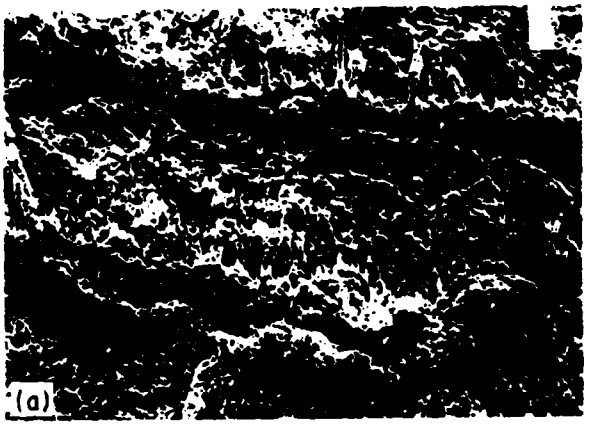

Figure 3 Blend compound wear surfaces and debris as a function of frictional work input. (a, b) 2160 J m^{-2}, (c, d) 1430 J m^{-2}, (e) 730 J m^{-2}.

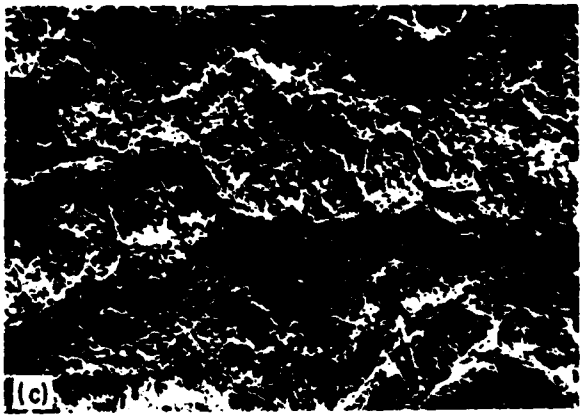

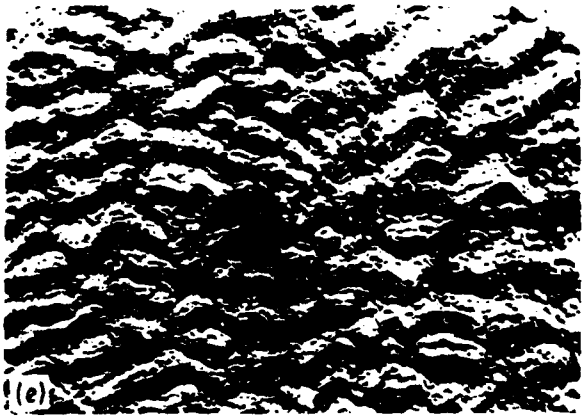

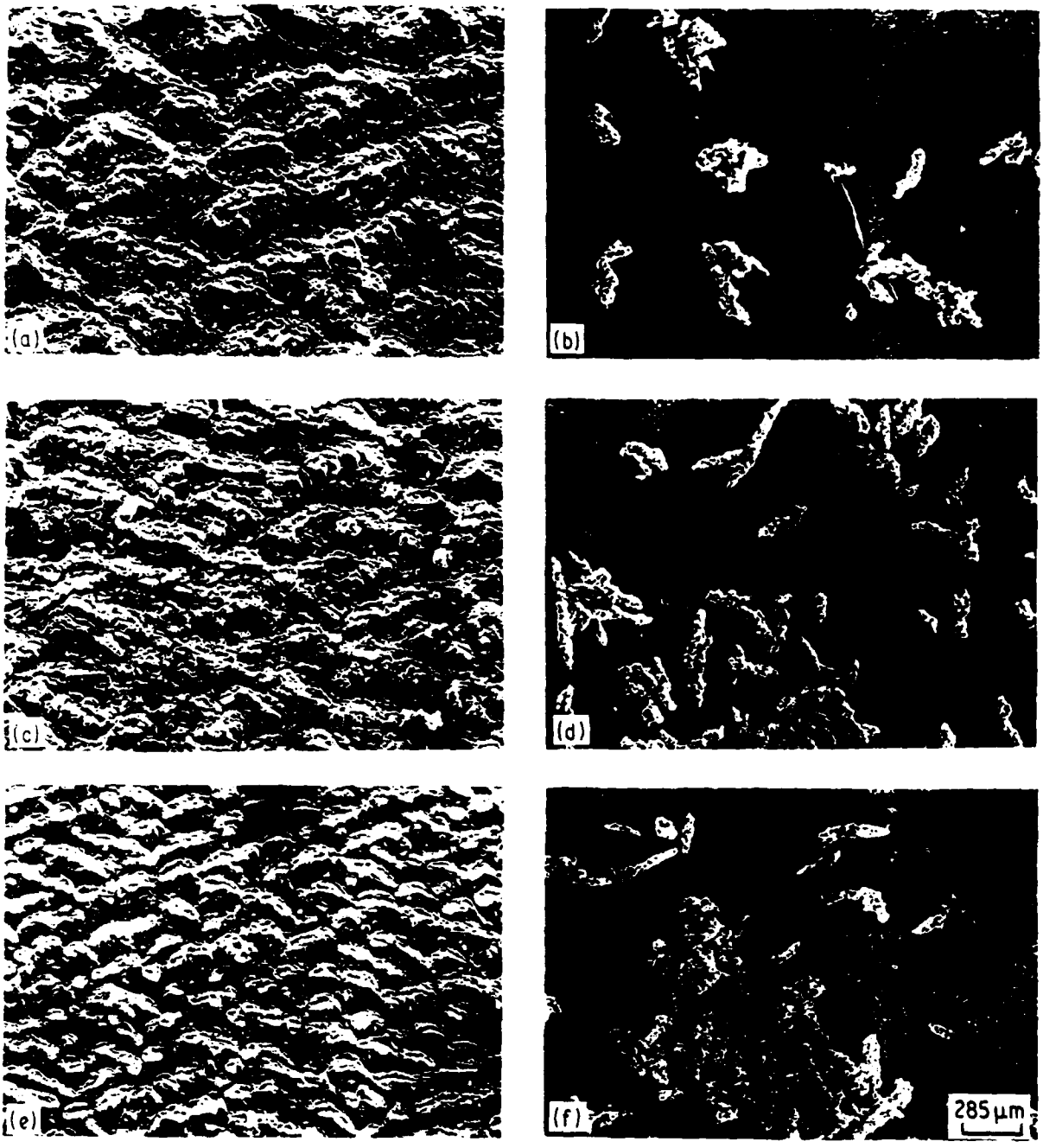

Figure 4 Polybutadiene rubber wear surfaces and debris as a function of frictional work input. (a, b) 1790 J m^{-2}, (c, d) 1220 J m^{-2}, (e, f) 650 J m^{-2}

3.2. Analysis

The profilometer traces were mounted on 1 mm thick paper board. An Exacto-knife was used to cut along the rugged line. This produced a relief image of the trace. The relief was glued to a long sheet of paper where perimeter estimates were made by rolling discs of various diameters along the length of the trace edge. A hole in the centre of each disc allowed a pencil lead to record on the paper each path taken. Small discs conformed closely to the irregular outline, whereas large discs were unable to penetrate into many of the irregularities (Fig. 5). The length of each path was measured with an architect's scale, and was normalized by dividing by the projected length of the original profilometer trace. Measuring the profilometry trace

TABLE II Wear parameters k and n

Compound	k	n
NR	8.6×10^{-3}	1.83
Blend	2.0×10^{-2}	1.64
PBD	3.9×10^{-2}	1.65

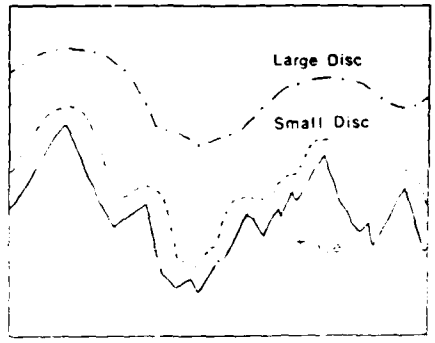

Figure 5 The effect of profilometer "radius" (disc diameter) on profilometer trace

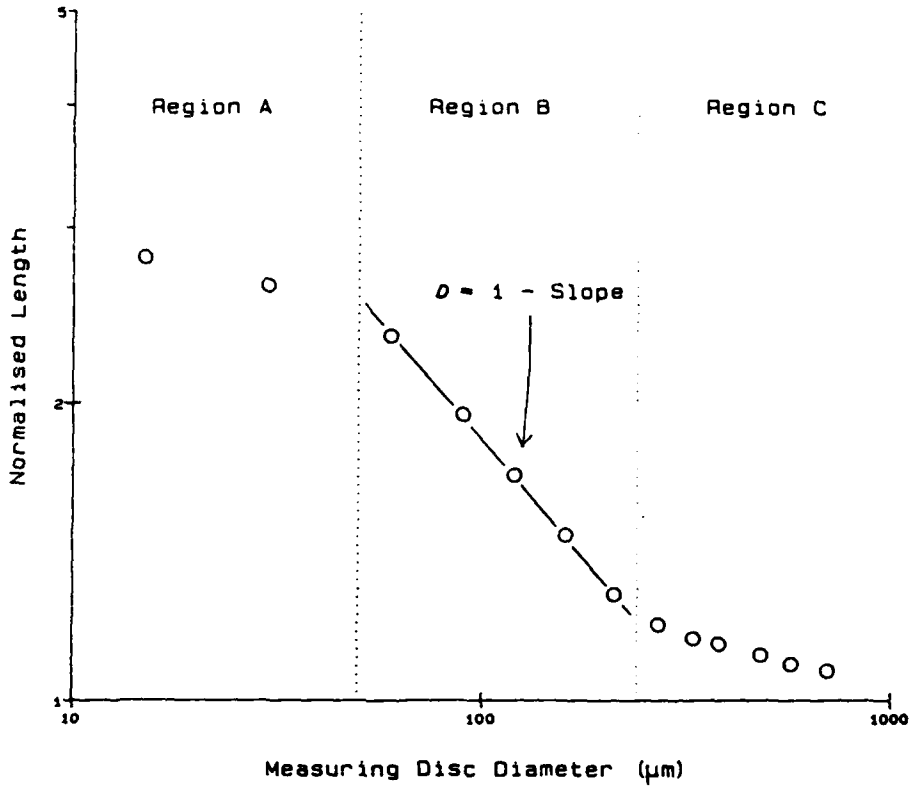

Figure 6 Typical fractal plot of profilometry data

with discs is analogous to measuring surface roughness with a profilometer employing styli of different diameters [15].

3.3. Results and discussion

The fractal dimension of the surface traces was determined from the graphical representation of Equation 1, where L was the normalized length, the measuring unit R was the disc diameter, and the slope equalled $(1 - D)$. A typical result is shown in Fig. 6.

The fractal dimension was not constant over the entire range of measuring diameters because of the limited self-similarity of the wear surface. The graph was divided into three regions: A, B and C. As the disc size decreased in region A the path length approached the true length of the original stylus trace, whereas, in region C the surface features became less significant as the disc size increased. Therefore the fractal dimension in these zones decreased toward the Euclidean value $D = 1$. The fractal dimension was obtained from the approximately linear region B, Fig. 6. The resulting value is considered a meaningful descriptor of the surface because it applies to the range of disc sizes that correspond to the scale of the actual surface features.

Fractal plots as a function of frictional work input are shown in Fig. 7, and corresponding values of D are given in Table III. When compared with respect to the frictional work input, the measured fractal dimension values could be divided into two categories; constant over a work input range or deviant.

When D was constant with frictional work the curves could be superimposed over their entire lengths (regions A, B and C), by shifting the curves only along the measuring unit axis (Fig. 8). This demonstrates that although the fractal dimension was changing over the measuring size range, it changed at the same rate for each surface. The suggested physical interpretation of superposition is that the wear process creates surfaces that are morphologically similar except for a scale factor. This suggests that the same wear mechanism operates at each work input. In the case of the PBD material, this view is supported because PBD exhibits only dry wear. Oily wear does not occur because the reactive species generated during wear preferentially react with the bulk rubber, not with the oxygen present in the atmosphere [2]. Therefore, for these compounds, the fractal dimension and superposition could be used to identify similarities in wear mechanism.

The amount of shift required to superimpose the curves, the fractal shift factor (log S), was related to the frictional work used to form the wear surfaces by

$$\log S = kF + b \qquad (4)$$

where k is the slope and b is the intercept when the

TABLE III Fractal dimension of wear surfaces

Compound	Frictional work ($J\,m^{-2}$)	Fractal dimension
NR	2000	1.46
NR	1670	1.47
NR	1340	1.47
NR	690	1.32
Blend	2160	1.48
Blend	1750	1.49
Blend	1430	1.49
Blend	730	1.13
PBD	2080	1.55
PBD	1790	1.58
PBD	1220	1.52
PBD	650	1.51

reference fractal plot was the highest frictional work measured (Fig. 9). Rewriting this relation to make its physical meaning more apparent gives

$$F = K \log S + B \quad (5)$$

and noting that B is the reference frictional work. Then, if the reference frictional work is taken as zero, the equation becomes

$$F = K \log S \quad (6)$$

and the wear rate can be written as

$$W = A(K \log S)^n \quad (7)$$

Thus fractal analysis shows that the wear topography can be quantitatively relative to the wear rate. The values of log S and K for each material are listed in Table IV.

It is natural to note the similarity between the character of the fractal shift factor and the Williams, Landel and Ferry shift factor used to create master

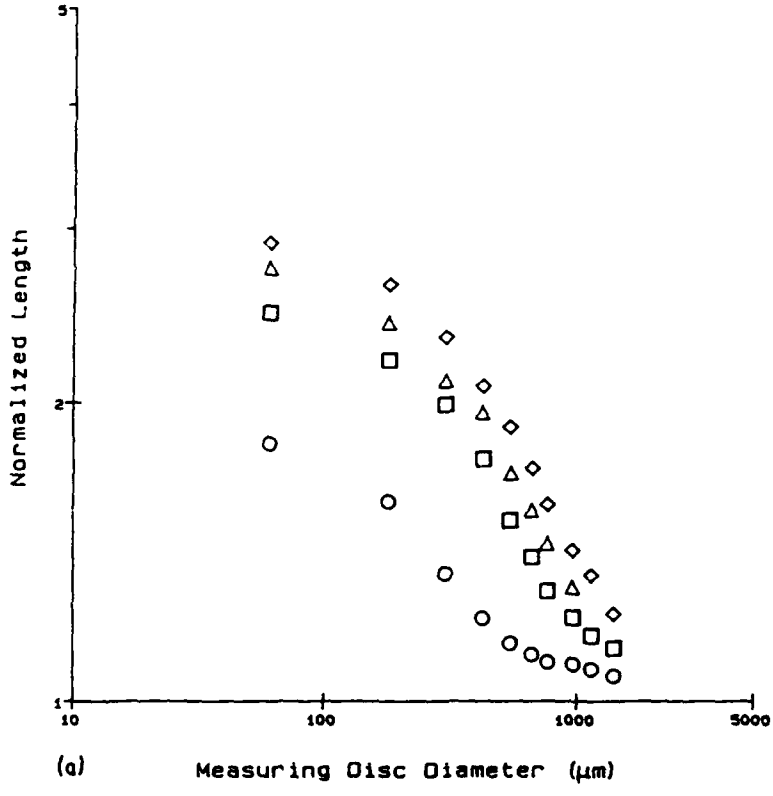

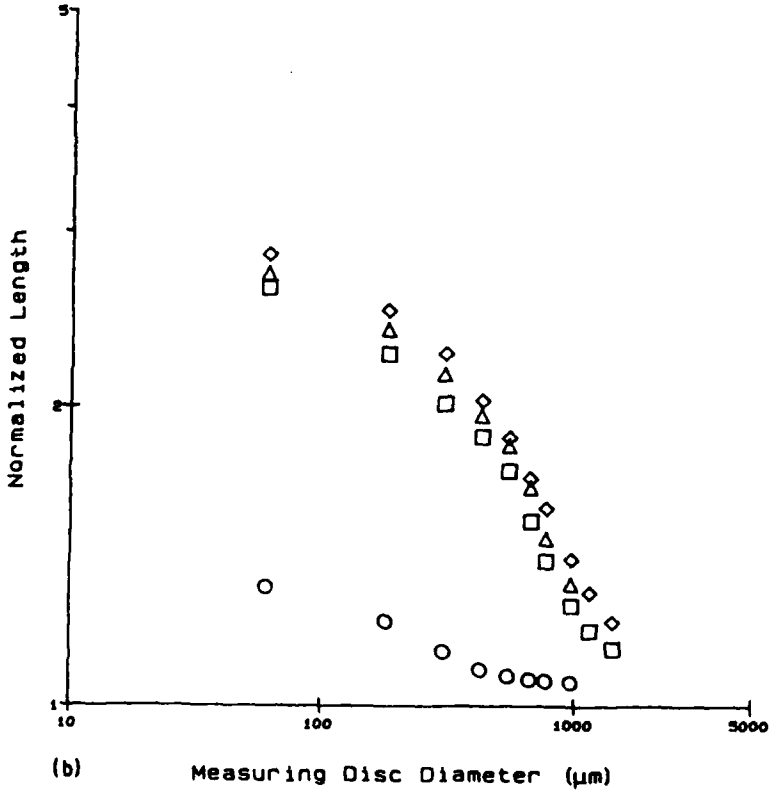

Figure 7 Fractal plot of profilometry data for (a) NR, (b) Blend, and (c) PBD compound. (a) (○) 690, (□) 1350, (△) 1670, (◇) 2000 J m^{-2}. (b) ○) 730, (□) 1430, (△) 1750, (◇) 2160 J m^{-2}. (c) (○) 650, (□) 1220, (△) 1790, (◇) 2080 J m^{-2}.

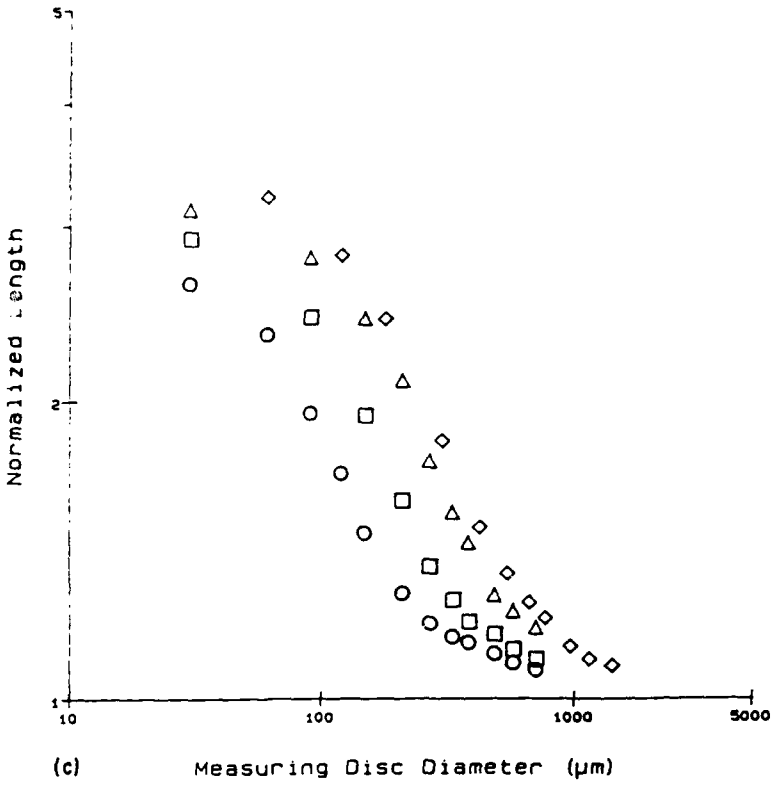

Figure ? Continued.

curves of material behaviour controlled by viscous deformation. In fact, the ability to form master curves for wear rate as a function of load by taking in the account the rise in near surface temperature as a function of wear load has been demonstrated [6]. Efforts to correlate the fractal shift factor with near surface temperatures and wear load are in process.

However, the experimental results for the Blend and NR samples tested at reduced frictional work (690, 920 J m^{-2}, respectively), displayed lower dimension values than their neighbouring curves and superimposed only over a small region. This was due to a distinct change is surface morphology in both cases. The Blend transformed from dry wear at high frictional work to oily wear at low frictional work, while the surface of the NR material changed from a series of discontinuous, irregular ridges at high work inputs to small, uniformly spaced ridges at low work inputs. This change may be due to effects of strain crystallization [6] or the initiation of an oily mode transition.

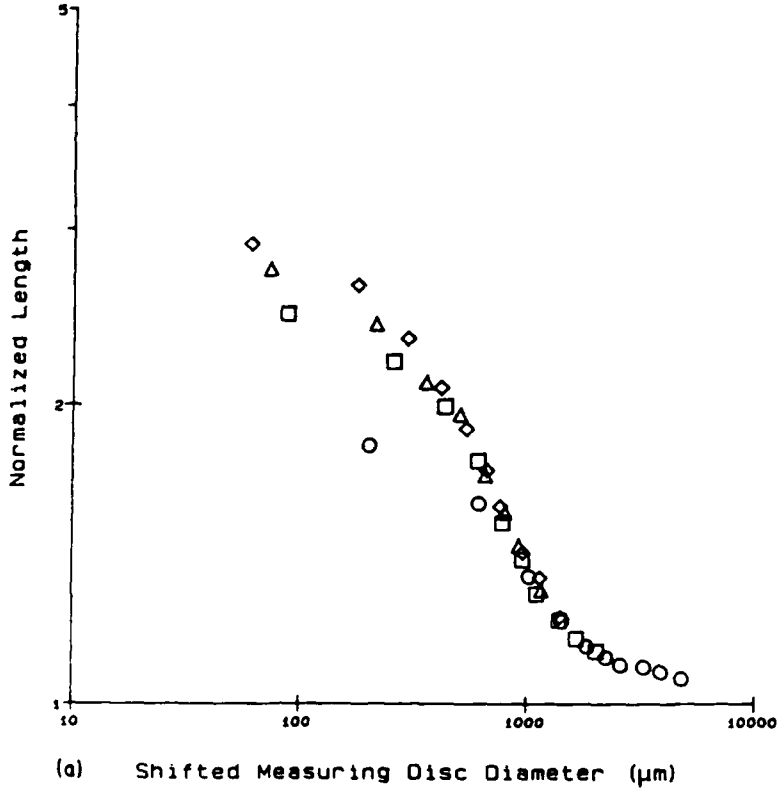

Figure 8 Shifted fractal plot for (a) NR, (b) Blend, and (c) PBD compound. (a) (○) 690, (□) 1350, (△) 1670, (◇) 2000 J m^{-2}. (b) (○) 730, (□) 1430, (△) 1750, (◇) 2160 J m^{-2}. (c) (○) 650, (□) 1220, (△) 1790, (◇) 2080 J m^{-2}.

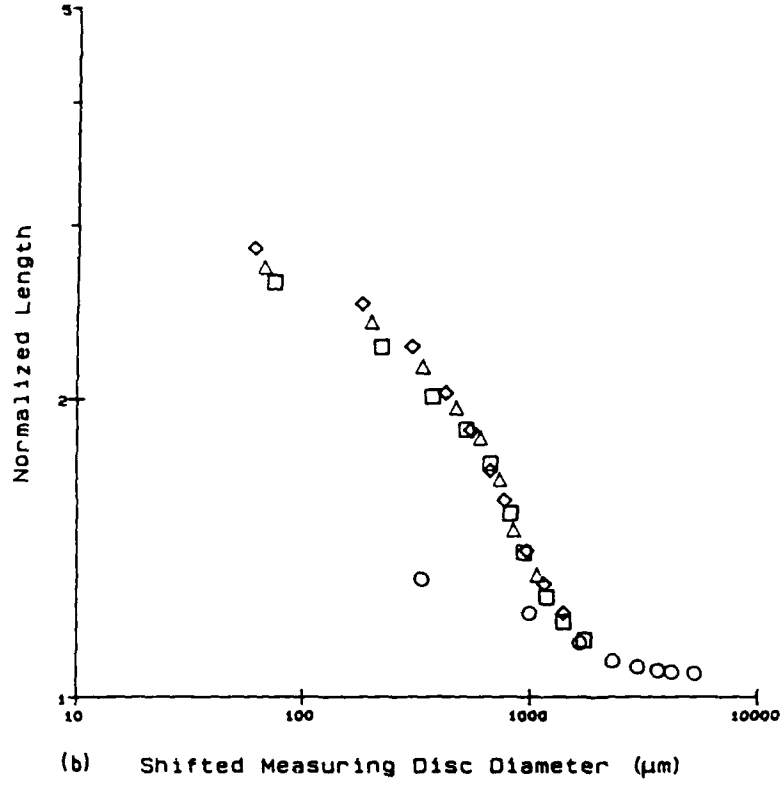

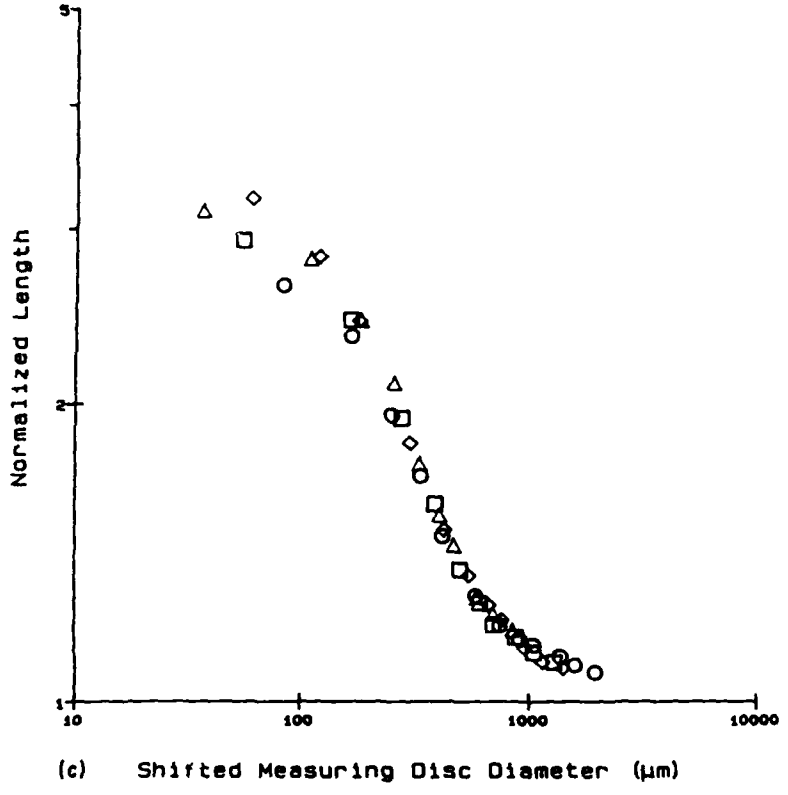

The interpretation in both cases is that a change in the operative wear mechanism changes the fractal dimension and negates superposition.

These results show that although natural objects are not fractal over all scales, important practical information can be obtained from fractal analysis. The special ability of fractal analysis to describe a surface at all scales gives a complete topographic picture which can be effectively exploited through additional parameters such as the fractal shift factor. In brief, it is not necessary that a single fractal descriptor be found for every natural object. In fact, to attempt to do so would be equally as erroneous as promoting Euclidian geometry as a universal descriptor (i.e. mountains are not cones!) [10].

4. Wear debris

4.1. Experimental methods

Wear debris was collected for each surface analysed with profilometry except the oily mode specimen

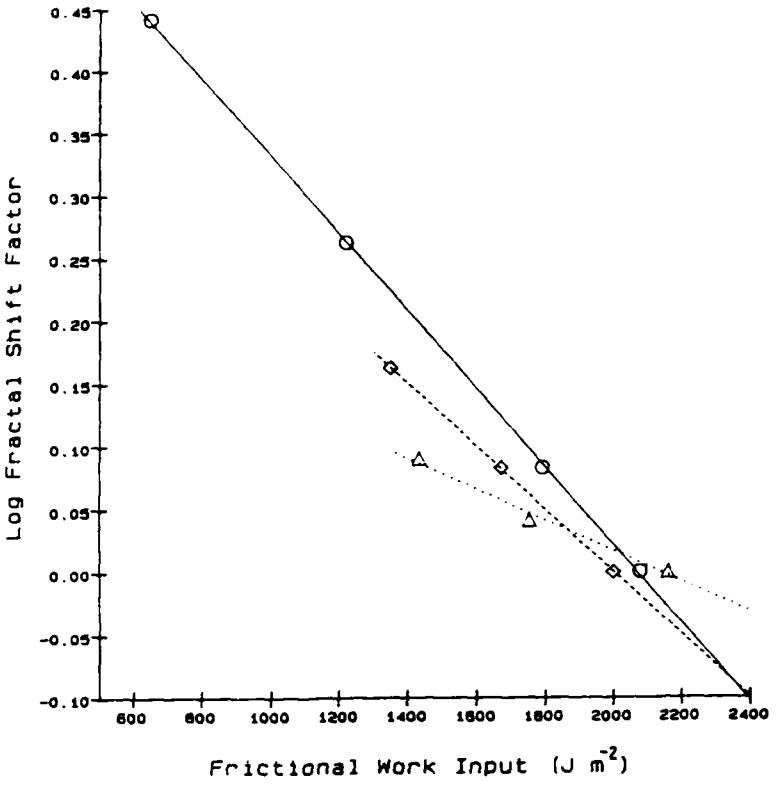

Figure 9 Log fractal shift factor as a function of frictional work input. (△) Blend, (◇) NR, (○) PBD

which produced no debris. The particles were photographed in a scanning electron microscope at a fixed magnification. The micrographs were Xeroxed on to transparencies and projected onto a large sheet of heavy-weight paper where their boundary images were traced. The length of the irregular perimeter of each particle was measured with the architect's scale and the projected area was determined by weighing the particle image.

4.2. Results and discussion

The fractal dimension of the debris (D_d) was determined using Equation 4 relating the perimeter, P, to the projected area, A, found at a fixed magnification according to

$$P \propto A^{1.2D_d} \tag{8}$$

The data and D_d as a function of frictional work, are shown in Fig. 10 and Table V. A minimum of ten particle images were analysed to determine the fractal dimension of the debris at each frictional work input. For all materials tested, D_d for the debris increased with F (Fig. 11); for the NR and PBD compounds this can be expressed as

$$D = mF + 1 \tag{9}$$

where m equals 2 and 2.5×10^{-10} m^2 J^{-1} for the NR and PBD, respectively. However, for the blend the relation was not followed, apparently because the nature of the debris was radically different from NR and PBD. The blend debris was very sticky, adherent and cylindrical, rather than dry and particulate for the other compounds. Also, because of the sticky nature of the blend debris the size of the debris analysed only ranged over one order of magnitude, while the NR and PBD particles were significantly smaller and ranged over several orders of magnitude.

Currently it is thought that the physical origin of this expression is not related to the wear mechanism alone, but rather is a strong function of the scheme by which the debris is formed under the scraping action of the blade. In fact, the results from the wear surface

TABLE IV Log fractal shift factors for NR, Blend, and PBD compounds

Compound	Frictional work (J m^{-2})	Log shift factor	K (J m^{-2})
NR	2000 (Reference)	0.0000	
NR	1670	0.0828	−4000
NR	1350	0.1621	
NR	690	0.5310	
Blend	2160 (Reference)	0.0000	
Blend	1750	0.0414	−8330
Blend	1430	0.0897	
Blend	730	0.7379	
PBD	2080 (Reference)	0.0000	
PBD	1790	0.0828	−3230
PBD	1220	0.2621	
PBD	650	0.4414	

TABLE V Fractal dimension of NR, Blend, and PBD debris

Compound	Frictional work (J m^{-2})	Fractal dimension
NR	2000	1.42 ± 0.04
NR	1340	1.24 ± 0.04
NR	690	1.12 ± 0.06
Blend	2160	1.36 ± 0.08
Blend	1430	1.14 ± 0.06
PBD	1790	1.44 ± 0.04
PBD	1220	1.34 ± 0.04
PBD	650	1.16 ± 0.04

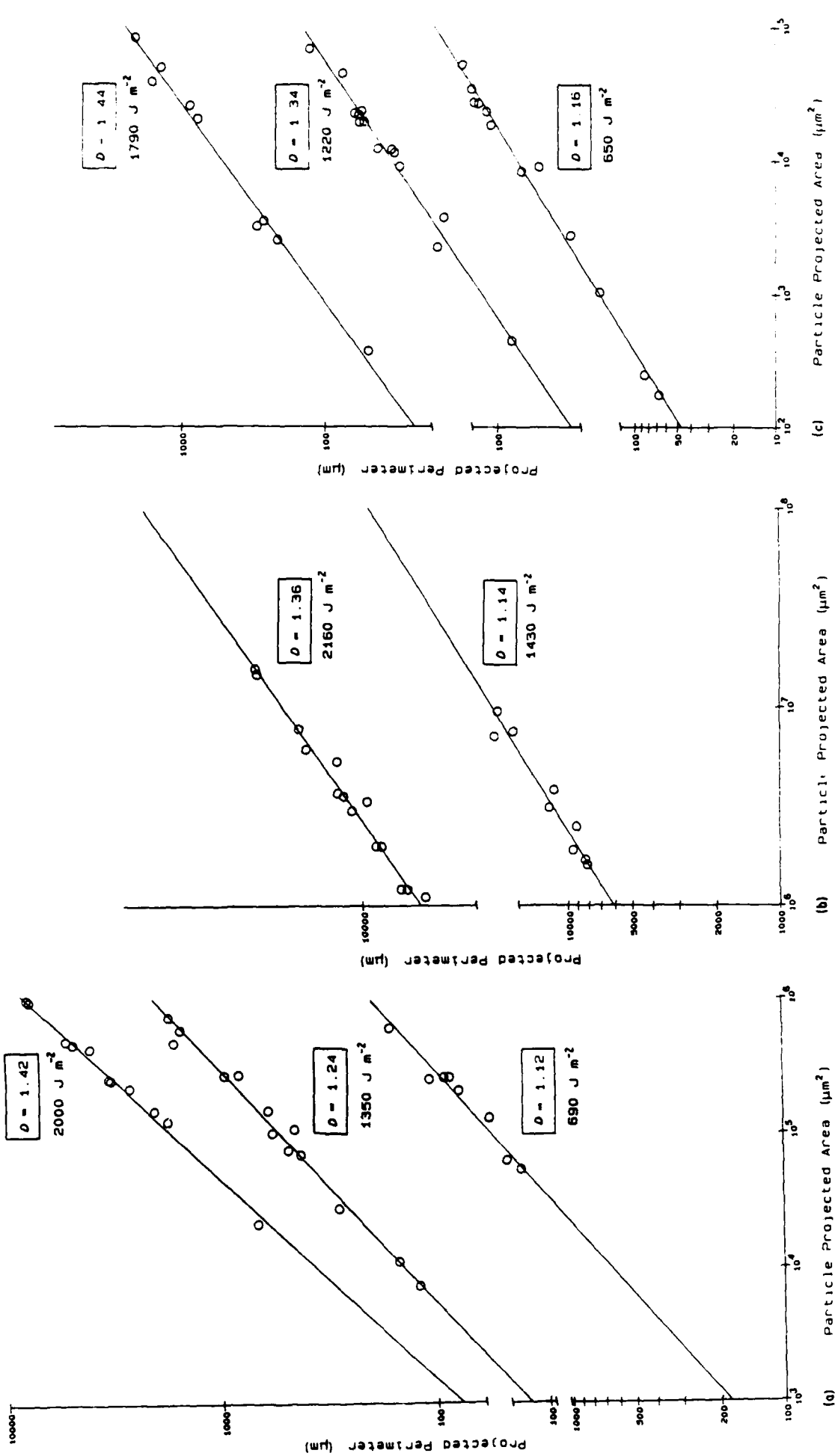

Figure 10 Fractal plots of (a) NR, (b) Blend, and (c) PDB debris.

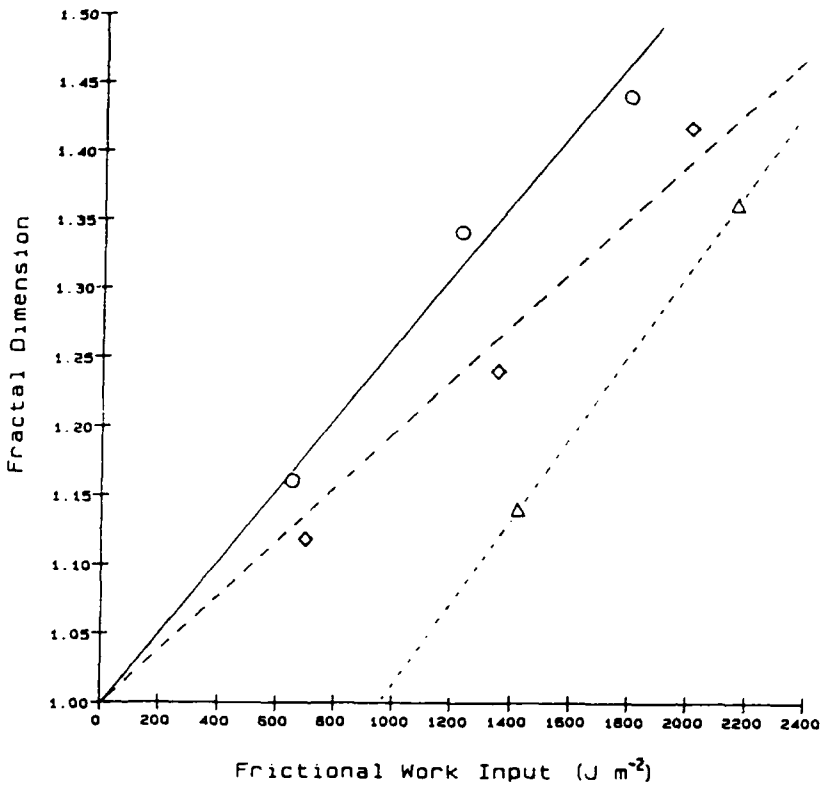

Figure 11 Fractal dimension of debris as a functional work input (△) Blend, (◇) NR, (○) PBD.

analysis indicates that over a large range of frictional work the surfaces are formed by the same mechanism. Therefore, if the debris was formed solely by this mechanism, its fractal dimension would be expected to have the same value!

It is proposed that at increasing wear rates more debris particles, which consist of primary particles and severed ridge tips, are produced per revolution and agglomerate with each pass of the blade until they are eventually removed. It is also believed that the detailed agglomeration mechanism is a function of the frictional work and responsible for the variation in the fractal dimension. A large body of information exists regarding the application of fractals to computer simulated random flocs in two and three dimensions [16–18]. Further interpretation of the precise agglomeration process would logically begin there.

Another feature of large random accreations of particles is an extensive range of self-similarity. This is evident from the many magnitudes over which the fractal dimension describes the rubber debris. This is further demonstrated in Fig. 12, where micrographs of the same debris particle continue to reveal more detailed irregularities with increasing magnification.

5. Conclusions

The dimension of rubber wear surfaces was fractal over a limited scale, and if the wear mechanism remained the same then the fractal plots could be superimposed. The required fractal shift factor was linearly related to the wear load. The fractal shift factor is highly suggestive of the classic WLF shift factor that relates viscous deformation processes to material properties. This relation is the focus of future research.

The wear debris was fractal and its dimension also increased with the wear load, but because the debris are agglomerates of wear particles the relation to wear load is thought to result from the effect of the wear load on the agglomeration mechanism.

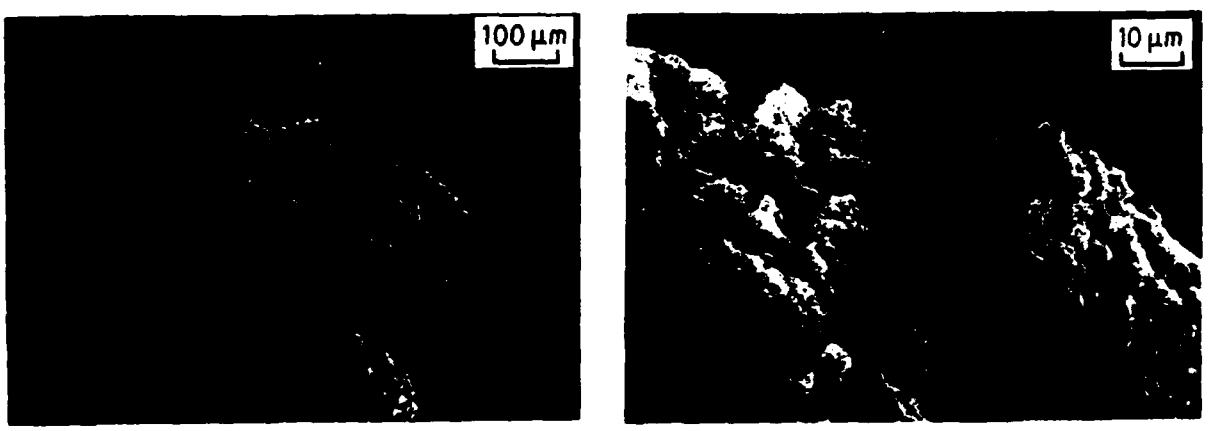

Figure 12 Self-similarity of debris particles.

Acknowledgements

The financial support of the US Army Research Office, Durham, is gratefully acknowledged and appreciated. We also thank P. Touchet and G. Rodriguez, US Army Belvoir R and D Center for supplying the materials.

References

1. M. L. DANNIS, *Rubber Chem. Technol.* **47** (1974) 1011.
2. A. N. GENT and C. T. R. PULFORD, *J. Appl. Polym. Sci.* **28** (1983) 943.
3. E. M. DANNENBURG, *Rubber Chem. Technol.* **59** (1986) 497.
4. V. I. DYRDA, V. I. VETTEGREN and V. P. NADUTYI, *Int. Polym. Sci. Technol.* **3** (1976) 26.
5. R. W. SMITH and A. G. VEITH, *Rubber Chem. Technol.* **55** (1982) 469.
6. A. SCHALLAMACH, *ibid.* **41** (1968) 209.
7. A. G. THOMAS, *ibid.* **48** (1974) 902.
8. E. SOUTHERN and A. G. THOMAS, *ibid.* **52** (1979) 1008.
9. S. W. ZHANG, *ibid.* **57** (1984) 755.
10. B. B. MANDELBROT, "The Fractal Geometry of Nature" (Freeman, New York, 1982).
11. S. LOVEJOY, *Science*, **216** (1982) 185.
12. B. B. MANDELBROT, D. E. PASSOJA and A. J. PAULLAY, *Nature* **308** (1984) 721.
13. C. S. PANDE, L. R. RICHARDS and S. SMITH, *J. Mater. Sci. Lett.* **6** (1987) 295.
14. E. F. UNDERWOOD and K. BANERJI, *Mater. Sci. Engng* **80** (1986) 1.
15. D. FARIN, S. PELEG, D. YAVIN and D. AVNIR, *Langmuir* **1** (1985) 399.
16. P. MEAKIN, *J. Coll. Int. Sci.* **96** (1983) 415.
17. P. MEAKIN and Z. R. WASSERMAN, *Chem. Phys.* **91** (1984) 492.
18. R. C. BALL and T. A. WITTEN, *J. Stat. Phys.* **36** (1984) 873.

Received 27 July
and accepted 23 October 1987

DRAFT

THE EFFECT OF CARBON BLACK AND STRESS STATE ON STRAIN-INDUCED CYSTALLIZATION IN NATURAL RUBBER

H. Liu, R. F. Lee and J. A. DONOVAN

Department of Mechanical Engineering

University of Massachusetts, Amherst, MA 01002

INTRODUCTION

Natural rubber (cis-polyisoprene) is mostly amorphous, except for a small percentage of semi-crystalline spherulites[1], if the material has been between 223-283K[2] for a long time. In temperature induced crystals (TIC) the long chain molecules in the crystalline lemella are parallel to the spherulite surface[1], therefore randomly oriented throughout the specimen. TIC is generally undesirable, since it hardens and decreases the recoverable strain of the rubber.

However, when natural rubber (NR) is uniaxially stressed, it is well known that strain induced crystallization occurs in the amorphous matrix. The strain induced crystals (SIC) have a shish-kebab structure with the extended chain crystals alligned in the direction of extension[3]. Since the covalent bonds along the chain are much stronger than the Van der Waals bonds between the

chains, the strength of the strecthed material[2] is anisotropic. In a stressed, cracked NR specimen the material in the crack tip region is most extended, therefore highly crystalline and the molecular chains are oriented in the maximum principle stress direction. Thus the strong intermolecular bonds hinder crack growth. Also the crystallization is a reversible process that dissipates energy in the crack tip region which is not therefore available for crack propagation.

The maximum degree of crystallinity, SIC and TIC, determined by X-ray diffraction experiments does not exceed about 30 percent[4].

Recent work showed carbon black (CB) filler in NR increased the energy required for crack initiation[5,6], and facilitates the development of molecular orientation[7] and crystallization[5]. Therefore an important mechanism of CB reinforcement, as measured by the increase in fracture resistance, is associated with the CB facilitated, strain induced crystallization occurring in the crack tip region.

Gent and Kim[8] showed that the critical energy release rate for crack growth was decreased by pre-stretching the specimen in the crack direction, and was larger in a trouser test than in a single edge notched specimen (SEN). It also has been shown that the critical strain energy release rate to initiate a crack in a pure shear (PS) specimen was less than in a SEN specimen; and that the state of biaxial stress

is greater in the crack tip region in the PS specimen[3] than in the SEN specimen[9]. The relation of SIC to fracture resistance suggests that the state of stress may affect the extent of SIC. Therefore, the objective of this work was to determine the effect of biaxial stress on the extent of SIC and relate these data to the role of SIC in fracture resistance.

Differential scanning calorimetry (DSC) is a standard method to determine the percent crystaliinity of semi-crystalline polymers. By measuring the heat absorbed by the melting of the crystals, the percent crystallinity can be calculated. Goritz and coworkers[10] were the first to use DSC to directly measure the crystallization behavior in uniaxial stretched NR. Lyon and Farris[11] developed another DSC technique and measured the SIC in an elastomer. In this work, a special fixture was designed for crystallization measurements of biaxially stressed CB filled NR by DSC.

EXPERIMENTAL

The NR used for this study was filled with 0, 10, 25 and 40 pph HAF carbon black and 10 percent regrind, compounded by B. F. Goodrich Rubber Company.

To measure SIC as a function of biaxial stress, a three-piece brass fixture was designed to hold a biaxial stretched rubber sample. A NR strip 0.6 mm thick, 15 mm wide and variable length was first clamped in a stretching

device, and extended to a desired elongation ratio λ_1^4 as shown in Figure 1 at room temperature. If the specimen was long enough, the NR would be uniaxially stressed and $\lambda_2=1/\sqrt{\lambda_1}$; if the specimen was short compared to the width, the sample could be in the same stress state as the PS with $\lambda_2=1$. Thus by changing the specimen length, the sample could be biaxially stretched to different degrees with $0<\lambda_2<1$.

Then, the stretched rubber sample was clamped between part A and B of the fixture (Figure 2) with the aid of a hand vice. The rubber outside the clamping fixture was cut off, part C was screwed tightly into part B to prevent contraction of the sample after the holding force was released. To check if any slippage of the sample ocurred in the fixture, several white dots' were pressed on the stretched sample, and their relative position was measured before and after clamping. The weight of the fixture averaged 370±10mg, and the rubber samples weighed between 15 to 30mg. The fixture containing the sample was then placed opposite a reference fixture in a DSC, and scanned at a rate of 20K/min from 173 to 423K. After the DSC measurement, the sample was released from the fixture, and the center part of the sample was trimmed along the clamping mark and re-weighed. Since the circumferential part of the sample was unstreched no SIC developed in this part of the material, the weight of the center was used for calculations of ΔH, the enthalpy of melting, and the crystallinity. Also, the

net weight of NR was used in the calculations by substracting the weight of the CB.[5]

To measure TIC, unstretched rubber was annealled at 423K, cooled to and kept at 253K for 3 days, than the DSC trace was determined by scanning at 20K/min from 253 to 373K. Samples stored at room temperature for about six months after curing were also measured in a similar way.

RESULTS AND DISCUSSION

A typical DSC curve for the materials studied is shown in Figure 3, where the glass transition temperature, T_g is about 213K, ΔC_p is the change in the heat capacity at T_g, and ΔH, the area under the peaks, is the enthalpy of fusion of the crystals. ΔCp is proportional to the free amorphous molecules present, while ΔH is proportional to the mass of crystalline material melted. The first peak corresponds to the melting of TIC. The second peak only appeared when the extension ratio reached a critical value, therefore the higher temperature peak is identified as the exothermic peak due to the melting of SIC.

CB Effects on Temperature Induced Crystallization

The amount of TIC in NR formed near the temperature of the maximum crystallization rate[12] (253K) was not a function of CB content as shown Figure 4, although the rate of crystallization may be[13]. But, for material stored at room

temperature (T~294K)[6], the extent of TIC decreased slightly with CB content as shown in Figure 4. The melting point Tm was independent of CB content (Table I).

CB and Stress Effects on Strain Induced Crystallization

Deformed NR had SIC in addition to the TIC that pre-existed as shown in Figure 3. Figure 5 shows ΔH, the heat absorbed due to the melting of SIC, as a function of CB and uniaxial extension ratio. Extension increased the extent of SIC in natural rubber as expected. CB increased the crystallinity at comparable extension ratios and decreased the critical strain at which SIC occurred in agreement with previous X-ray studies[5,14].

The critical extension ratio to induce crystallization for unfilled NR was 3.5, below which SIC did not occur. However, 10pph CB filled NR crystallized at λ=2 and 40pph NR crystallized almost immediately upon extension. This agrees with Gehman and Field's discovery[14,15] that X-ray diffraction spots appeared at lower elongations when NR was filled with CB, and with the Mullin-Tobin study[16] of volume changes with stretching which indicated that CB caused NR to crystallize at much lower elongations.

At the same extension ratio, ΔH, or crystallinity, increased with the increase of CB content. The CB interacts with the rubber molecules and forms additional network

points[17]. Among the range of filler-rubber bonds, the over-stressed molecules are released by successive rupture and re-establishment of CB-rubber bonds, accompanied by sliding of the rubber chains over the filler. Therefore, the stresses in filled NR are more evenly distributed among the rubber chains than in unfilled NR. This promotes orientation of the molecular chains in the stress direction, and therefore, increases SIC. Marei et al.[18] suggested that fillers in polymers have the same effect on the mechanism and kinetics of crystallization as the application of uniaxial stress, since fillers act as heterogeneous crystallization sites which promote the rate of crystallization and the formation of bi- and uni-directional crystals.

Figure 6 shows that SIC is less in biaxial stretched specimens than in uniaxial stretched specimens even when λ_2 in the biaxial case is not much larger than in the uniaxial case. Zuyev[7] has suggested that biaxial stress will hinder the formation of molecular orientation. When contraction of NR is restricted in the λ_2 direction the stress, σ_2 will restrict molecular rearrangement in the λ_1 direction through molecular entanglements. Therefore, the crystallization is impeded.

CB and Stress Effects on Melting Temperature of SIC

The melting temperature, defined as the temperature at which the last trace of crystals melt, increased with both

uniaxial or biaxial stress (Figure 7), but was unchanged by CB content[8](Figure 8). The increase of Tm with stress is theoretically expected from the classical thermodynamics of rubber. The Gibbs free energy ΔG is

$$\Delta G=\Delta H-T*\Delta S, \quad (1)$$

and at the melting point $\Delta G=0$, so

$$Tm=\Delta H/\Delta S=\Delta H/(Sam-Scr), \quad (2)$$

where ΔH is the enthalpy change, Tm is the melting temperature of crystals, ΔS is the entropy change and Sam and Scr are the entropy of the amorphous and the crystalline phase, respectively. Deformation decreases Sam according to

$$\Delta Sam=-\frac{1}{2}Nk(\lambda_1^2+\lambda_2^2+\lambda_3^2-3), \quad (3)$$

where λ_1, λ_2, λ_3 are the extension ratios in the three principle directions. Therefore Sam decreases and Tm increases with the increase of λ_1, λ_2 , λ_3 or any combination of λ.

Crystallinity Calculation

The crystallinity of unfilled NR can be determined either by[19]

$$Wc = \Delta H/\Delta H_{100}, \quad (4)$$

or by[20]

$$Wc = 1 - \Delta Cp_{cr}/\Delta Cp_{am}, \quad (5)$$

where ΔH_{100} is the enthalpy of fusion for a perfectly crystalline polymer, ΔCp_{cr} is the change of heat capacity at the glass transition temperature Tg of the amorphous phase in a

semi-crystalline rubber and ΔCp_{am} is the change of heat capacity at Tg for an 100 percent amorphous rubber.[9]

For CB filled NR, Equation 5 should be modified because of the presence of the bound rubber between filler aggregates and rubber molecules:

$$Wc=[1-\Delta Cp_{cr}(filled)/\Delta Cp_{am}(filled)]*(1-\nu), \quad (6)$$

where ν is the fraction of bound rubber which could be determined by[20]

$$\nu = 1 - \Delta Cp_{am}(filled)/\Delta Cp_{am}(unfilled), \quad (7)$$

Equating Equation (4) and (6) and noting that the total crystallinity equals the sum of TIC and SIC gives

$$(1-\Delta Cp_{cr}/\Delta Cp_{am})*(1-\nu)$$
$$=(\Delta H_{TIC}/\Delta H_{TIC^{100}})+(\Delta H_{SIC}/\Delta H_{SIC^{100}}) \quad (8)$$

in which $\Delta H_{TIC^{100}}$= 64.1 J/gm (15.3 cal/gm)[21], ΔH_{TIC} (Figure 4b), ΔH_{SIC} (Figure 5), ΔCp_{cr} and ΔCp_{am} (Figure 9) can all be obtained from the DSC curves.

Equation 8 provides a method to determine $\Delta H_{SIC^{100}}$, instead of assuming, as is usually done, that it is the same as $\Delta H_{TIC^{100}}$[22]. The $\Delta H_{SIC^{100}}$ values obtained for all CB contents and strains considered are shown in Table II to be in the range of 44-52 J/gm, which is less than the usually assumed value of 64.1 J/gm. The percent of SIC (Figure 5) was determined with $\Delta H_{SIC^{100}}$=48 J/gm.

SIC in the Crack Tip Region

Since CB in NR increases the extent of SIC[10] and decreases the critical extension ratio to induce SIC, the concentration of SIC in the crack tip region and the SIC zone size are greater in CB filled than in unfilled NR specimen at crack initiation or propagation. Therefore more energy, that otherwise would be available for crack growth, is dissipated and the crack growth resistance is improved by CB filler[5,6].

But, if the stress state in the crack tip region of one specimen is more biaxial than another, the former specimen would have lower crack growth resistance than the other, since the crystallinity and the size of the crystalline zone in the crack tip region is reduced by biaxial stress. This explains the smaller crack growth resistance in PS specimens compared with SEN specimens[9].

CONCLUSIONS

1. CB enhances SIC, but has little effect on TIC.
2. The formation of SIC is hindered by biaxial stresses
3. Strain increases the Tm of SIC, but CB has no effect on Tm of SIC and TIC.

REFERENCES

[1] J. L White, J. Poly. Eng., 5(3), 235 (1985).

[2] E. H. Andrews, Proc. Roy. Soc., A270, 232 (1962).

[3] E. H. Andrews, J. Poly. Sci, Phys. Ed., 4, 668 (1966).

[4] G. Parks, J. Chem. Phys., 4, 459 (1937).

[5] D. J. Lee and J. A. Donovan, Rubber Chem. Technol., 60, 911 (1987).

[6] R. F. Lee and J. A. Donovan, ibid, 59, 282 (1986).

[7] Yu. S. Zuyev, Poly. Sci. USSR, 21, 1351 (1980).

[8] A. N. Gent and H. J. Kim, Rubber Chem. Technol., 51, 35, (1978).

[9] H. Liu, R. H. Lee and J. A. Donovan, Rubber Chem. Technol., 60, 893 (1987).

[10] D. Goritz and F.H. Muller, Kolloid Z. Z. Polymer,251,892 (1973).

[11] R. E. Lyon, R. J. Farris, and W. J. Macknight, J. Poly. Sci., Poly. Letters Ed., 21, 323 (1983).

[12] E. H. Andrews, Proc. Roy. Soc., A270, 232 (1962).

[13] A. N. Gent, Rubber Chem. Technol., 36, 697 (1963).

[14] S. D. Gehman and J. E. Field, Ind. Eng. Chem., 32, 140 (1940).

[15] F. Bueche and J. C. Halpin, J. Appl. Phys., 35, 36 (1964).

[16] L. Mullins and N. R. Tobin, Trans. Inst. Rubber Ind., 33, 1 (1956).

[17] L. Bateman, "The Chemistry and Physics of Rubber-like Substances", P. 303.

[18] A. I. Marei, S. K. Kurlyand and G. Ye. Novikova, Poly.

12
Sci. USSR, 13(3), 790 (1971).

[19]Hans-Georg Elias, "Macromolecules--Structure and Properties", 2nd ed., 161 (1985).

[20]Yu. S. Lipatov, "Physical Chemistry of Filled Polymer", Translated from Russion, International Polymer Sience and Technology Monograph No.2, Translated by R. J. Molesley, originally published by Khimiya, Moscow.

[21]D. F. Roberts and L. Mandelkern, J. Am. Chem. Soc., 77, 881 (1955).

[22]D. Goritz and M. Kiss, Rubber Chem Tech., 59, 41 (1986).

13

TABLE I

Tm OF TIC FOR DIFFERENT CB CONTENT

CB CONTENT	0	10	25
Tm(°K)	335.3	336	335.5

TABLE II

$\Delta H_{SIC^{100}}$(J/gram) CALCULATED FROM EQUATION (8)

λ_1	λ_2	0(pph)	10(pph)	25(pph)
2.5	1	--	48.4	49.4
3	1	--	47.6	51.6
4	1	46.9	47.2	45.4
2.5	.63	--	49.4	49.3
3	.58	--	46.7	45.8
4	.5	44.3	48.9	48.0

FIGURE CAPTIONS

FIG. 1.--Biaxially stretched rubber piece.

Fig. 2.--Three-piece brass fixture for DSC of a biaxially stretched rubber sample.

Fig. 3.--A Typical DSC curve for the material studied.

Fig. 4.--ΔH for TIC as a function of CB at a) 253°K b) 294°K.

Fig. 5.--ΔH for SIC of uniaxially stretched NR as a function of extension ratio.

Fig. 6.--ΔH for SIC of biaxially stretched NR as a function of extension ratio.

Fig. 7.--Tm of SIC as a function of extension ratio.

Fig. 8.--Tm of SIC as a function of CB content.

Fig. 9.--ΔCp_{cr} as functions of extension ratio and CB.

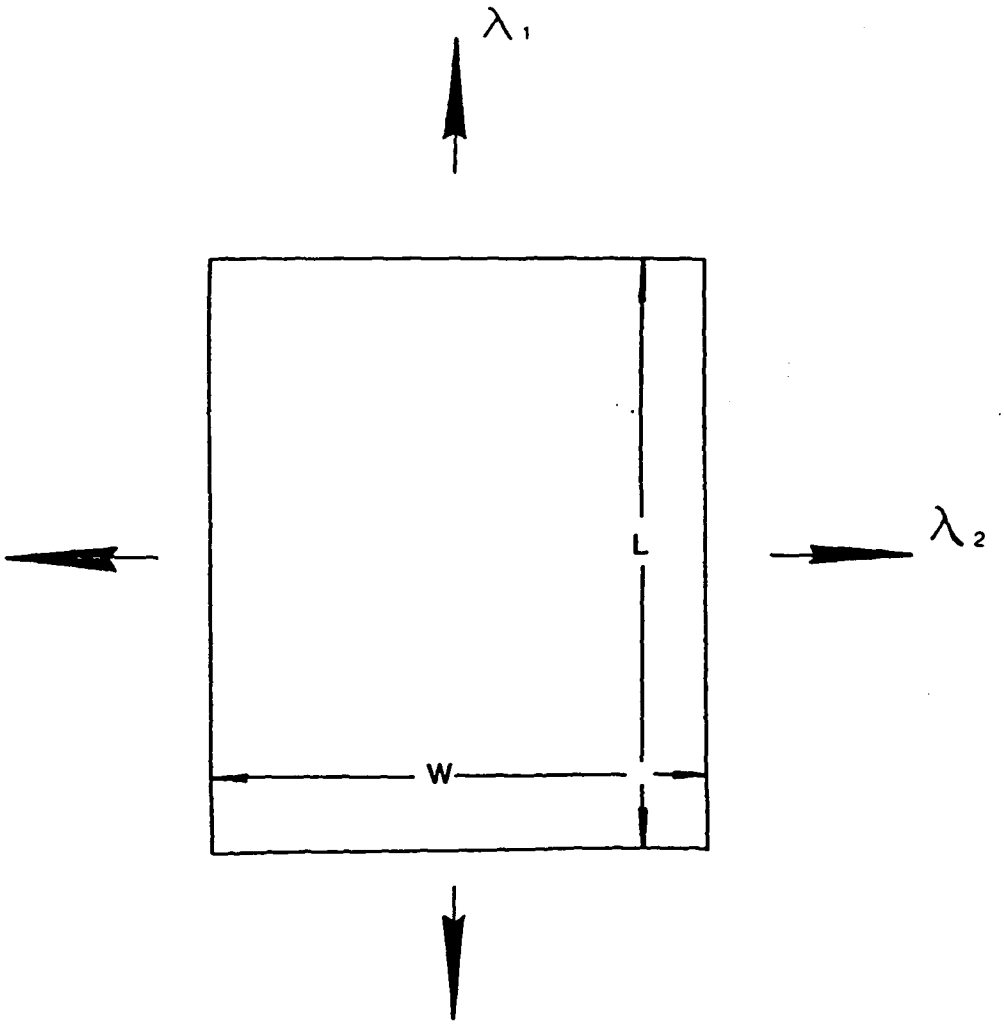
λ1
λ2
L
W

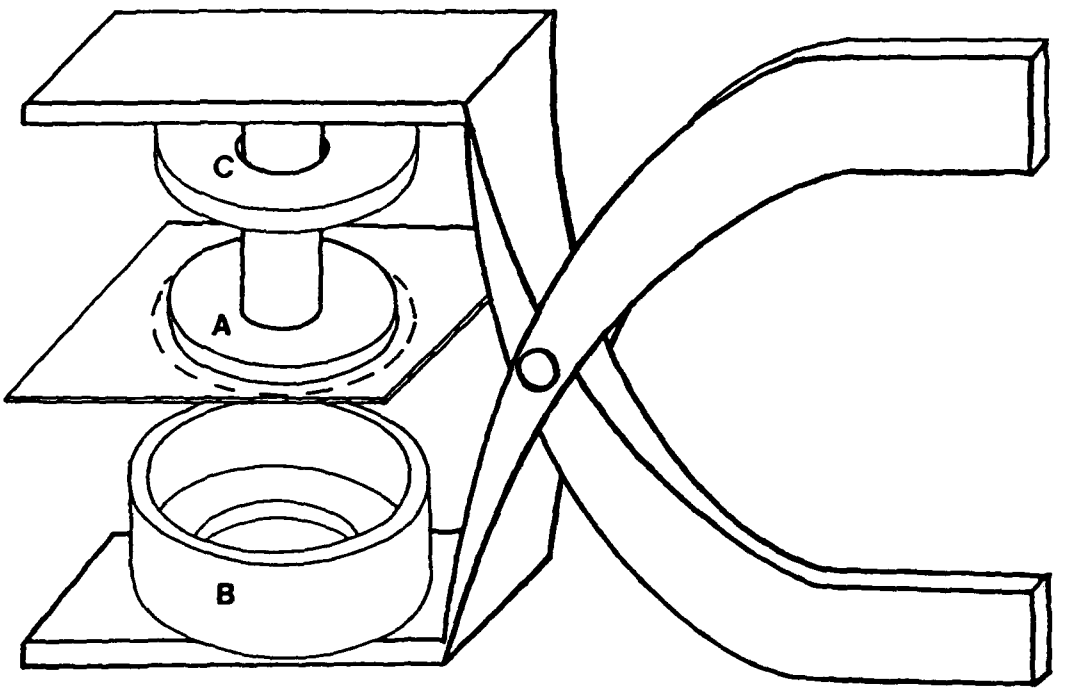
C
A
B

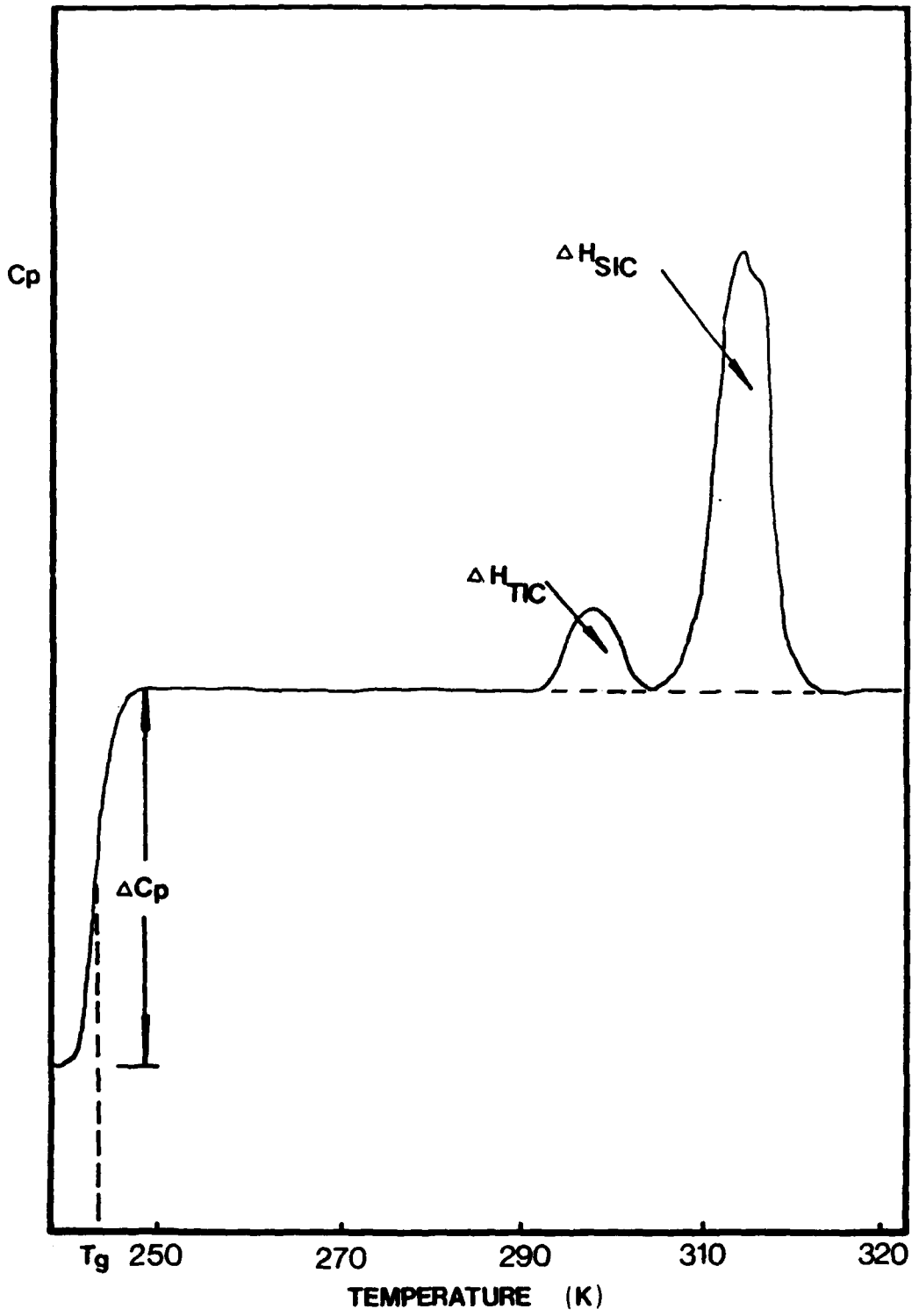
Cp
ΔH_SIC
ΔH_TIC
ΔCp
Tg
250
270
290
310
320
TEMPERATURE (K)

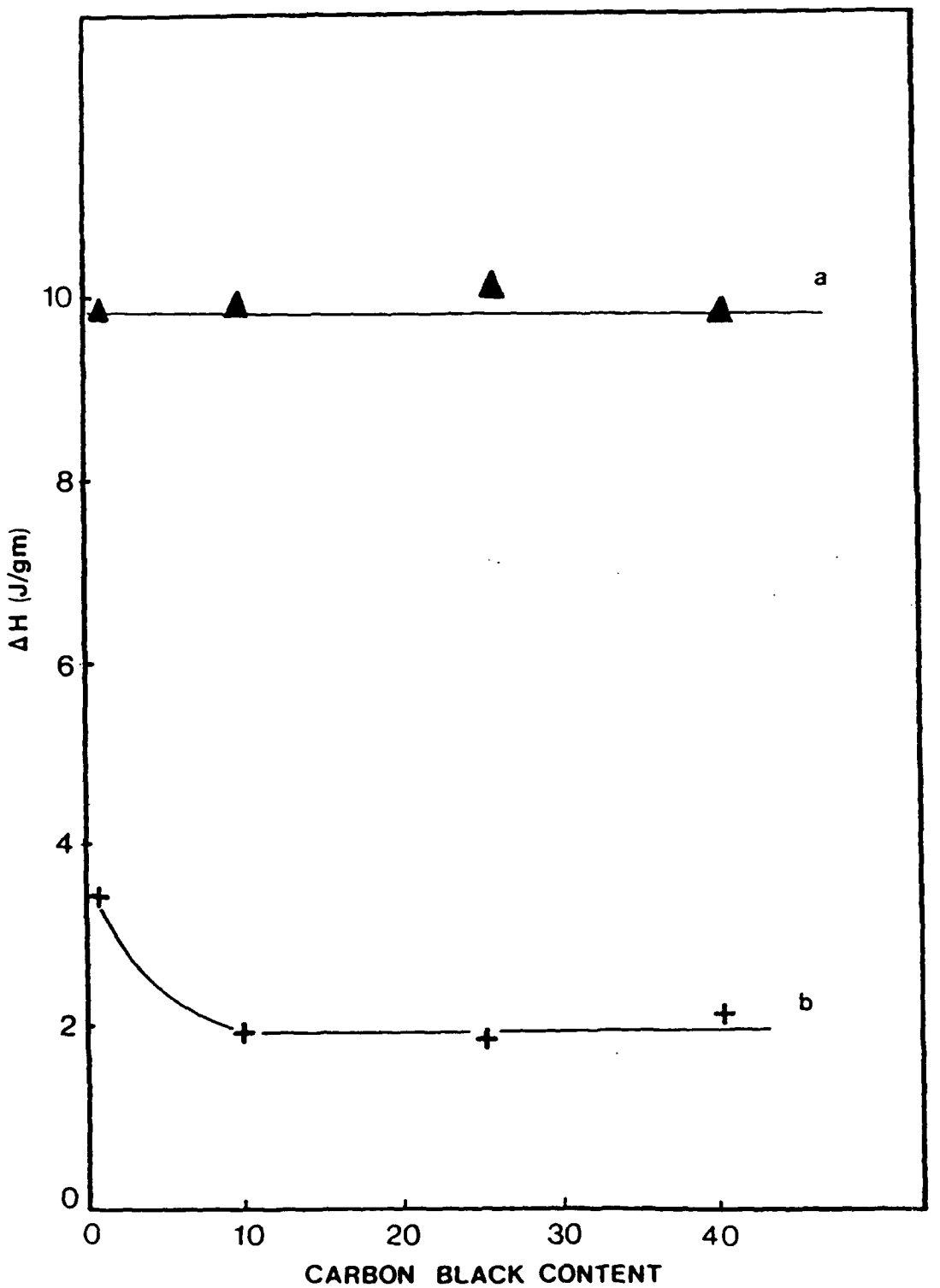
10
8
6
4
2
0
ΔH (J/gm)
a
b
0
10
20
30
40
CARBON BLACK CONTENT

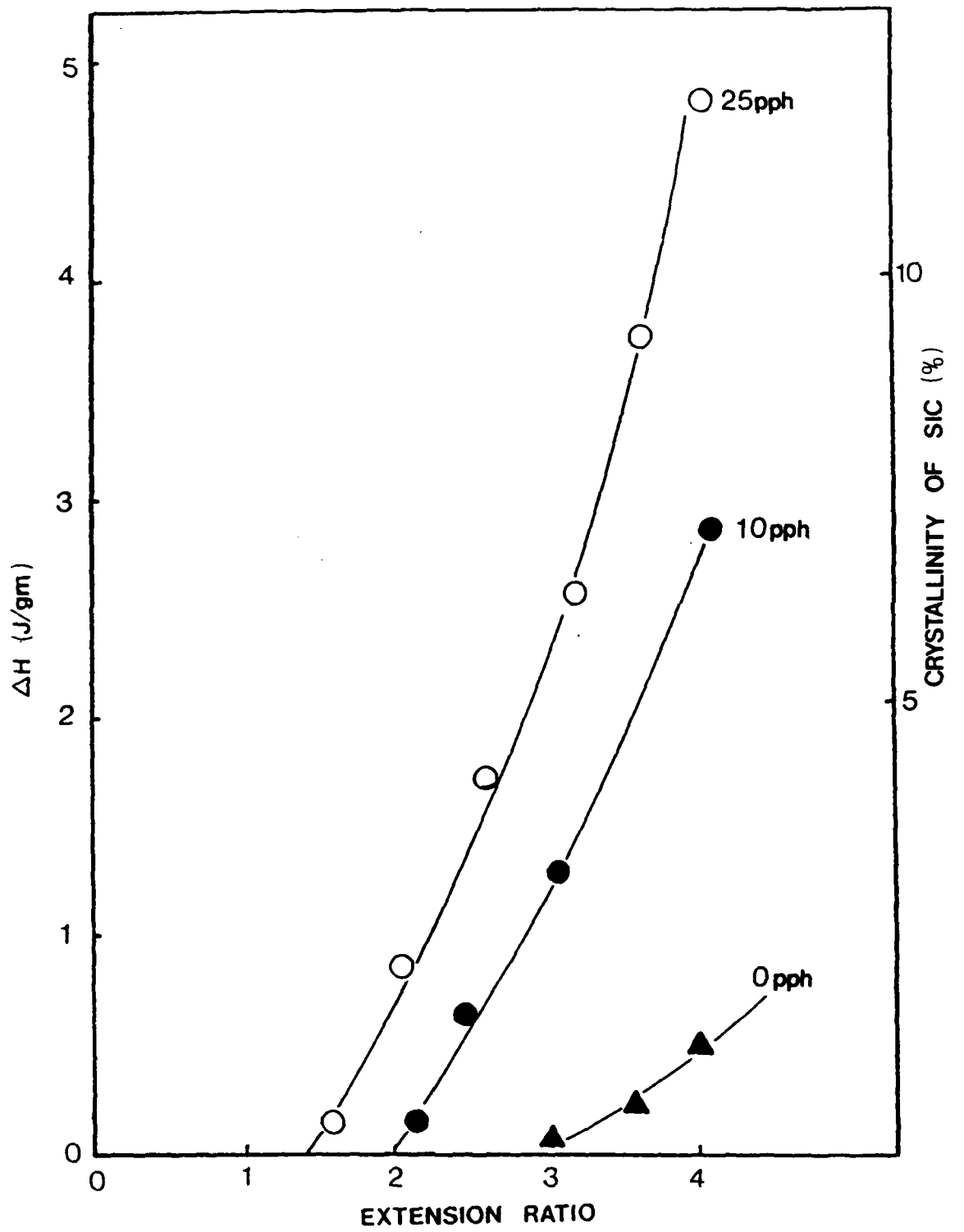
25pph
10pph
0pph
ΔH (J/gm)
CRYSTALLINITY OF SIC (%)
EXTENSION RATIO
0
1
2
3
4
5
10

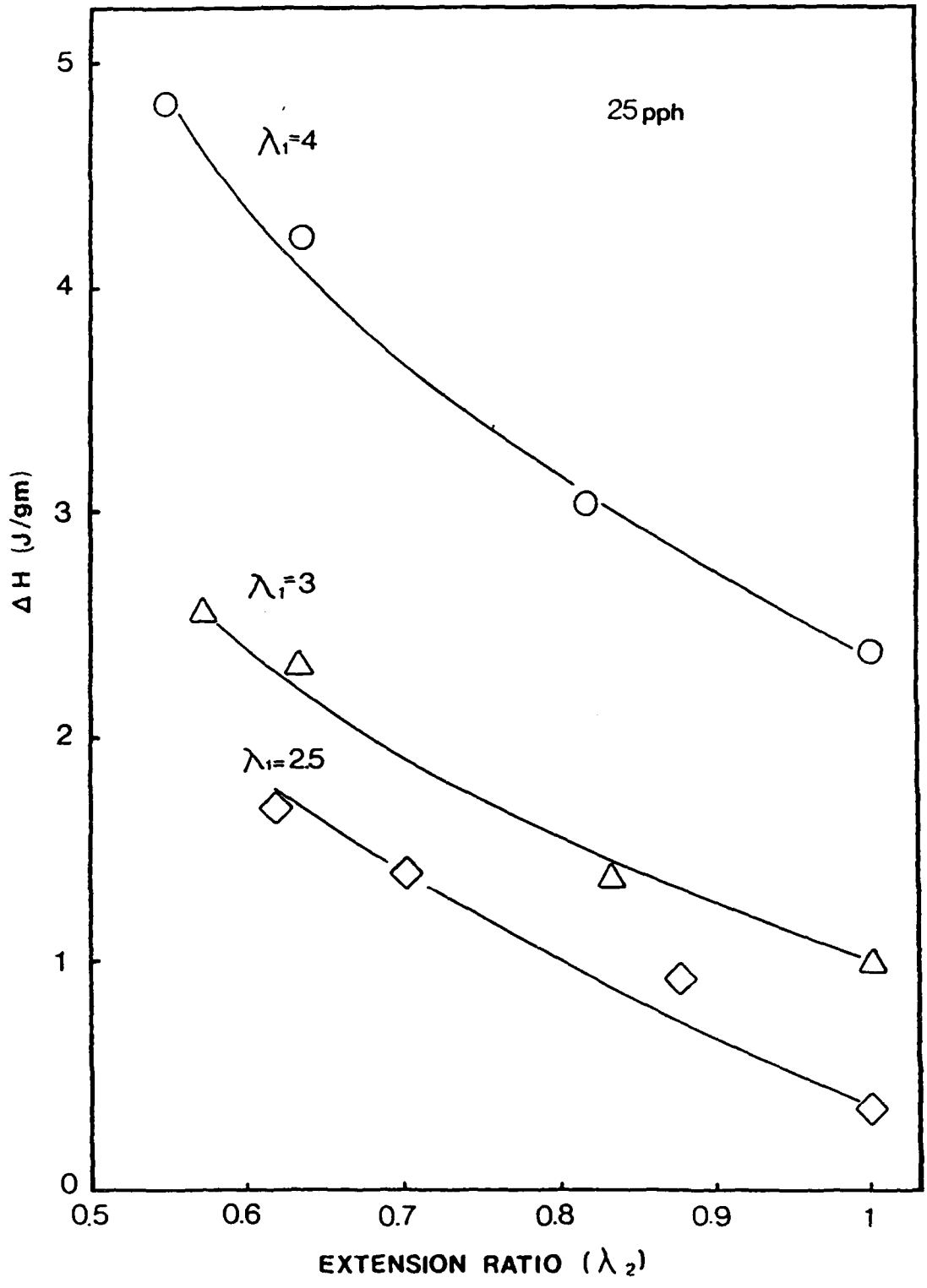
25 pph
λ1=4
λ1=3
λ1=2.5
ΔH (J/gm)
EXTENSION RATIO (λ2)
0
1
2
3
4
5
0.5
0.6
0.7
0.8
0.9
1

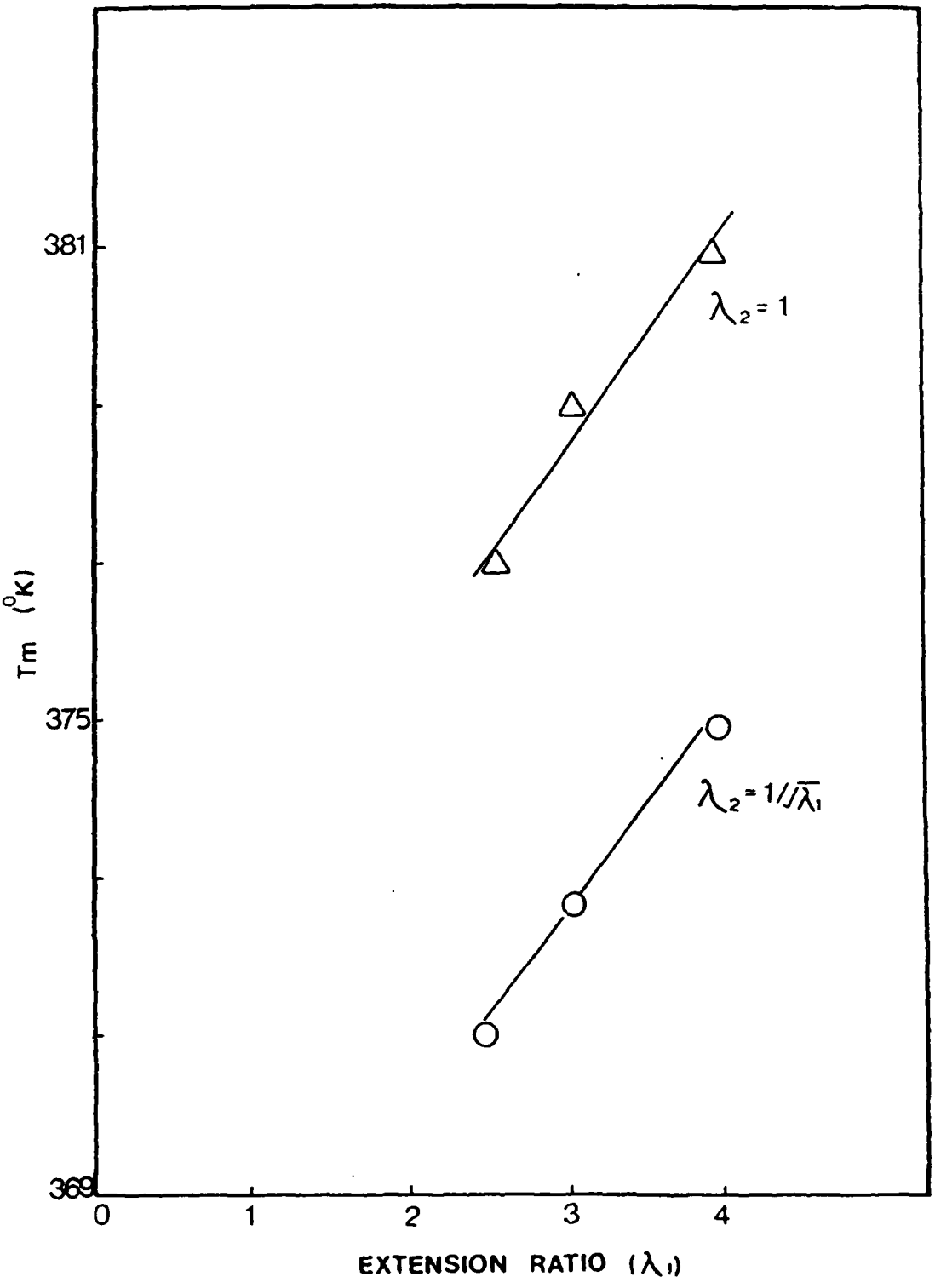
381
375
369
Tm (°K)
0
1
2
3
4
EXTENSION RATIO (λ1)
λ2 = 1
λ2 = 1/√λ1

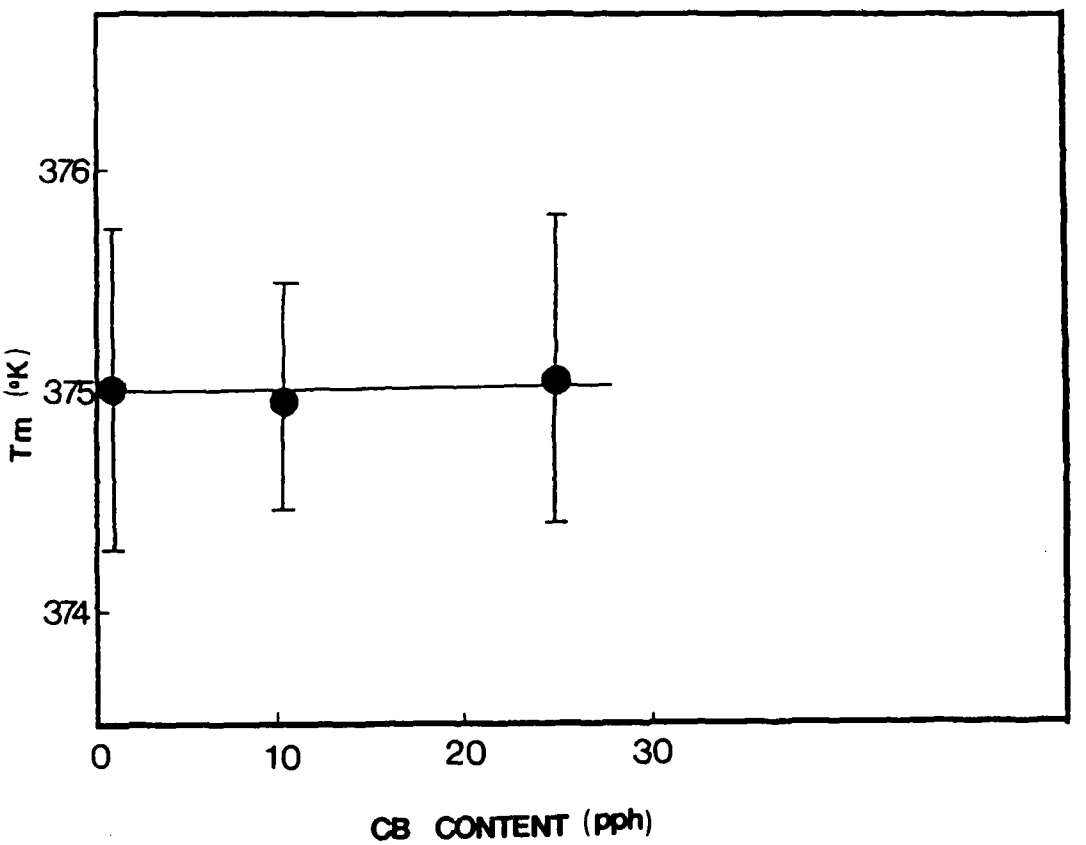
376
375
374
Tm (°K)
0
10
20
30
CB CONTENT (pph)

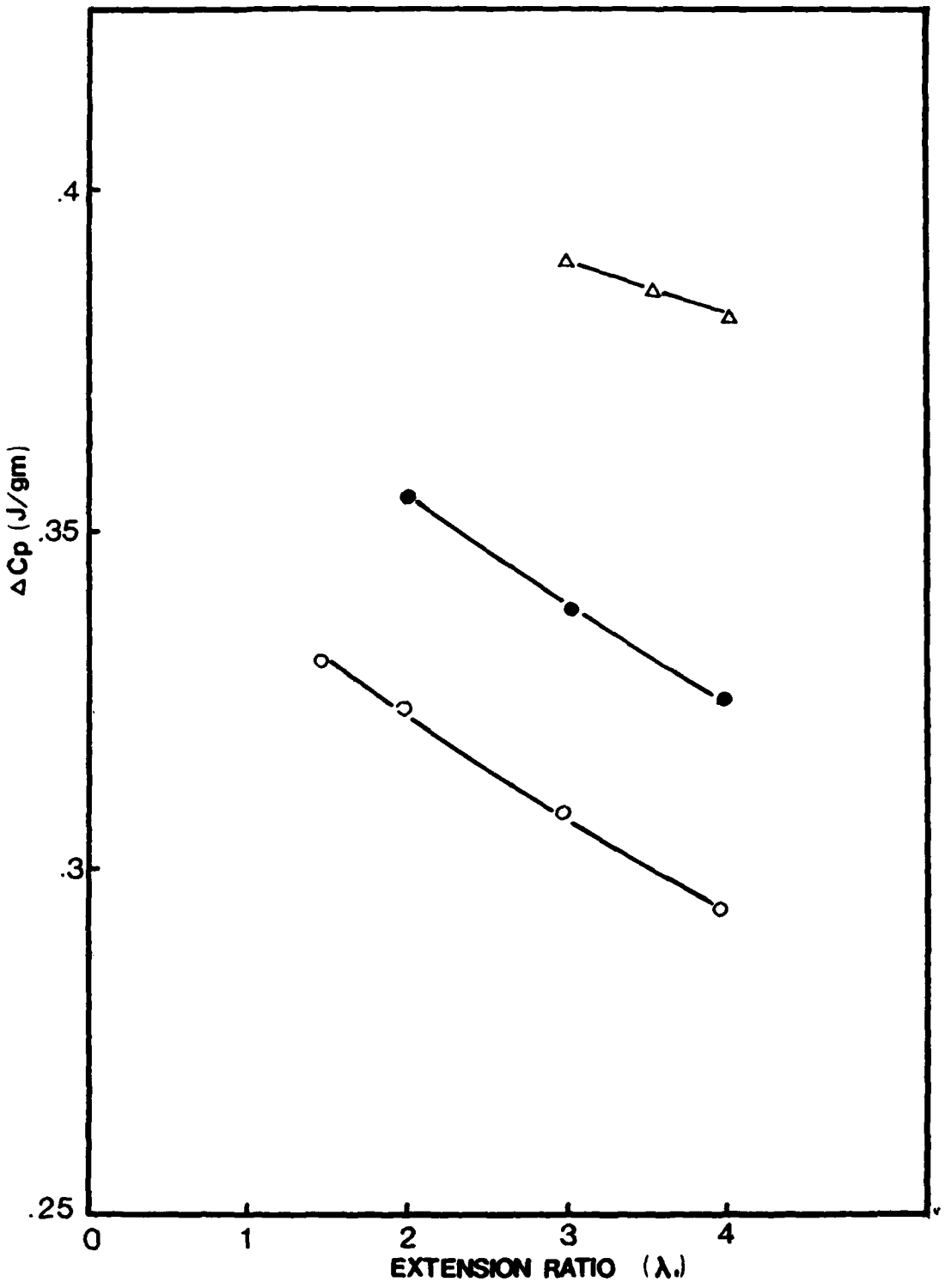
.4
.35
.3
.25
ΔCp (J/gm)
0
1
2
3
4
EXTENSION RATIO (λ1)

Presentations

The majority of the work has been presented at the Rubber Division Meetings of the American Chemical Society, but other presentations have been made at the American Physical Society, Materials Research Society, and the North American Thermal Analysis Society. Also, several posters have been presented and one won the Best Poster Award, 1986 Rubber Division Meeting.

In addition, invited presentations of this research were made at the Sagamore Army Materials Research Conference (1985), Elastomers Gordon Research Conference (1987), and will be made at the Frontiers in Rubber Science Symposium (1989).

Participating Scientific Personnel

1. D.J. Lee, Ph.D., 1987

2. R.F. Lee, Ph.D., 1988

3. P.R. Stupak, M.S., 1988

4. H. Liu, Ph.D., expected June 1989

5. J.H. Kang, M.S. expected June 1989

6. J.A. Donovan